

**MINISTRY OF EDUCATION AND SCIENCE OF UKRAINE  
ODESSA STATE ENVIRONMENTAL UNIVERSITY**

**Glushkov A.V., Kruglyak Yu.A.,  
Khetselius O.Yu., Buyadzhi V.V**

**NUMERICAL METHODS IN QUANTUM  
GEOMETRY AND CHAOS THEORY,  
PART 1 THEORY MANY-BODY  
SYSTEMS**

**Lecture's Notes**

**Odessa - 2015**

ББК 22.193  
GX55  
УДК 539.184:539.27

Glushkov A.V., Kruglyak Yu.A., Khetselius O.Yu., Buyadzhi V.V.,  
Numerical methods in quantum geometry and chaos theory, part 1 Theory of  
many-body systems, Lecture's Notes.-Odessa: TEC.-2015.

In the book there are presented new and reviewed known quantum theory, including geometry, quantum mechanics and theoretical nanoelectronics methods and new computational algorithms, which are used in solving some important and complicated classes of problems in computational mathematics, quantum geometry and mechanics, theoretical nanoelectronics and so on. For magisters and PhD students of the specialties: "Computational Mathematics", "Mathematical Physics", "Optics and Laser Physics" and so on.

У книзі представлені нові, а також відомі методи квантової теорії, у тому числі, геометрії, квантової механіки та теоретичної наноелектроніки і нові обчислювальні алгоритми, які можуть бути використані у вирішенні цілого ряду важливих і складних класів задач обчислювальної математики, квантової геометрії та механіки, теоретичної наноелектроніки та інших. Для магістрів та аспірантів спеціальностей «Обчислювальна математика», «Оптика та лазерна фізика» «Математична фізика», тощо.

В книге представлены новые а также хорошо известные методы квантовой теории, в том числе, геометрии, квантовой механики и теоретической нанoeлектроники и новые вычислительные алгоритмы, которые могут быть использованы в решении целого ряда важных и сложных классов задач вычислительной математики, квантовой геометрии и механики, теоретической нанoeлектроники и др. Для магистров и аспирантов специальностей «Прикладная математика» («Вычислительная математика»), Физика и астрономия («Оптика и лазерная физика»), «Математическая физика» и др.

*Published by the decision of Methodical council of Odessa State  
Environmental University.*

*Навчальне видання*

д-р фіз.-мат.наук, професор Глушков О.В. (Glushkov A.V.),  
д-р хім.наук, професор Кругляк Ю.О. (Kruglyak Yu.A.),  
д-р фіз.-мат.наук, професор Хецеліус О.Ю., (Khetselius O.Yu.),  
канд.фіз.-мат.наук Буюджи В.В. (Buyadzhi V.V.)

Обчислювальні методи в квантовій геометрії і теорії хаосу, Част. 1. Теорія  
багаточастинових систем

ISBN

© Odessa State Environmental University, 2015  
© Glushkov A.V., Kruglyak Yu.A., Khetselius O.Yu.,  
Buyadzhi V.V., 2015

# CONTENT

	Pages
<b>Introducing Remarks</b> .....	5
<b>Abbreviations (used in the text)</b> .....	6
 <b>Chapter 1 THE METHOD OF NON-EQUILIBRIUM GREEN'S FUNCTIONS AND MODEL THE TRANSPORTATION PROBLEM</b>	
1.1 Introduction.....	7
1.2 One-level resistor: a quantum approach.....	16
1.3 Quantum broadening.....	20
1.4 Quantum transport through multi-level conductor.....	23
1.5 Modeling 1D conductor.....	31
1.6 Modeling 2D conductor.....	41
1.7 Contact its own energy for 2D conductor.....	49
1.8 A general method for the construction of the contact matrices.....	56
1.9 Ballistic conductance of grapheme.....	60
 <b>Chapter 2 HALL EFFECT MEASURING ELECTROCHEMICAL POTENTIALS</b>	
2.1 Introduction.....	62
2.2 The spatial profile of the electrochemical potential.....	69
2.3 Measurement of electrochemical potential. Formula Landauer and Buttiker.....	73
2.4 Buttiker's formula.....	81
2.5 Quantum Hall effect, Landau levels and edge states in grapheme.....	91
 <b>Chapter 3 TRAFFIC SPIN MODEL NEGF AND QUANTUM SPIN HALL EFFECT</b>	
3.1 Introduction.....	101

3.2	One-level spin valve.....	105
3.3	Rashba Hamiltonian.....	113
3.4	The spin precession.....	120
3.5	The quantum spin Hall effect.....	123
3.6	Method NEGF and diffusive transport.....	125

**Chapter 4 QUANTUM INTERFERENCE AND DEPHASING IN  
METHOD NON-EQUILIBRIUM GREEN'S FUNCTIONS**

4.1	Introduction.....	131
4.2	1D conductor with two or more scattering centers.....	135
4.3	The potential jump on defects.....	140
4.4	The quantum nature of the classics.....	147

<b>References to Chapter 1</b> .....	<b>153</b>
--------------------------------------	------------

<b>References to Chapter 2</b> .....	<b>157</b>
--------------------------------------	------------

<b>References to Chapter 3</b> .....	<b>160</b>
--------------------------------------	------------

<b>References to Chapter 4</b> .....	<b>163</b>
--------------------------------------	------------

## Introducing Remarks

In the book there are presented new and reviewed known quantum theory, including geometry, quantum mechanics and theoretical nanoelectronics methods and new computational algorithms, which are used in solving some important and complicated classes of problems in computational mathematics, quantum geometry and mechanics, theoretical nanoelectronics and so on.

Especially attention is devoted to review of quantum transport in nanoelectronic devices includes the following topics discussed in the frame of the «bottom – up» approach: 1). Non-equilibrium Green's functions (NEGF) method in matrix representation with applications to model transport problems for 1D and 2D conductors using the nearest neighbor orthogonal tight-binding model. General method to account for electric contacts in Schrödinger equation when solving electron quantum transport problems is also given; 2). Classical and quantum Hall effects, measurement of electrochemical potentials, the Landauer formulae and Buttiker formula, measurement of Hall potential, inclusion of magnetic field in the NEGF formalism as well as the quantum Hall effect, Landau levels, and edge states in graphene; 3). Spin transport via the NEGF formalism in the spinor representation, in particular, spin valve, rotating magnetic contacts, spin precession and rotating spins, Zeeman and Rashba spin Hamiltonians, quantum spin Hall effect, calculation of the spin potential, and four-component description of electron transport; 4). Elastic and spin dephasing modeling, account for the non-coherent processes using Buttiker probe, 1D conductor with two and more scatterers, quantum interference, strong and weak localization, potential drop across scatterers, quantum oscillations in NEGF method without dephasing and with its account under phase and impulse relaxation regimes, destructive and constructive interference effects, four-component description of spin transport with account for dephasing and finally ending with discussion of quantum nature of classics including spin coherence and pseudo-spin formalism. This part of the review is closely based on lectures of Prof. Supriyo Datta «Fundamentals of Nanoelectronics, Part II: Quantum Models» given on-line in 2012 under initiative of Purdue University/nanoHUB-U [[www.nanohub.org/u](http://www.nanohub.org/u)].

Для магістрів та аспірантів спеціальностей «Обчислювальна математика», «Оптика та лазерна фізика» «Математична фізика», тощо.

### **Abbreviations (used in the text):**

AGNR-	armchair graphene nanoribbon,
LL-	Landau levels,
MBPT-	many-body perturbation theory,
NEGF-	non-equilibrium Green's function,
STM-	scanning tunneling microscope,
QSH-	quantum spin Hall effect,
ZGNR-	zigzag graphene nanoribbon.

# Chapter 1

## THE METHOD OF NON-EQUILIBRIUM GREEN'S FUNCTIONS AND MODEL THE TRANSPORTATION PROBLEM

### 1.1 Introduction

In continuation of previous publications [1 – 3] under the concept of "bottom – up" nanoelectronics [4, 5] consider the method of non-equilibrium Green's functions in the matrix formulation and apply it to the analysis and solution of model transport problems of electron transport on the example of the homogeneous and inhomogeneous 1D and 2D conductors, including graphene, and we formulate a General method of accounting for electrical contacts in the Schrodinger equation.

Modern laptop contains almost a billion or more field-effect transistors with long channel conductivity  $\sim 40 - 50$  nm, which corresponds to a few hundred atoms. Decreasing the length of the conduction channel of a physical nature electron transport varies qualitatively (Fig. 1.1).

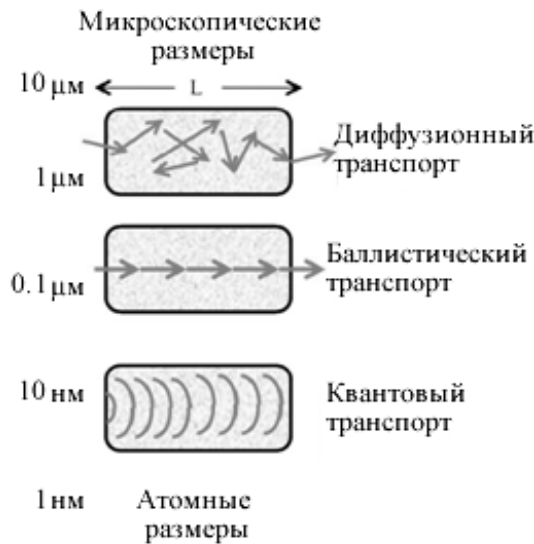


Figure 1.1 – With the reduction in the length of the conduction channel,  $L$  is the physical nature of electron transport varies qualitatively from diffusive to ballistic and further to quantum

For long enough conductors transport is diffusive with a trajectory resembling a random walks. If the length of the conduction channel becomes

less than the average mean free path, transport of electrons goes into ballistic mode of transfer. When shorter lengths of channel conductivity begins to show the wave nature of electrons in these quantum effects such as interference and tunneling.

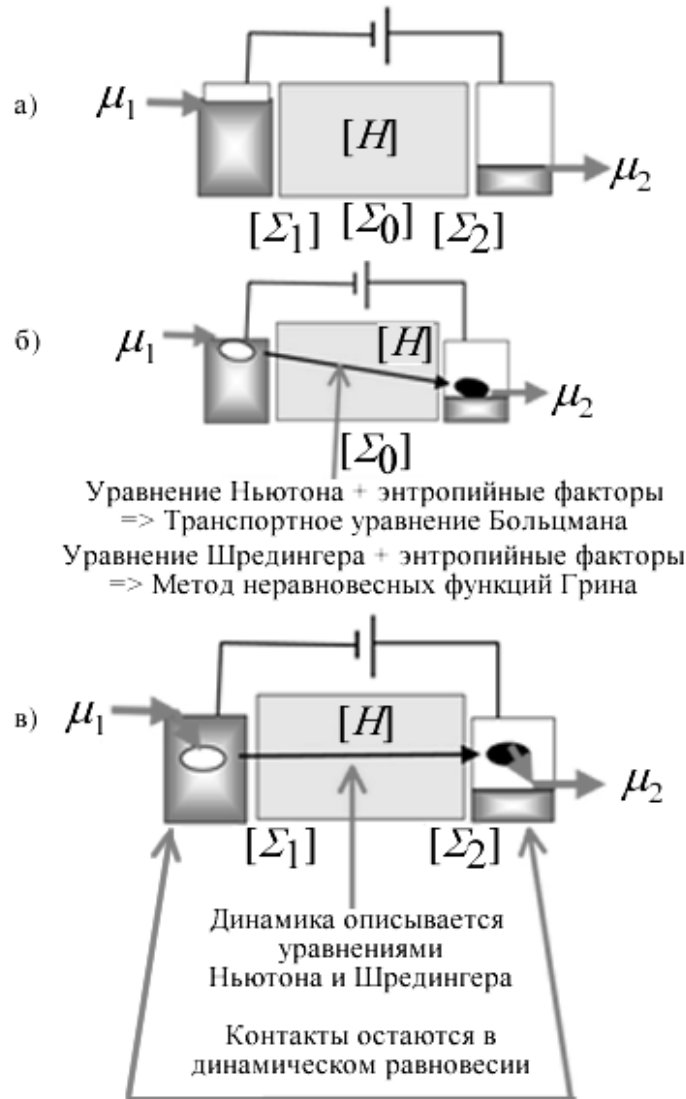


Figure 1.2 – Schematic description of (a) active channel conductivity interacting with the source and drain, and two limiting cases – (b) diffusive transport in macroscopic conductors and (b) ballistic transport in nanotransistors

Historically a deeper understanding of the physical nature of electrical conductivity occurred top – down: from the massive macroscopic conductors transistors to molecular and even atomic dimensions. Even 20 years – 25 ago there were the usual arguments about how to understand the concept about

electrical resistance, if the conductor size is approaching atomic dimensions. Despite the extraordinary achievements in the field of experimental metafisica and Nanophysics, and to this day when discussing the conductivity is dominated by the concept of top – down instead of the more natural concept of bottom – up, which makes the analysis and discussion of nanoelectronics devices sometimes ludicrously complicated [6, 7]. The concept of bottom – up is illustrated in Fig.1.2.

Any device nanoelectronics has active channel conductivity, which is described by the Hamiltonian  $[H]$ , which includes potential energy  $U$ , obliged all other charges as external (on the electrodes) and internal (in the channel). The channel conductance interacts with the source and drain and with all other contacts in a specific device, which are in local equilibrium, as defined by the relevant electrochemical potentials (Fig. 1.2a). The interaction between the channel and the contacts is described by the matrices of the self-energy (self-energy)  $[\Sigma_1]$  and  $[\Sigma_2]$  [8]. The interaction of the electron in the channel with its surroundings is described by the self-energy matrix  $[\Sigma_0]$ , which in contrast to the matrix  $[\Sigma_1]$  and  $[\Sigma_2]$ , must be calculated consistent. The dimension of these square matrices is determined by the number  $N$  of basis functions used for the quantum-mechanical description of the conduction channel and contacts. The specific form of the matrices used method of solving the Schrodinger equation is semi-empirical, based on the density functional theory or from first principles, as well as the choice of basis functions. Once these matrices are composed, the further procedure for the calculation of conductivity, current and other electrical properties of a standard, to which this paper is devoted to model transport problems, representing not only scientific, but also informative and educational interest.

In Fig. 1.2 shows two extreme cases of the electron transport is diffusive (Fig. 1.2b) and ballistic (Fig. 1.2b). In the ballistic limit of transport of electrons is controlled by the contact matrix  $[\Sigma_1]$  and  $[\Sigma_2]$ , whereas interactions within the channel are negligible. In contrast, in the diffusion limit of transport of electrons is controlled by the interactions inside the channel, described by a matrix  $[\Sigma_0]$ , and the role of the contact matrices  $[\Sigma_1]$  and  $[\Sigma_2]$  is negligible. Not surprising that until about 1990, the contacts are not even depicted in the diagrams. Between the Hamiltonian matrix  $[H]$  and matrix  $[\Sigma_{0,1,2}]$  there is an important difference: the matrix of the Hamiltonian is conservative dynamic forces and is

Hermitian, whereas the matrix of the self-energy into account entropic factors and are not Hermitian.

The Schrodinger equation itself is not suitable to explain such seemingly obvious processes, such as spontaneous transition of an electron from the excited state to the ground and the impossibility of a spontaneous return process. This tendency for systems of any complexity to relax unidirectionally downward energy seems obvious and has no explanation in the framework of quantum mechanics. Such processes as diverse unidirectional phenomena in the world around us, are entropic in nature. In the design and analysis of any electronic devices, quantum or classical dynamics equations must be supplemented by entropic forces. So there was a statistical mechanics of non-equilibrium processes, Central to which is 140 years old is transport Boltzmann equation [9, 10]. The quantum analogue of the Boltzmann equation is the method of non-equilibrium Green's functions (NEGF), whose foundations were laid in the works of Martin and Schwinger [11], Kaganova and Bame [12] and Keldysh [13].

Both approaches – classical Boltzmann and quantum formalism NEGF consolidates the fact that they are simultaneously taken into account and dynamic and entropic forces. In the ballistic limit, however, dynamic and entropic processes are spatially separated (Fig. 1.2b). Electrons skips from one contact to another under the action of dynamic forces. Inside contacts, the electrons are not in equilibrium, but quickly come to equilibrium under the action of the entropic forces. A similar development model in the ballistic limit is called the elastic resistor model Landauer proposed by Rolf Landauer in 1957 [14 – 16] long before its triumphal experimental confirmation in nanotransistors. Today is really securely mounted, ballistic resistors can withstand fairly strong currents due to the fact that the allocation of Joule heat is negligible. The heat released on contact due to its relative massiveness quickly dissipated it. Spatial separation of dynamics and thermodynamics in ballistic devices is a strong argument in favor of the concept of "bottom – up", which seems to us to be attractive not only scientific, but also pedagogically.

The equations of the method of non-equilibrium Green functions. The objective of the present work, we see it, to give a compact presentation of the formalism NEGF with the model of Landauer in relation to nanoelectronic devices. Based on pioneering work from Schwinger to Keldysh [11 – 13], based

on quantum many-body perturbation theory (MCT) and diagrammatic technique, it is not enough for a few semesters to master the method NEGF. In this presentation, we will follow the works Datta, Meira and Wingina [4 – 7, 17 – 20], as most adequate to the task before us. We begin with the elastic resistor, entropic processes in which heat dissipation occurs only at the contacts, and the problem of the resistance of the resistor will look at the single-particle approximation with the addition of the Schrodinger equation

$$[H]\{\psi\} = E\{\psi\} \quad (1.1)$$

two more members describing the outflow of electrons in the contacts (outflow)

$$[\Sigma] = [\Sigma_1] + [\Sigma_2], \quad (1.2)$$

and the flow of electrons in a conductor with contacts (inflow)

$$\{s\} = \{s_1\} + \{s_2\}, \quad (1.3)$$

namely:

$$E\{\psi\} = [H]\{\psi\} + [\Sigma]\{\psi\} + \{s\}, \quad (1.4)$$

where the Schrodinger equation directly written in matrix form, keeping in mind that the base functions are chosen so that the square matrices taken in the square brackets, and matrix-columns – in braces. Now the solution of the Schrodinger equation can be directly recorded using inverse matrix

$$\{\psi\} = [EI - H - \Sigma]^{-1}\{s\}. \quad (1.5)$$

where I is the identity matrix.

Matrix

$$G^R = [EI - H - \Sigma]^{-1} \quad (1.6)$$

got the name delayed (Retarded) Green's function, and the Hermitian conjugate of her matrix

$$G^A = [G^R]^+ \quad (1.7)$$

called advanced (Advanced) Green's function. The origin of these and other terms, generally accepted formalism NEGF, for us the future is not significantly more acquainted with the terminology suggest [6, 11 – 13]. We note only that the formalism NEGF as applied to problems in nanoelectronics is reduced to four equations, the first of which is the expression (1.6) for the retarded Green's function. Now the Schrodinger equation (1.5) can be rewritten in the form

$$\{\psi\} = [G^R]\{s\}. \quad (1.8)$$

The product of the column  $\{\psi\}$  on Hermitian conjugated string  $\{\psi\}^+$  gives

$$\{\psi\}\{\psi\}^+ = [G^R]\{s\}\{s\}^+[G^A], \quad (1.9)$$

where it is considered that the transposition of matrix multiplication changing the order of factors is reversed.

Non-equilibrium Green's function is defined as

$$G^n = 2\pi\{\psi\}\{\psi\}^+, \quad (1.10)$$

so the number of electrons is given by the expression

$$N = Tr [G^n] / 2\pi. \quad (1.11)$$

Likewise describes the flow of electrons

$$\Sigma^{in} = 2\pi\{s\}\{s\}^+, \quad (1.12)$$

so now the equation (1.9) has the form

$$G^n = G^R \Sigma^{in} G^A \quad (1.13)$$

and will be the second equation in the formalism NEGF. Completeness sake, we denote by comparison with [6] is simplified, namely:  $\Sigma$  instead  $\Sigma^R$ ,  $G^n$  instead  $-iG^<$ ,  $\Sigma^{in}$  instead  $-i\Sigma^<$ , however, the first and second equations (1.6) and (1.13) is substantially the same as that of equation (75) – (77) in his fundamental work of Keldysh [13] obtained diagrammatic technique MCTV. We believe that highlighting these two equations, and then two more from MCTV, originally used to display them, will make the method NEGF more transparent and accessible, and it will read to students physicists and electronic engineers to solve problems when the need arises to take into account the electrical contacts in the Schrodinger equation.

Give the remaining two equations formalism NEGF. The third equation is the matrix form of the density of States  $D(E)$ , multiplied by  $2\pi$ , and is called the spectral function  $A$

$$2\pi \cdot D(E) = A = G^R \Gamma G^A = G^A \Gamma G^R = i[G^R - G^A], \quad (1.14)$$

where the matrix  $G^R$  and  $G^A$  are given by equations (1.6) and (1.7), the matrix  $[\Gamma]$  is Skew-Hermitian part of the corresponding contact matrix

$$\Gamma = i[\Sigma - \Sigma^+] \quad (1.15)$$

and describes the interactions of electrons in the channel with contacts. The derivation of formula (1.14) for the spectral functions and the equivalence of all three expressions will perform below.

All of the matrix  $[\Sigma]$ ,  $[\Gamma]$  and  $[\Sigma^{in}]$  contain terms relating to specific terminals (contacts) included in a particular task. In equations (1.6), (1.13) and (1.14) the summation over all terminals have already been implemented. The fourth equation in the formalism NEGF is the equation for current through the terminal room  $m$

$$\tilde{I}_m = \frac{q}{h} \text{Trace} \left[ \sum_m^{in} A - \Gamma_m G^n \right], \quad (1.16)$$

which includes only those components of the matrices that belong to a given terminal  $m$ . This specific current (per unit energy), you need to integrate

across the spectrum of energies to get the total current through the terminal  $m$ . Next, we consider a simple model of the transportation problem, then go back to the rationale and the derivation of the equations of the method NEGF and discuss more complex transportation problems.

One-level resistor: semiclassical approach. To feel the physics of the method NEGF you can have a simple transport problem on a single-tier conductor, described by the matrices  $1 \times 1$ , i.e. numbers with  $[H] = \varepsilon$ . In this example we will see how to count the contacts in the Schrodinger equation, and then move on to the conductor with an arbitrary number of channels described by the matrices  $N \times N$ . First, however, let us consider a single-level task in the semiclassical approximation (Fig. 1.3).

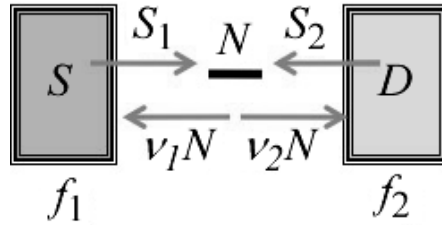


Figure 1.3 – Single-level model of a conductor in a semi-classical approximation

One-level conductor is in contact with two contacts with the Fermi population  $f_1(\varepsilon)$  and  $f_2(\varepsilon)$ . Initially assume that the source  $S$  of the Fermi function  $f_1 = 1$ , and the drain  $D$  function  $f_2 = 0$ . This means that the source seeks to fill the level with energy  $\varepsilon$ , and flow seeks only to extract the electrons from this level. Finally when calculating total current multiply it on

$$f_1(\varepsilon) - f_2(\varepsilon),$$

keeping in mind that the injection of electrons occurs from both contacts, and the total current has a differential effect.

When  $f_1 = 1$  on the source and  $f_2 = 0$  drain is the average number of electrons  $N$  satisfies the equation

$$\frac{d}{dt} N = -(\nu_1 + \nu_2) N + S_1 + S_2, \quad (1.17)$$

where  $v_1$  and  $v_2$  are the speed with which the electrons leave the conductor in the direction of the contacts, and  $S_1$  and  $S_2$  is the speed with which the electrons injected by the contacts in the conductor. In the conditions of dynamic equilibrium  $dN/dt = 0$ , so the population of the single-level electron

$$N = \frac{S_1 + S_2}{v_1 + v_2}. \quad (1.18)$$

If mentally disabled runoff, the number of electrons is equal to the Fermi functions at the source, but if disconnect the source, the number of electrons is equal to the Fermi functions at the drain

$$\frac{S_1}{v_1} = f_1(\varepsilon) \quad \text{and} \quad \frac{S_2}{v_2} = f_2(\varepsilon). \quad (1.19)$$

Let us regroup the equation (1.17) in

$$\frac{dN}{dt} = (S_1 - v_1 N) + (S_2 - v_2 N), \quad (1.20)$$

then the first term is the flow of electrons generated by the source, and the second term is the flow. In the conditions of dynamic equilibrium of both streams are equal and oppositely directed, and the current is

$$I = q(S_1 - v_1 N) = q(v_2 N - S_2), \quad (1.21)$$

while any of these two expressions can be used to calculate the current. From (1.18) and (1.19) have an occupancy level in the conditions of dynamic equilibrium

$$N = \frac{v_1 f_1(\varepsilon) + v_2 f_2(\varepsilon)}{v_1 + v_2}, \quad (1.22)$$

substituting in the expression for the current (1.21) and bearing (1.19), for the current  $I$  via the Fermi functions have finally

$$I = q \frac{v_1 v_2}{v_1 + v_2} (f_1(\varepsilon) - f_2(\varepsilon)). \quad (1.23)$$

## 1.2 One-level resistor: a quantum approach

The stationary Schrodinger equation

$$[H]\{\psi\} = E\{\psi\}$$

follows from the time-dependent Schrodinger equation

$$i\hbar \frac{\partial}{\partial t} \{\tilde{\psi}(t)\} = [H]\{\tilde{\psi}(t)\} \quad (1.24)$$

as a result of lookup

$$\{\tilde{\psi}(t)\} = \{\psi\} e^{-iEt/\hbar}. \quad (1.25)$$

To describe dynamic equilibrium is usually sufficient stationary Schrodinger equation, but in some cases, can not do without time-dependent equation (1.24), for example, as we will see later, in the interpretation of some dependency matrices from their own energies.

For the single-level problem  $[H] = \varepsilon$ , the evolution of the wave function is described by the equation

$$i\hbar \frac{d}{dt} \tilde{\psi} = \varepsilon \tilde{\psi}, \quad (1.26)$$

with the use of which he comprehensively have paired

$$\frac{d}{dt} (\tilde{\psi} \tilde{\psi}^*) = 0, \quad (1.27)$$

in other words, the population of the isolated energy level does not change with time.

What we need here is not an isolated system, and a conductor connected to two contacts. Standard textbooks on quantum mechanics, unfortunately, does not show how to describe for us the situation. Modify the Schrodinger equation as follows

$$i\hbar \frac{d}{dt} \tilde{\psi} = \left( \varepsilon - i \frac{\gamma_1 + \gamma_2}{2} \right) \tilde{\psi} \quad (1.28)$$

so that the evolution of the electron density

$$\frac{d}{dt} \tilde{\psi} \tilde{\psi}^* = - \left( \frac{\gamma_1 + \gamma_2}{\hbar} \right) \tilde{\psi} \tilde{\psi}^* \quad (1.29)$$

like the dynamic equation semi-classics (1.17), with the possible exception of speeds  $S_1$  and  $S_2$ , with which the electrons injected by the contacts to the conductor, but we'll come back later. Equations (1.29) and (1.17) are consistent with each other, if you put

$$\gamma_1 = \hbar v_1, \quad (1.30)$$

$$\gamma_2 = \hbar v_2. \quad (1.31)$$

Stationary analogue of the equation (1.28)

$$E\psi = \left( \varepsilon - i \frac{\gamma_1 + \gamma_2}{2} \right) \psi \quad (1.32)$$

is obtained by substituting the solution for a single value of energy  $E = \varepsilon$

$$\tilde{\psi}(t) = \psi(E) e^{-iEt/\hbar}. \quad (1.33)$$

Equation (1.32) has the obvious solution  $\psi = 0$ , which indicates that the dynamical equilibrium of the electrons are not able to populate the level with energy  $E = \varepsilon$ . While not included source  $S_1$  of receipt of electrons in conductor electrons can only leave the vehicle, leaving the contacts (Fig. 1.4).

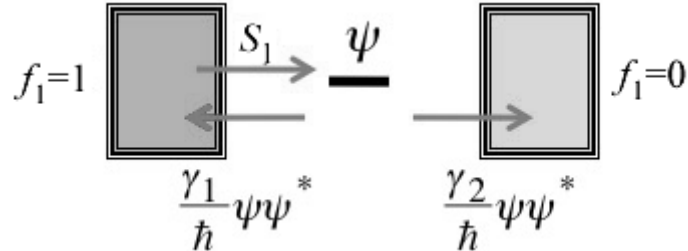


Figure 1.4 – Evacuation and the flow of electrons in the quantum model, one level of conductor

Introduce the stationary Schrodinger equation (1.32) of the contact members  $s_1$  as the source of electrons

$$E\psi = \left( \varepsilon - i\frac{\gamma}{2} \right) \psi + s_1, \quad (1.34)$$

where

$$\gamma = \gamma_1 + \gamma_2.$$

In contrast to the semiclassical model (1.17) in the quantum model introduces a single source of electrons instead of two, the reason why will become clear below. Equation (1.34) allows you to associate the wave function with the electron source

$$\psi = \frac{s_1}{E - \varepsilon + i(\gamma/2)}. \quad (1.35)$$

We note that the wave function takes on its maximum value when the electron energy  $E$  becomes equal to the energy level  $\varepsilon$ . The peculiarity of the quantum model is that the wave function is not substantially disappears when

the deviation  $E$  from  $\varepsilon$  by an amount less  $\gamma$ . This is an example of "broadening" or uncertainty of the energy missing in semiclassical.

Rate the quality of the electron source  $s_I$  as follows. Will index the total number of electrons in the entire spectrum of energies and equate it to the semiclassical expression (1.22) given the fact that  $f_I = 1$  and  $f_2 = 0$  (Fig. 1.4)

$$\int_{-\infty}^{+\infty} dE \psi \psi^* = \frac{\nu_1}{\nu_1 + \nu_2} = \frac{\gamma_1}{\gamma_1 + \gamma_2}, \quad (1.36)$$

where the second equality is obtained taking into account (1.30) and (1.31). Calculate the left part of equation (1.36) using the expression for the wave function (1.35),

$$\int_{-\infty}^{+\infty} dE \psi \psi^* = \int_{-\infty}^{+\infty} dE \frac{s_1 s_1^*}{(E - \varepsilon)^2 + \left(\frac{\gamma}{2}\right)^2} = \frac{2\pi s_1 s_1^*}{\gamma}, \quad (1.37)$$

where

$$\int_{-\infty}^{+\infty} dE \frac{\gamma}{(E - \varepsilon)^2 + \left(\frac{\gamma}{2}\right)^2} = 2\pi. \quad (1.38)$$

Equating (1.36) and (1.37), we obtain

$$2\pi s_1 s_1^* = \gamma_1. \quad (1.39)$$

In other words, the source of electrons is proportional to the rate of removal of electrons from a conductor, which seems plausible: if the contact is well connected with the conductor, the electrons just as well leave the contact as you come back from Explorer.

As in the case of the classical expression for the current (1.21), the current in quantum models will receive from the rate of change of the electron density (1.29)

$$\frac{d}{dt} \tilde{\psi} \tilde{\psi}^* = (\text{Inflow of contact 1}) - \frac{\gamma_1}{\hbar} \tilde{\psi} \tilde{\psi}^* - \frac{\gamma_2}{\hbar} \tilde{\psi} \tilde{\psi}^* \quad (1.40)$$

adding a flow of an injecting contact s1 that are not included in the temporary Schrodinger equation (1.28).

The left and right side of equation (1.40) is zero, since we are talking about the current state of dynamic equilibrium. As in the classical model, the current can be calculated either as the sum of the first two terms, or as the third summand in equation (1.40)

$$\frac{I}{q} = (\text{Inflow of contact 1}) - \frac{\gamma_1}{\hbar} \tilde{\psi} \tilde{\psi}^* = \frac{\gamma_2}{\hbar} \tilde{\psi} \tilde{\psi}^* . \quad (1.41)$$

Integrating across the entire spectrum of energies, for the current received

$$I = q \int_{-\infty}^{+\infty} dE \frac{\gamma_2}{\hbar} \psi \psi^* \quad (1.42)$$

and substituting (1.35) and (1.39) for the current in quantum models have finally

$$I = \frac{q}{\hbar} \frac{\gamma_1 \gamma_2}{2\pi} \int_{-\infty}^{+\infty} dE \frac{1}{(E - \varepsilon)^2 + (\lambda / 2)^2} , \quad (1.43)$$

what can be compared with the expression for the current in a semi-classical model (1.23), bearing in mind that  $f_1 = 1$  and  $f_2 = 0$ ,  $\gamma = \gamma_1 + \gamma_2$ ,

$$I = \frac{q}{h} \frac{\gamma_1 \gamma_2}{\gamma_1 - \gamma_2} . \quad (1.44)$$

### 1.3 Quantum broadening

Calculation of the current in the quantum model (1.43) involves integration over the entire spectrum of energies, because the quantum consideration of a

single localized level blurred into a continuous energy distribution (Fig. 1.5) according to the density of states  $D(E)$

$$D = \frac{\gamma / 2\pi}{(E - \varepsilon)^2 + (\gamma / 2)^2}. \quad (1.45)$$

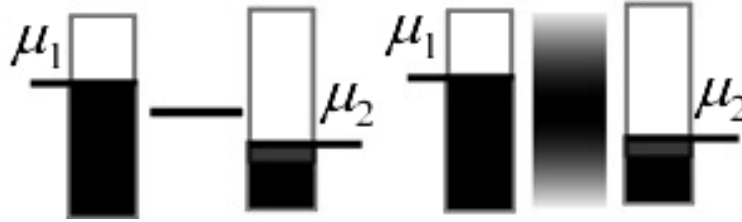


Figure 1.5 – Unlike classical views (left) single localized energy levels in the quantum model (right) was being undermined by the Heisenberg uncertainty principle

Direct experimental measurement of the conductivity of single molecules of hydrogen [21], the spectrum of which actually corresponds to the single-level model of the resistor, can serve as a direct proof of validity of quantum broadening of energy levels.

Comparing (1.43) with the expression for the current of the elastic resistor (32) in [1] obtained the conductivity of the single-level model taking into account the quantum broadening

$$G(E) = \frac{q^2}{h} \frac{\gamma_1 \gamma_2}{(E - \varepsilon)^2 + \left(\frac{\gamma}{2}\right)^2}. \quad (1.46)$$

Assuming equal communication conductor with two contacts

$$\gamma_1 = \gamma_2 = \frac{\gamma}{2} \quad (1.47)$$

and the temperature low enough to ensure that the measured conductivity was equal to  $G(E = \mu_0)$ , have

$$G \approx G(E = \mu_0) = \frac{q^2}{h} \frac{(\gamma/2)^2}{(\mu_0 - \varepsilon)^2 + (\gamma/2)^2}. \quad (1.48)$$

Thus, the quantum model one-level resistor shows that the measured conductivity will be maximum and equal to the quantum of conductance  $q^2/h$ , if the electrochemical potential  $\mu_0$  will be sufficiently close to the energy level  $\varepsilon$ . Experimentally measured conductance quantum is equal to  $2q^2/h$ , where the deuce is associated with degeneration on the back, because in reality all energy levels come in pairs with spins  $\alpha$  and  $\beta$ , so the single layer model of the resistor actually has a two-level taking into account the spin degeneracy.

**To the question about the interference of sources of electrons in a conductor.** Unlike classical models of resistor, which simultaneously took into account both the source of the electrons with the two contacts in the conductor (1.17), in the quantum model (1.34) was based on the injection of electrons only from the source ( $f_1 = 1$ ), and flow was maintained empty ( $f_2 = 0$ ).

It's not a question of convenience of reasoning. If instead of (1.34) in the Schrodinger equation simultaneously consider both an injecting contact

$$E\psi = \left( \varepsilon - i\frac{\gamma}{2} \right) \psi + s_1 + s_2, \quad (1.49)$$

for the wave function will receive

$$\psi = \frac{s_1 + s_2}{E - \varepsilon + i\frac{\gamma}{2}}, \quad (1.50)$$

so in the electron density shows two cross-interference terms

$$\psi\psi^* = \frac{1}{(E - \varepsilon)^2 + \left(\frac{\gamma}{2}\right)^2} (s_1 s_1^* + s_2 s_2^* + s_1 s_2^* + s_2 s_1^*), \quad (1.51)$$

which has never been observed experimentally, since the injection of two separate contacts, the electrons enter the conductor with uncorrelated phases, evolving in time in an arbitrary manner and on average gives zero contribution.

The first two pairwise works give positive contributions and are observed experimentally.

Contacts in electronic devices are usually not coherent, and this fact must be taken into account while modeling. The Schrodinger equation cannot simultaneously take into account multiple electrical contacts. To consider contacts need one by one to calculate properties that depend on works of the wave functions, such as electron density, the current, and the other, and then sum the contributions from different contacts.

### 1.4 Quantum transport through multi-level conductor

Generalize the single layer model (1.34) in a multi-level (Fig. 1.6) of the Hamiltonian matrix  $N \times N$  with  $N$  eigenvalues. The Schrodinger equation with two contacts,

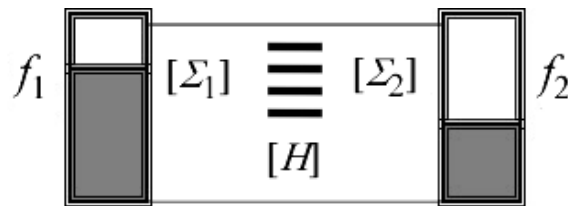


Figure 1.6 – Transport model for multi-level conductor

one injects, has the form

$$E\{\psi\} = [H + \Sigma_1 + \Sigma_2]\{\psi\} + \{s_1\}, \quad (1.52)$$

where the wave function and an injecting contact is columnar  $N \times 1$  matrix and the contact  $N \times N$  matrix  $\Sigma_1$  и  $\Sigma_2$  not eremit with antihermit components

$$\begin{aligned} \Gamma_1 &= i[\Sigma_1 - \Sigma_1^+], \\ \Gamma_2 &= i[\Sigma_2 - \Sigma_2^+], \end{aligned} \quad (1.53)$$

performing role  $\gamma_1$  and  $\gamma_2$  in a single-level task.

First we will show how the four basic equations of the method NEGF (1.6), (1.13), (1.14) and (1.16) follow from the Schrodinger equation with posted contacts (1.52).

From (1.52) are directly

$$\{\psi\} = [G^R] \{s_1\}, \quad (1.54)$$

where the retarded Green function  $G^R$  is given by the expression (1.6) with

$$\Sigma = \Sigma_1 + \Sigma_2. \quad (1.55)$$

Non-equilibrium Green's function

$$G^n = 2\pi \{\psi\} \{\psi\}^+ = 2\pi [G^R] \{s_1\} \{s_1\}^+ [G^A], \quad (1.56)$$

where the advanced Green's function  $G^A$  there is the ermitian conjugate of the retarded function (1.7).

For a single-level task  $2\pi s_l s_l^* = \gamma_l$  (1.39), and for multi-level - is the matrix

$$2\pi \{s_1\} \{s_1\}^+ = [\Gamma_1], \quad (1.57)$$

so

$$G^n = [G^R] [\Gamma_1] [G^A]. \quad (1.58)$$

This unequal Green's function for one of the injection source. For a number of sources of electron density matrix, despite the wave functions, all add up, weighted corresponding Fermi function to obtain (1.13) with the matrix  $\Sigma^{in}$ , which is a non-coherent sum of all the independent sources, so in our case, two sources.

$$[\Sigma^{in}] = [\Gamma_1] f_1(E) + [\Gamma_2] f_2(E). \quad (1.59)$$

Equation (1.13) to (1.59) gives a matrix of electron density  $G^n$  Fermi function through two contacts. If both the Fermi function equal to unity, then all states are occupied by electrons, so that electron density matrix becomes a matrix density of states, called in the method NEGF matrix spectral function  $[A]$ . Assuming in (1.13) and (1.59)  $f_1 = 1$  and  $f_2 = 1$ , spectral function

$$[A] = [G^R][\Gamma][G^A] \quad (1.60)$$

with  $\Gamma = \Gamma_1 + \Gamma_2$ .

We obtain two other expressions for the spectral function given in (1.14). From (1.54) with (1.52) and (1.55) we have

$$G^R = [EI - H - \Sigma]^{-1}, \quad (1.61)$$

so that the inverse matrix of the retarded Green's function, we have

$$[G^R]^{-1} = EI - H - \Sigma. \quad (1.62)$$

After completing the ermitian conjugate equation (1.62), we obtain

$$\left[ [G^R]^{-1} \right]^+ = \left[ [G^R]^+ \right]^{-1} = EI - H - \Sigma^+ \quad (1.63)$$

or else, considering (1.7),

$$[G^A]^{-1} = EI - H - \Sigma^+. \quad (1.64)$$

Subtracting (1.62) from (1.64) and bearing

$$\Gamma = i[\Sigma - \Sigma^+], \quad (1.65)$$

next from (1.53), we obtain

$$[G^R]^{-1} - [G^A]^{-1} = i[\Gamma]. \quad (1.66)$$

Multiplying (1.66) the left on  $[G^R]$ , and the right to  $[G^A]$ , obtain another expression for the spectral function  $A$  (1.14)

$$i[[G^R] - [G^A]] = G^R \Gamma G^A. \quad (1.67)$$

Multiplying (1.66) the left on  $[G^A]$ , and the right to  $[G^R]$ , obtain third expression for the spectral function  $A$  (1.14)

$$i[[G^R] - [G^A]] = G^A \Gamma G^R. \quad (1.68)$$

It remains to obtain the expression for the current. As in the case and considering the classical and quantum-tier model, we obtain the expression for the current change in time as the number of electrons. We start with temporary Schrodinger equation

$$i\hbar \frac{d}{dt} \{\psi\} = [H + \Sigma] \{\psi\} + \{s\} \quad (1.69)$$

and its ermitian conjugate

$$-i\hbar \frac{d}{dt} \{\psi\}^+ = \{\psi\}^+ [H + \Sigma^+] + \{s\}^+. \quad (1.70)$$

have

$$\begin{aligned} i\hbar \frac{d}{dt} \{\psi\} \{\psi\}^+ &= \left( i\hbar \frac{d}{dt} \{\psi\} \right) \{\psi\}^+ + \{\psi\} \left( i\hbar \frac{d}{dt} \{\psi\}^+ \right) = \\ &= ([H + \Sigma] \{\psi\} + \{s\}) \{\psi\}^+ - \{\psi\} \left( \{\psi\}^+ [H + \Sigma^+] + \{s\}^+ \right) = \\ &= [(H + \Sigma) \psi \psi^+ - \psi \psi^+ (H + \Sigma^+)] + [s s^+ G^A - G^R s s^+], \end{aligned} \quad (1.71)$$

which is already used by well-known relation (1.54) and its ermitian conjugate

$$\{\psi\} = [G^R] \{s\} \quad \text{и} \quad \{\psi\}^+ = \{s\}^+ [G^A]. \quad (1.72)$$

As trace of a matrix  $[\psi\psi^+]$  gives the number of electrons, the derivative of the matrix over time, we find the matrix of the current operator, which will trace current. Using (1.10) and (1.12), for the current operator of the matrix (1.71), we have

$$I^{op} = \frac{[HG^n - G^n H] + [\Sigma G^n - G^n \Sigma^+] + [\Sigma^{in} G^A - G^R \Sigma^{in}]}{i2\pi\hbar}. \quad (1.73)$$

Considering that trace of the product matrix is independent of the order of the factors for the rate of change of the number of electrons in the channel have

$$\frac{dN}{dt} = \frac{-i}{h} Tr \left( [\Sigma G^n - G^n \Sigma^+] + [\Sigma^{in} G^A - G^R \Sigma^{in}] \right), \quad (1.74)$$

and including further (1.14) and (1.15) we finally obtain

$$\frac{dN}{dt} = \frac{1}{h} Tr [\Sigma^{in} A - \Gamma G^n]. \quad (1.75)$$

Next you need to consider the following. In equation (1.73), both sides are equal to zero, because it is a current in the system (Fig. 1.6) in a state of dynamic equilibrium. Both parts of the equation (1.73) are broken down into terms related to terminals 1 and 2. The amount of zero in accordance with Kirchhoff's law for electric circuits in a state of dynamic equilibrium. Generalizing to an arbitrary number of contact  $m$ , we obtain the already mentioned equation (1.16) for the current

$$\tilde{I}_m = \frac{q}{h} Tr [\Sigma_m^{in} A - \Gamma_m G^n]. \quad (1.76)$$

Classical and quantum models are compared in Fig. 1.7, where the factor  $D$  in the classical model takes into account the multilevel classical task.

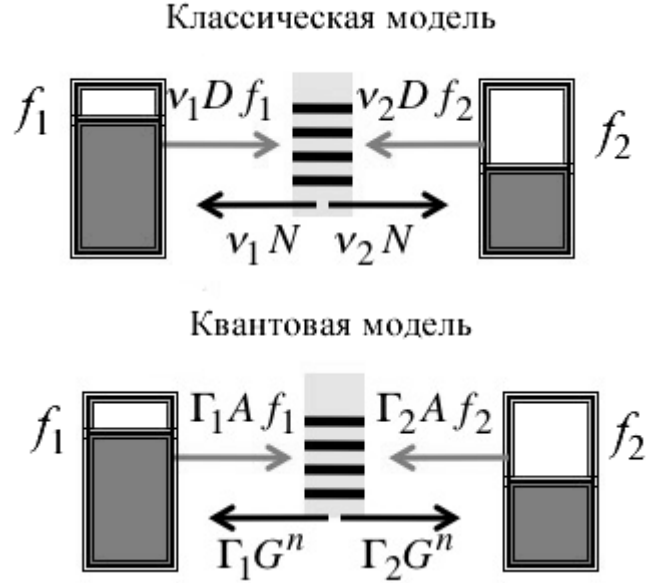


Figure 1.7 - Updating and empty conduction channel in the classical and quantum models of electron transport

**The function of the conduction for coherent transport.** Transform equation (1.76) as follows. We take into account (1.13) and (1.14), and

$$\Gamma = \sum_n \Gamma_n, \quad \Sigma^{in} = \sum_n \Sigma_n^{in}, \quad \Sigma_n^{in} = \Gamma_n f_n(E). \quad (1.77)$$

Then have

$$\tilde{I}_m = \frac{q}{h} \sum_n \bar{T}_{mn} (f_m(E) - f_n(E)), \quad (1.78)$$

where transmission coefficient between the contacts  $m$  and  $n$

$$\bar{T}_{mn} \equiv Tr[\Gamma_m G^R \Gamma_n G^A]. \quad (1.79)$$

using permutation matrix under the trace, easily proved useful feature of the transmission coefficient

$$\sum_n \bar{T}_{mn} = \sum_n \bar{T}_{nm} = Tr[\Gamma_m A]. \quad (1.80)$$

rewrite the expression for the current (1.78) using (1.79) for two-terminal device

$$\tilde{I}(E) = \frac{q}{h} \text{Tr} \left[ \Gamma_1 G^R \Gamma_2 G^A \right] (f_1(E) - f_2(E)) \quad (1.81)$$

and comparing it to the current expression to the same expression for the current in the elastic resistor (32) in [1], we obtain the quantum analogue of the conductivity

$$G(E) = \frac{q^2}{h} \text{Tr} \left[ \Gamma_1 G^R \Gamma_2 G^A \right] = \frac{q^2}{h} \bar{T}_{12}. \quad (1.82)$$

To interpret the experimental data obtained in multi-terminal devices Buttiker [22] proposed an elegant formula relating the current  $I_m$  on contact  $m$  electrochemical potentials on the remaining contacts

$$I_m = (1/q) \sum_n G_{m,n} (\mu_m - \mu_n), \quad (1.83)$$

where  $G_{m,n}$  has a conductivity determined transmission coefficient between the contacts  $m$  and  $n$ .

In the linear response use our normal decomposition of the difference of the Fermi functions in Taylor (21) in [1] for the corresponding electrochemical potential difference, then the equation (1.78) will actually Buttiker equation (1.83) with a conductivity

$$G_{m,n}(E) \equiv \frac{q^2}{h} \text{Tr} \left[ \Gamma_m G^R \Gamma_n G^A \right],$$

which still need to be averaged for the elastic resistor in the usual way

$$G_{m,n} = \int_{-\infty}^{+\infty} dE \left( -\frac{\partial f_0}{\partial E} \right) G_{m,n}(E).$$

Until now we have considered only physical contact  $[\Sigma_{1,2}]$  in quantum coherent transport model in which the electrons move coherently from the source to the drain through the channel described by static Hamiltonian  $[H]$  in

the absence of electron interaction with the environment  $[\Sigma_0]$  during its movement through the channel (Fig. 1.2a). Allowance for the interaction  $[\Sigma_0]$  from a formal point of view the problem is not. All equations method NEGF remain the same, in the same matrices  $\Sigma$ ,  $\Gamma$  and  $\Sigma^{in}$  will only additional members

$$\begin{aligned}\Sigma &= \Sigma_1 + \Sigma_2 + \Sigma_0, \\ \Gamma &= \Gamma_1 + \Gamma_2 + \Gamma_0, \\ [\Sigma^{in}] &= [\Gamma_1] f_1(E) + [\Gamma_2] f_2(E) + [\Sigma_0^{in}].\end{aligned}\tag{1.84}$$

However, what is of himself physically reacting  $\Sigma_0$ ? From the point of view of an electron moving in a solid, Wednesday is not a static electron described static Hamiltonian  $[H]$ , but a very turbulent environment with a randomly varying potential  $U_R$ , which fluctuates in the picosecond time scale. Even at low temperatures frozen phonon modes electron moves in the fluctuating potential produced by all other electrons (the self-consistent field approximation). Even in this case, there are phase fluctuations (dephasing), leading to fluctuations in current. Typical current measurements give us the average value in the range of several nanoseconds, microseconds or even milliseconds. The effect of averaging should be adequately model if we are to correctly interpret the experimental data.

Method NEGF was originally developed to account for inelastic quantum transport processes in thick samples. We spoke of it in relation to the elastic resistors. The issues of skew and a generalization NEGF on inelastic transport processes would require a separate publication. Now we consider the model problem of quantum transport, which is not only pedagogical, but also of scientific interest. We begin with the quantum transport in 1D conductors not only in the regime of ballistic transport, but also taking into account scattering centers. Reasonable to neglect the effects of interference on the defects and assume that the electrons diffuse as classical particles? This question was put by Anderson in 1958 [23] and concluded that diffusion can be substantially suppressed or even it can be completely neglected as a result of quantum interference between scattering centers. We do not intend to delve into the theory andersonsc localization [24], we will only show how even a simplified model NEGF provide insight into the physics of quantum transport. For any

transportation problem you need to write the Hamiltonian [ $H$ ] and the self-energy matrix [ $\Sigma$ ]. Once this is done, further calculations by the method of NEGF made routine.

### 1.5 Modeling 1D conductor

For our purposes it is enough one-dimensional model unbounded homogeneous conductor in the strong-coupling approximation taking into account only interaction of neighboring atoms (Fig. 1.8) in the orthogonal basis. This approximation is known in quantum chemistry since 1931 as a method of molecular orbitals of Hückel [25]. Even this simple model describes correctly not all, but many of the properties of polyene long  $-(CH=CH-)_nCH=$  [26 – 28], graphene [29, 30], polyacetylenes and cumulenes  $=(C=)_nC=$  [31 – 33], in the past, though, each atom supplies two mutually orthogonal  $\pi$ -electrons, which requires only a small modification of the model.

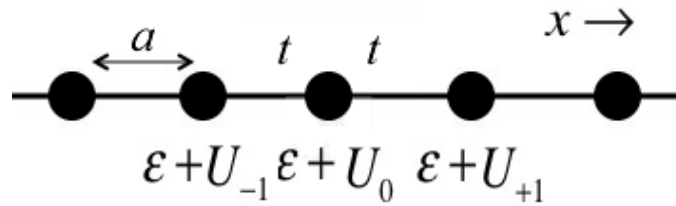


Figure 1.8 – To take account of changing along the conduction channel potential  $U(x)$  in the translationally invariant chain of atoms with a period of  $a$ , each supplying one electron, and characterized by the Hückel two parameters - the Coulomb integral  $\epsilon$  and resonance integral  $t$

Uniform 1D conductor described by the standard theory of one-dimensional model crystal Kronig - Penny and obeys a parabolic dispersion relation with the effective mass

$$E = E_c + \frac{\hbar^2 k^2}{2m} . \quad (1.85)$$

We need to rewrite the dispersion relation (1.85) for we use the approximation of strong coupling with the interaction of a neighboring atoms

(Fig. 1.8) in an orthogonal basis. In other words, how to select the parameters, and  $\varepsilon$   $t$ , to approximate dispersion relation (1.85).

From the Schrodinger equation

$$E\psi_n = \sum_m H_{nm}\psi_m \quad (1.86)$$

have

$$E = \sum_m H_{nm} \frac{\psi_m}{\psi_n}. \quad (1.87)$$

Solutions of the Schrodinger equation (1.86) is a flat wave (Bloch theorem)

$$\psi_n = \exp(ik na), \quad (1.88)$$

so that (1.87) implies

$$E(k) = \sum_m H_{nm} \exp(ik(m-n)a). \quad (1.89)$$

The matrix  $[H]$  is as follows: on the main diagonal Coulomb integrals  $\varepsilon$ , on the adjacent upper and lower diagonals are resonance integrals  $t$ , the other elements are equal to zero,

$$H = \begin{bmatrix} \ddots & & \dots & & \ddots \\ & \varepsilon & t & 0 & \\ \vdots & t & \varepsilon & t & \vdots \\ & 0 & t & \varepsilon & \\ \ddots & & \dots & & \ddots \end{bmatrix},$$

So for any row  $n$  of the matrix  $[N]$  according to the Schrödinger equation (1.86) we have

$$E\psi_n = t\psi_{n-1} + \varepsilon\psi_n + t\psi_{n+1} \quad (1.90)$$

else

$$E = t \frac{\psi_{n-1}}{\psi_n} + \varepsilon + t \frac{\psi_{n+1}}{\psi_n}, \quad (1.91)$$

and taking into account (1.88) and regrouping

$$E(k) = \varepsilon + t \exp(+ika) + t \exp(-ika) = \varepsilon + 2t \cos ka. \quad (1.92)$$

At low  $k$

$$\cos ka \approx 1 - \frac{(ka)^2}{2}. \quad (1.93)$$

Comparing the dispersion relation (1.92) for a homogeneous chains in the Hückel approximation at small  $k$  with the correct dispersion parabolic approximation (1.85), we find the resonance and Coulomb integrals

$$E_c = \varepsilon + 2t, \quad (1.94)$$

$$-t \equiv t_0 \equiv \frac{\hbar^2}{2ma^2}. \quad (1.95)$$

If the simulation of the electronic device is required to take into account changing the conductivity along the channel potential  $U(x)$ , this is done by adding local value to the Coulomb potential  $U$  integral (Fig. 1.8).

Now, of course, the translational invariance is violated, the dispersion relation will be different, but the new Hamiltonian is quite suitable for numerical calculations and satisfactorily describes the physics of transport for a potential  $U(x)$ , not too fast in changing the scale of interatomic distances.

With the obtained values of integrals  $\varepsilon$  (1.94) and  $t$  (1.95) is easily written out of the Hamiltonian matrix  $[H]$ . Now let's discuss the matrix contact their own energies. The basic idea is that an infinitely long conductors, described by the Hamiltonian  $[H]$ , replaced by a conductor of finite length, described by the matrix  $[H + \Sigma_1 + \Sigma_2]$ , with open boundary conditions at the ends, meaning by this "good" contacts, not creating at the ends of the reflected fluxes (Fig. 1.9).

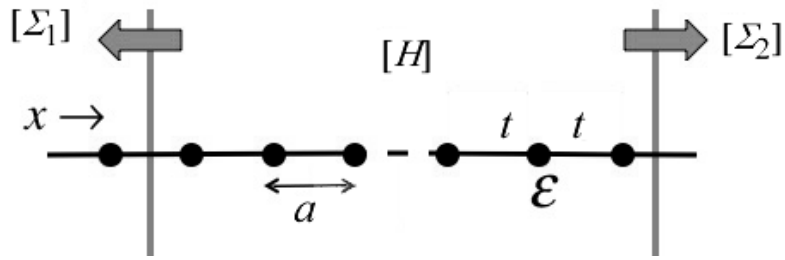


Figure 1.9 – Open boundary conditions correspond to "good" contacts, do not create at the ends of the reflected streams

Let us illustrate this idea into a one-dimensional lattice. Let conductor of limited length is  $n$  atoms, numbered from 1 to  $n$ . Then the left track 1 begins to atom chain with the number 1, and the right track 2 - after the atom chain number  $n$  (Fig. 1.10). Contacts do not have the incoming streams only care.

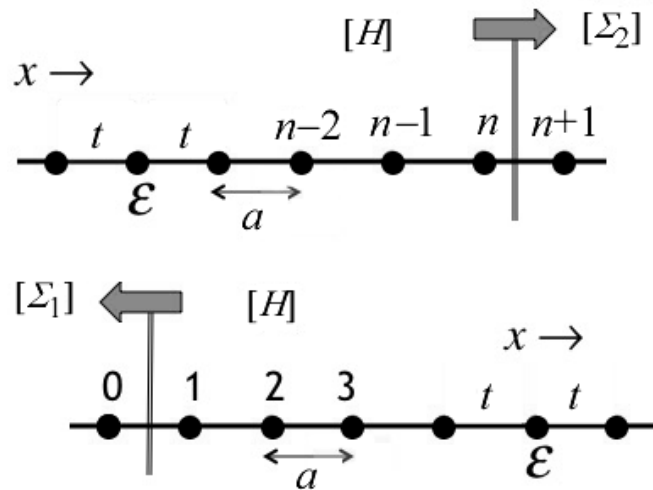


Figure 1.10 – For the compilation of the contact matrices 1D conductor of  $n$  atoms

In the  $n$ -th row (1.90) of the Schrodinger equation (1.86) the term  $t\psi_{n+1}$  already own terminal 2, which, according to equation (1.91), contributes to the energy equal to  $t\psi_{n+1} / \psi_n$ . This energy is the energy of the private contact 2. subject to

$$\psi_{n+1} = \psi_n e^{ika} \quad (1.96)$$

instead of (1.90) we have

$$E\psi_n = t\psi_{n-1} + (\varepsilon + te^{ika})\psi_n, \quad (1.97)$$

wherein the additive Coulomb integral to the  $n$ -th row (1.97) is a self-energy contacts 2 and placed it as an element of  $(n, n)$  corresponding to the contact matrix

$$\Sigma_2 = \begin{bmatrix} \ddots & & \dots & & \\ & 0 & 0 & 0 & \\ \dots & 0 & 0 & 0 & \\ & 0 & 0 & te^{ika} & \end{bmatrix}. \quad (1.98)$$

The same self-energy has a pin 1, and the corresponding contact matrix placed it as an element  $(1, 1)$

$$\Sigma_1 = \begin{bmatrix} te^{ika} & 0 & 0 & \dots \\ 0 & 0 & 0 & \\ 0 & 0 & 0 & \\ \dots & & & \ddots \end{bmatrix}. \quad (1.99)$$

The remaining elements of the matrix  $\Sigma_1$  и  $\Sigma_2$  zero.

**Ballistic 1D conductor.** The energy matrix  $H$ ,  $\Sigma_1$  и  $\Sigma_2$  drawn, calculate the retarded Green's function  $G^R$  (1.6), anticipatory function  $G^A$  (1.7), matrix  $\Gamma_1$  and  $\Gamma_2$  (1.53) and, lastly, the completion rate of  $T_{12}$  and conductivity  $G(E)$  (1.82). The calculation of the conductivity of 1D ballistic conductor is good check that the contact matrix defined properly. Conductivity should be equal to the quantum of conductance  $q^2/h$ , multiplied by the number of modes  $M(E)$  1D conductor equal to one (back not included). According to (1.82) this means that in the considered example, the transmission coefficient should be equal to unity in the energies  $0 < E - E_c < 4t_0$ ,

Covered by the dispersion relation

$$E = \varepsilon + 2t \cos ka = E_c + 2t_0(1 - \cos ka), \quad (1.100)$$

and zero outside this region (Fig. 1.11,  $U = 0$ ).

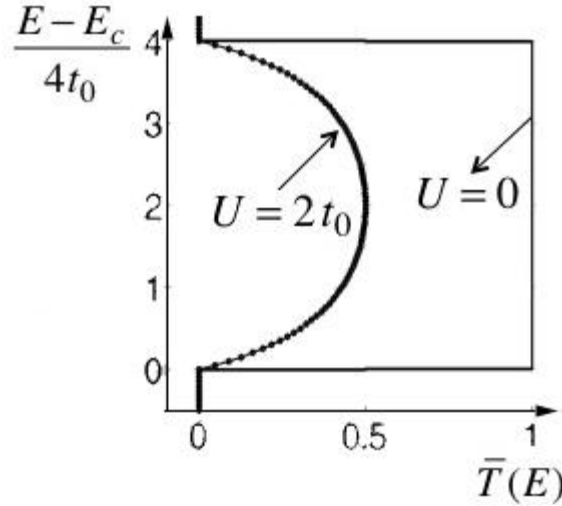


Figure 1.11 – Transmission coefficient in 1D ballistic conductor without scattering ( $U = 0$ ) and with one point scattering center ( $U = 2t_0$ )

**The density of States of 1D conductor.** First calculate the  $D(E)$  1D conductor from elementary considerations. According to (1.82) [1], the number of states of 1D conductor of length  $L$  with the values of the pulse smaller than the predetermined value  $p$ ,

$$N(p) = \frac{2L}{h/p}. \quad (1.101)$$

the density of states

$$D(E) = \frac{dN}{dE} = \frac{2L}{h} \frac{dp}{dE} = \frac{L}{\pi \hbar v}, \quad (1.102)$$

which takes into account the fact that for an isotropic dispersion law  $E(p)$  speed  $v = dE/dp$  [1, (1.80)].

We obtain the same expression for the density of states by NEGF. For isotropic 1D conductor is sufficient to consider only one atom in the chain (Fig. 1.12). In this case, the role of conductor length  $L$  plays the lattice constant  $a$ . For delayed

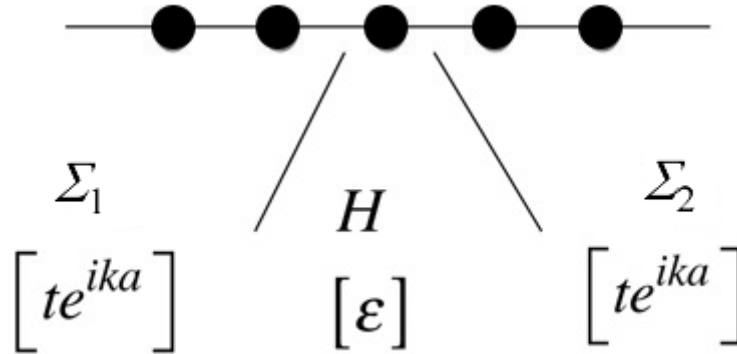


Figure 1.12 – For the calculation of the density of states  $D(E)=A/2\pi$  of the spectral function  $A$  (1.14)

Green's functions have

$$G^R = [E - \varepsilon - 2te^{ika}]^{-1}. \quad (1.103)$$

Introducing exponential through the sine and cosine, and using (1.100), we obtain

$$G^R = i / 2t \sin ka. \quad (1.104)$$

have

$$\hbar v = \frac{dE}{dk} = -2at \sin ka, \quad (1.105)$$

where the first equality follows from the isotropic 1D conductor, and the second - from (100). With regard to (105) to  $G^R$  finally have

$$G_R = \frac{i}{2t \sin ka} = \frac{-i}{\hbar v / a}, \quad (1.106)$$

and advanced Green functions

$$G^A = \frac{ia}{\hbar v}. \quad (1.107)$$

the spectral function

$$A = i[G^R - G^A] = \frac{2a}{\hbar v}, \quad (1.108)$$

and the density of states

$$D(E) = \frac{A}{2\pi} = \frac{a}{\pi \hbar v} \quad (1.109)$$

coincides with (1.102), the previously obtained from elementary considerations.

**1D conductor with a scattering center.** In the Hamiltonian model the scattering center by adding to the Coulomb integral of a continuous chain of atoms building U

$$H = \begin{bmatrix} \ddots & & & & \\ & \varepsilon & t & 0 & \\ \vdots & t & \varepsilon + U & t & \\ & 0 & t & \varepsilon & \\ & & \dots & & \ddots \end{bmatrix}. \quad (1.110)$$

In this formulation of the problem transmittance can be calculated analytically (Fig. 1.13). Contact 1x1 matrix defined by him figured  $\Gamma_1$  and  $\Gamma_2$  by

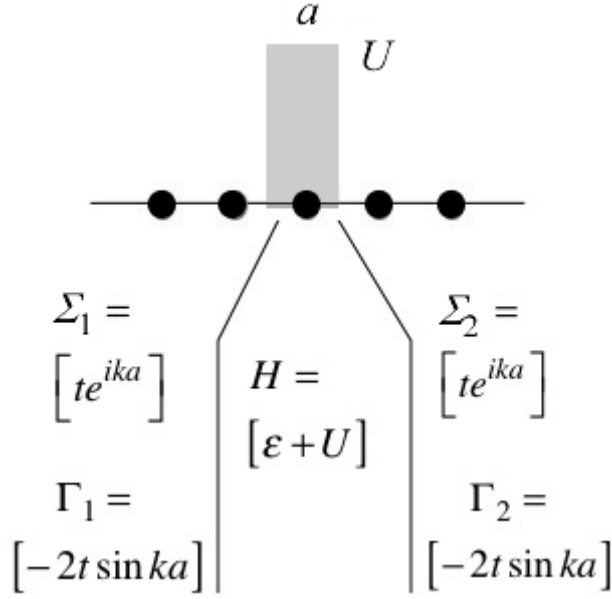


Figure 1.13 – Calculation of the transmission coefficient in the 1D conductor with a scattering center by NEGF

(1.53), Green's function with (1.100)

$$G^R(E) = \frac{1}{E - (\varepsilon + U) - 2te^{ika}} = \frac{1}{-U - i2t \sin ka}, \quad (1.111)$$

from her complex conjugation take anticipatory function  $G^A$  and immediately obtain the transmittance

$$\Gamma_1 G^R \Gamma_2 G^A = \frac{(2t \sin ka)^2}{U^2 + (2t \sin ka)^2} \quad (1.112)$$

or taking into account the (1.105) final

$$\bar{T}(E) = \frac{(2t \sin ka)^2}{U^2 + (2t \sin ka)^2} = \frac{(\hbar v / a)^2}{U^2 + (\hbar v / a)^2}. \quad (1.113)$$

The calculation results in the absence of scattering center ( $U = 0$ ), and taking it into account  $U = 2t_0$  shown in Fig. 1.11.

The expression for the transmission coefficient (1.113) withdraw as useful from elementary considerations (Fig. 1.14).

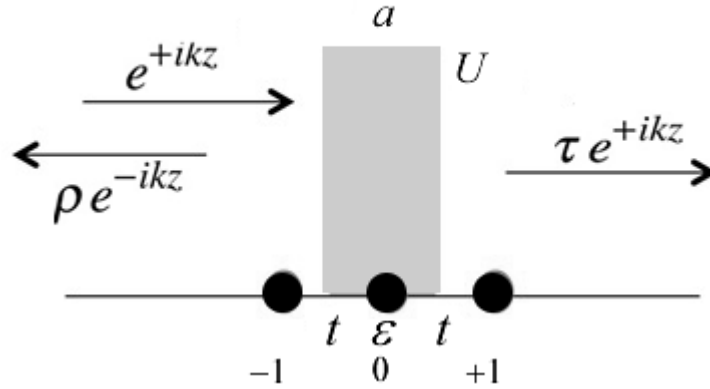


Figure 1.14 – For the calculation of transmission coefficient from the condition of continuity of the wave function

For convenience, renumber atoms of the conductor so that the defect was in the atom number 0. Incident on the wave scattering center  $\exp(+ikz)$  reflected  $\rho \cdot \exp(-ikz)$  reflection coefficient  $\rho$  and extends further  $\tau \cdot \exp(+ikz)$  with transmission coefficient  $\tau$ . From the Schrödinger equation in the Hückel approximation we have

$$E\psi_0 = (\varepsilon + U) \psi_0 + t\psi_{-1} + t\psi_{+1}. \quad (1.114)$$

From the law of conservation and continuity conditions for the wave function of the defect ( $z = 0$ ), we have

$$1 + \rho = \tau = \psi_0. \quad (1.115)$$

Substituting into (1.114) of wave functions at neighboring defective atoms and with (1.115) gives

$$(E - \varepsilon - U)\tau = t(e^{-ika} + (\tau - 1)e^{ika}) + t\tau e^{ika}, \quad (1.116)$$

after simple transformations and rearrangements taking into account the (1.100) and (1.105) for the transmission coefficient  $\tau$  get

$$\tau = \frac{i\hbar v / a}{-U + i\hbar v / a}, \quad (1.117)$$

after multiplication by its complex conjugate obtain previously been derived by NEGF expression for the transmission coefficient (1.113).

## 1.6 Modeling 2D conductor

Among the fundamental experiments 80s that led to the birth of mesophysics were monitoring the conductivity of 2D ballistic conductors, which turned integrally proportional to the quantum of conductance  $2q^2/h$ . To understand the physics and the interpretation of such experiments is necessary as much as possible simple model 2D conductor.

For our purposes, similar to 1D conductors, rather two-dimensional model of unlimited uniform conductors in the strong coupling approximation taking into account the only the interaction of neighboring atoms (Fig. 1.15) in an orthogonal basis, the so-called Hückel model. The model parameters  $\varepsilon$  and  $t$  is chosen so,

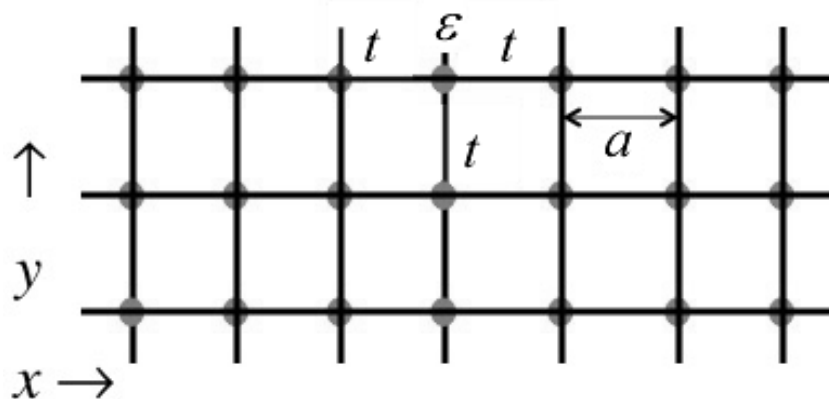


Figure 1.15 – Translationally invariant lattice of atoms with a period of  $a$ , each supplying one electron, and the Hückel characterized by two parameters - the Coulomb integral  $\varepsilon$  and resonance integral  $t$

to satisfy a standard dispersion relation with the effective mass

$$E(k_x, k_y) = E_C + \frac{\hbar^2 (k_x^2 + k_y^2)}{2m}. \quad (1.118)$$

The solution of the Schrodinger equation (1.86) is chosen in the form

$$\psi_n = \exp(i\vec{k} \cdot \vec{r}_n), \quad (1.119)$$

where the wave vector is determined by its projections  $k_x$  and  $k_y$  in the selected coordinate system, and position vector indicating the position of the  $n$  atom in the lattice. Substituting this solution into the equation (1.87), we obtain the dispersion relation

$$E(\vec{k}) = \sum_m H_{nm} \exp(i\vec{k} \cdot (\vec{r}_m - \vec{r}_n)), \quad (1.120)$$

Hückel is for lattice model provides

$$\begin{aligned} E(\vec{k}) &= \varepsilon + t \exp(+ik_x a) + t \exp(-ik_x a) + t \exp(+ik_y a) + t \exp(-ik_y a) = \\ &= \varepsilon + 2t \cos(k_x a) + 2t \cos(k_y a). \end{aligned} \quad (1.121)$$

Using the same reasons as for the one-dimensional chain, for resonance and Coulomb integrals as we get the model parameters

$$t = -\hbar^2 / 2ma^2, \quad (1.122)$$

$$\varepsilon = E_c - 4t \quad (1.123)$$

or a little differently

$$E_c = \varepsilon + 4t, \quad (1.124)$$

$$-t \equiv t_0 \equiv \frac{\hbar^2}{2ma^2}. \quad (1.125)$$

Drawing Hückel Hamiltonian  $H$  (Fig. 1.16) is not difficult, but it is necessary to discuss the construction of the contact matrices for 2D conductor. However,

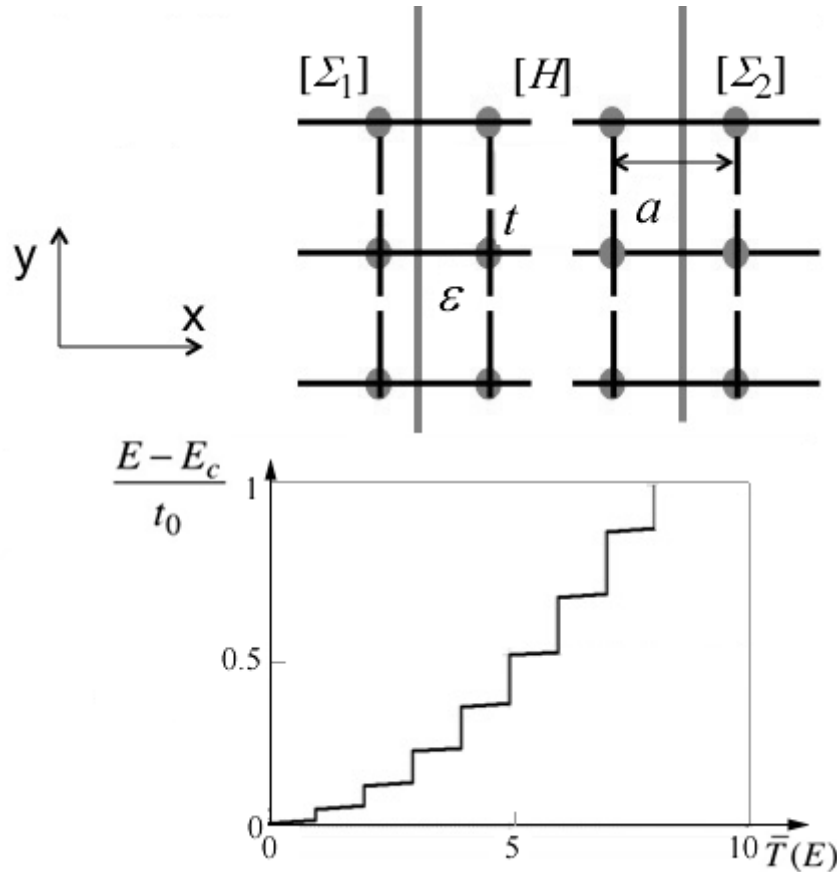


Figure 1.16 – The isolation of the two-dimensional lattice of the conductor and the field itself contacts for NEGF method and the results of calculating the transmission coefficient method NEGF when the number of atoms across the width of the conductor, equal to 25

first try to understand the causes of steps, depending on the energy transmission coefficient. A simple explanation of the experimentally observed fact may be as follows [1, formula (1.105)]. For ballistic conductor transmission coefficient is simply the number of modes  $M(E)$  equal to half the number of de-Broglie wavelengths fit into the cross-section  $W$ ,



matrix  $\alpha$  of order  $p$ . For example, when  $p = 3$  it has the form

$$\alpha = \begin{bmatrix} \varepsilon & t & 0 \\ t & \varepsilon & t \\ 0 & t & \varepsilon \end{bmatrix}. \quad (1.127)$$

The columns are connected to each other resonance integrals  $t$  follows. Consider the relationship between the columns adjacent to the numbers  $n$  and  $n+1$ . This relationship is described by a scalar matrix  $\beta = t \cdot I$  of order  $p$ , where  $I$  – the identity matrix. In our model of course,  $\beta = \beta^+$ . For example, when  $p = 3$

$$\beta = \begin{bmatrix} t & 0 & 0 \\ 0 & t & 0 \\ 0 & 0 & t \end{bmatrix}. \quad (1.128)$$

The Hamiltonian  $H$  has a block structure. On its main diagonal identical matrix  $\alpha$  of order  $p$ , and next to it diagonally from above and below are filled with matrices  $\beta$  also order  $p$ , the other elements are zero. If the length of the conductor is, for example,  $q = 10$  atoms, and the width of the conductor is  $p = 5$  atoms, the order of the matrix  $H$  is equal to  $p \times q = 50$ .

Solution of the problem on the eigenvalues of the Hamiltonian  $H$  is reduced to the diagonalization of the matrix  $[\alpha]$

$$[\tilde{\alpha}] = [V]^+ [\alpha] [V], \quad (1.129)$$

where the columns of the matrix  $[V]$  есть is the eigenvector matrix  $[\alpha]$ , so that

$$\tilde{\alpha} = \begin{bmatrix} \varepsilon_1 & 0 & 0 \\ 0 & \varepsilon_2 & 0 \\ 0 & 0 & \varepsilon_3 \end{bmatrix}. \quad (1.130)$$

It is always possible inverse of their own, or modal basis in the original lattice basis

$$[\alpha] = [V][\tilde{\alpha}][V]^\dagger. \quad (1.131)$$

Matrix  $\beta$  is not affected by the transformation of the base, since it is already diagonal. Diagonalization of the matrix  $\alpha$  form ( $p \times p$ ) leads to the vanishing of the resonance integrals  $t$ , connecting lines of the original matrix of the Hamiltonian, ie, to conversion a 2D conductor in  $p$  of parallel-connected contacts 1D conductors, each of length  $q$  atoms (Fig. 1.18) with energy  $\varepsilon_1, \varepsilon_2, \varepsilon_3, \dots, \varepsilon_p$ , equal to the eigenvalues of the matrix  $\alpha$

$$\varepsilon_n = \varepsilon - 2t_0 \cos k_n a \quad (1.132)$$

with

$$k_n a = \frac{n\pi}{p+1}. \quad (1.133)$$

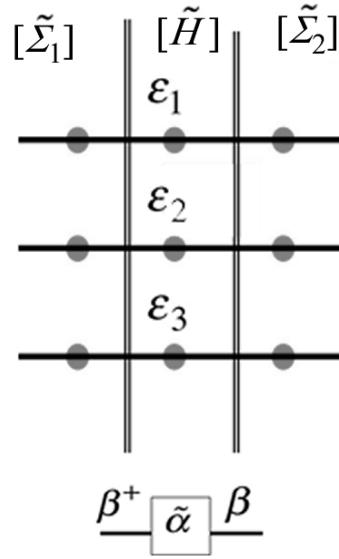


Figure 1.18 – 2D guide to the Hückel after diagonalization of the Hamiltonian  $H$

For each of  $p$  parallel 1D conductors transmittance is equal to unity in the energy ( $t_0 \equiv |t|$ )

$$\varepsilon_n - 2t_0 < E < \varepsilon_n + 2t_0,$$

as shown in Fig. 1.19. Folding transmission coefficients for all  $p$  mod conductor obtain the transmission coefficient dependence on energy in the form of rising steps at the bottom of the graph (Fig. 1.16) and descending stairs to the upper part of the graph.

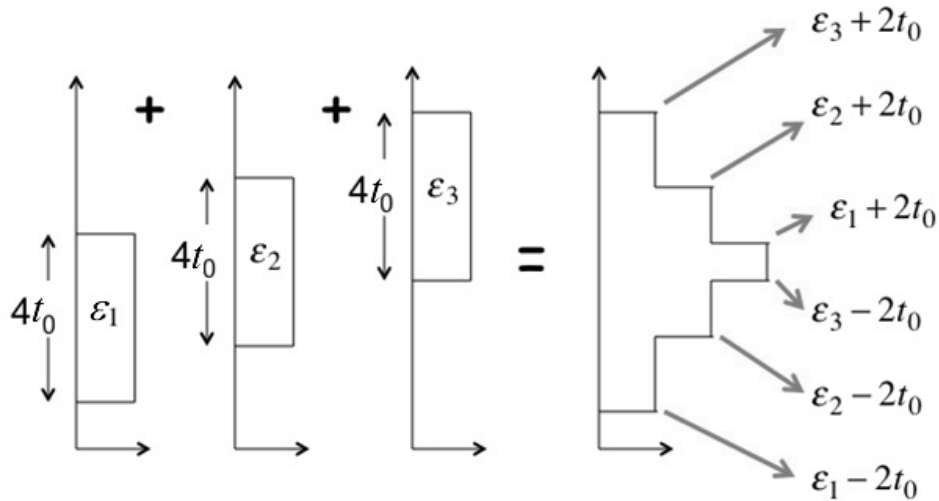


Figure 1.19 – To the formation of steps (Fig. 1.16) depending on the energy transmission coefficient

In the simulation, the n-type conductors are usually calculated the lower part of the zone (Fig. 1.16), and we see only going up the stairs with energies  $\epsilon_n - 2t_0$ .

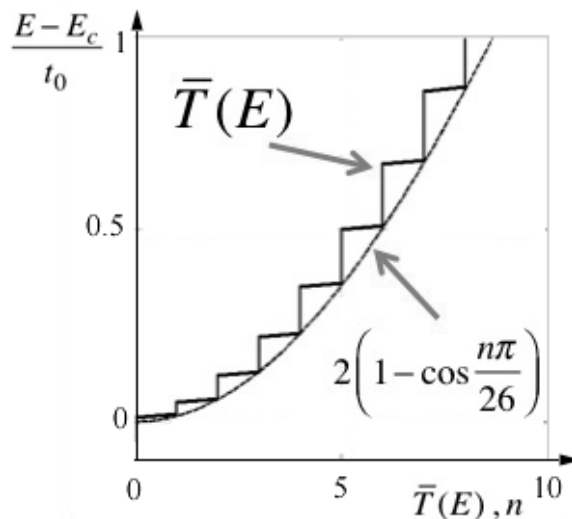


Figure 1.20 – Comparison of the numerical results of calculation of transmission coefficient method NEGF with the analytical approximation of (1.134) with  $p = 25$

Using (1.132) (1.133) and (1.124), we find the position of the steps

$$\varepsilon_n - 2t_0 = E_c + 2t_0 \left( 1 - \cos \frac{n\pi}{p+1} \right). \quad (1.134)$$

Fig. 1.20 the calculation results of the transmission coefficient at NEGF method including atoms conductor width  $p = 25$  (Fig. 1.16) are shown together with the envelope of steps calculated from (134) at the same conductor width  $p = 25$ .

Presentation of 2D / 3D conductor in parallel 1D conductors seems to us not only physically correct but also very useful approach when interpreting experimental data. Each of these 1D conductors called fashion or subzone with the dispersion relation

$$E_n(k_x) = \varepsilon_n - 2t_0 \cos k_x a, \quad (1.135)$$

as shown in Fig. 1.21.

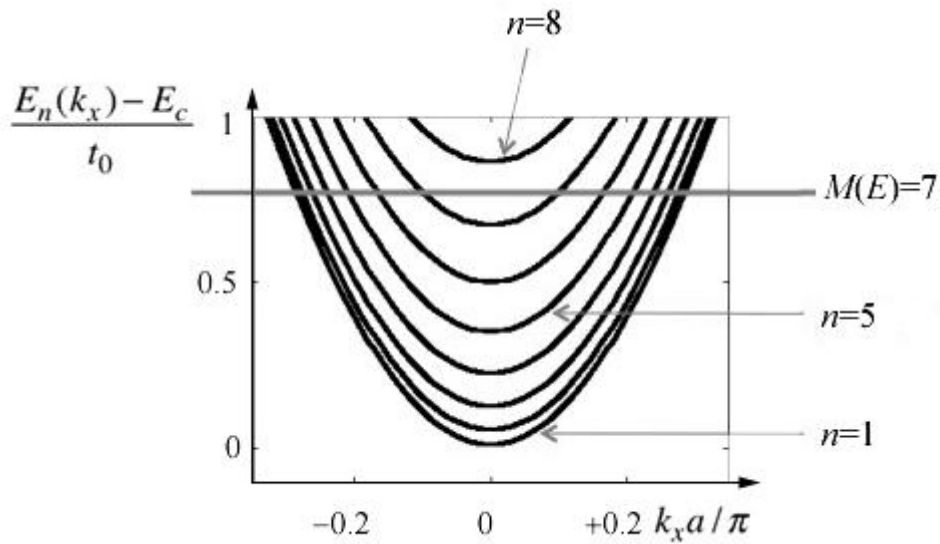


Figure 1.21 – The lower eight subzones Hückel model 2D conductor

Dispersion relations for subzones are obtained from the general expression (1.121) with the requirement that  $k_y$  took quantized values

$$k_y a = \frac{n\pi}{p+1}, \quad (1.136)$$

where each value of  $n$  gives rise to a corresponding sub-band (Fig. 1.21).

The horizontal line drawn at a certain energy  $E$ , the number of crosses subzones equal to twice the value of the events at this energy, because each mode generates two intersections, one for states with positive velocity, and the other - with a negative.

### 1.7 Contact its own energy for 2D conductor

Ideally, the contacts must be such that the electrons are free to leave the vehicle and did not return as a result of reflection from the boundary contacts. We consider the simplest model of such contacts, which boils down to the fact that the contact is a natural extension of the conductor.

2D conductor width  $p$  is equivalent to  $p$  parallel 1D conductors as a result of conversion basis

$$[\tilde{X}] = [V]^+ [X] [V], \quad (1.137)$$

where the matrix  $X$  in the lattice basis is transformed into a matrix  $X$  WITH a TILDE in the modal basis or vice versa

$$[X] = [V][\tilde{X}][V]^+, \quad (1.138)$$

as demonstrated above for the Hamiltonian  $H$ . As a result, for each of the  $p$  independent 1D conductors easily discharged its contact array, and then they all gather in the full matrix  $\Sigma$ .

The Hückel model 2D conductor each  $p$  1D conductors characterized own energy contact  $t \cdot \exp(ika)$  with the corresponding value  $ka$  for a particular 1D conductor at a given energy  $E$ . For a number mode  $n$

$$E = \varepsilon_n - 2t_0 \cos k_n a, \quad (1.139)$$

so that the contact matrix in the modal basis

$$[\tilde{\Sigma}_1] = \begin{bmatrix} te^{ik_1a} & 0 & 0 & \dots \\ 0 & te^{ik_2a} & 0 & \\ 0 & 0 & te^{ik_3a} & \\ \dots & & & \ddots \end{bmatrix}, \quad (1.140)$$

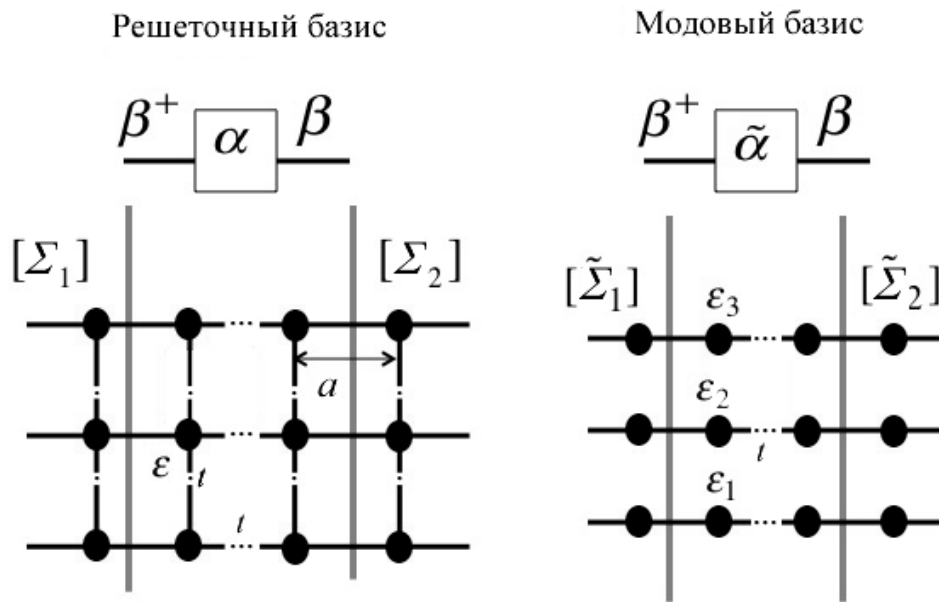


Figure 1.22 – Construction of the contact matrices in modal basis with the opposite conversion to the lattice basis

and after conversion into lattice basis (Fig. 1.22)

$$[\Sigma_1] = [V][\tilde{\Sigma}_1][V]^+. \quad (1.141)$$

The above method of constructing a contact matrix for uniform gratings, but is not suitable in the general case, since not always manage the same basis transform matrix and diagonalized simultaneously matrix  $\alpha$  and matrix  $\beta$ . And in the case we are considering all the scalar matrix  $\beta$  ie it has diagonalized. An example of this kind can serve as a lattice of graphene.

**Graphene.** In the discussion of homogeneous lattice (Fig. 1.15), each atom is in the same environment. The regular hexagonal graphene lattice (Fig. 1.23) there are two kinds of atoms. Atoms grades A and B are in different environments. Atom type A left one atom and two on the right, and the atom in the opposite sort. Translational invariance of the graphene lattice provide two atoms forming the unit cell of a regular diamond.

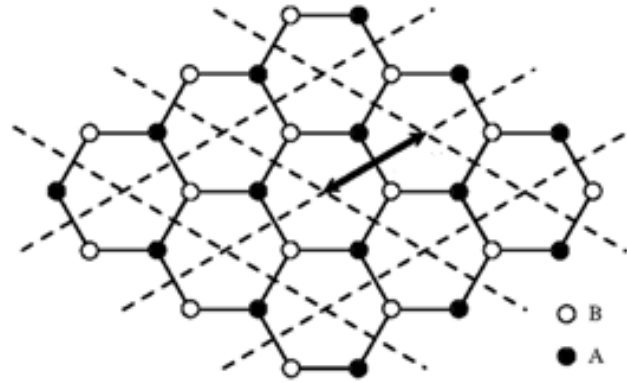


Figure 1.23 – The unit cell of the graphene and the translation vector Bravais lattices A and B

Given the presence of two non-equivalent atoms in the unit cell, the Schrodinger equation (1.86) in the form

$$E\{\psi\}_n = \sum_m [H]_{nm} \{\psi\}_m, \quad (1.142)$$

where  $\{\psi\}_n$  is a column vector form (2 x 1), the components which correspond to the two atoms of type A and B, forming a unit cell with number  $n$ . The Hamiltonian of the form (2 x 2) establishes a link between the atoms of type A and B cell number  $n$ , and the atoms of type A and B cell number  $m$ .

The solution can be written as

$$\{\psi\}_n = \{\psi\}_0 \exp(i\vec{k} \cdot \vec{r}_n), \quad (1.143)$$

after substituting into (1.142), we have

$$E\{\psi\}_0 = [h(\vec{k})]\{\psi\}_0, \quad (1.144)$$

where the Hamiltonian taking into account the phase factor

$$[h(\vec{k})] = \sum_m [H]_{nm} \exp(i\vec{k} \cdot (\vec{r}_m - \vec{r}_n)) \quad (1.145)$$

also it has the shape of (2 x 2). We calculate it using the notch of the columns containing the cell surrounded by its four nearest cells (Fig. 1.24).

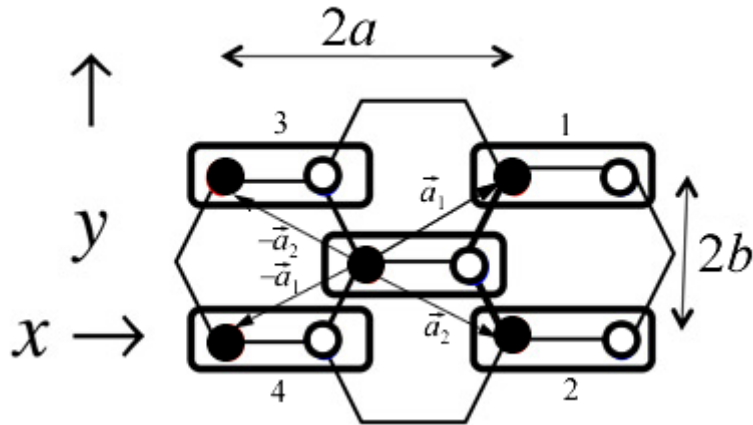


Figure 1.24 – The unit cell of the graphene with the number 0 is surrounded by four nearest cells with numbers 1, 2, 3, 4

It would also be two vectors

$$\begin{aligned} \vec{a}_1 &= a\hat{x} + b\hat{y} \\ \vec{a}_2 &= a\hat{x} - b\hat{y} \end{aligned} \quad (1.146)$$

associated with the geometric parameters of the graphene network

$$a = 3a_0 \text{ and } b = \sqrt{3}a_0 / 2, \quad (1.147)$$

where  $a_0$  – CC bond length in graphene is usually taken as  $1.42 \text{ \AA}$ .

Deposits in the Hamiltonian (1.145) of five cells taking into account the vectors (1.146) (Fig. 1.24)

$$\begin{aligned}
& e^{-i\vec{k}\cdot\vec{a}_2} \begin{bmatrix} 0 & t \\ 0 & 0 \end{bmatrix} & & \begin{bmatrix} 0 & 0 \\ t & 0 \end{bmatrix} e^{+i\vec{k}\cdot\vec{a}_1} \\
& & + & & + \\
& & & \begin{bmatrix} \varepsilon & t \\ t & \varepsilon \end{bmatrix} & \\
& & + & & + \\
& e^{-i\vec{k}\cdot\vec{a}_1} \begin{bmatrix} 0 & t \\ 0 & 0 \end{bmatrix} & & \begin{bmatrix} 0 & 0 \\ t & 0 \end{bmatrix} e^{+i\vec{k}\cdot\vec{a}_2}
\end{aligned} \tag{1.148}$$

to be summed together with the corresponding phase factor. At the center of the cell phase factor is absent, as it contributed to the diagonal Hamiltonian ( $n=m=0$ ). The interaction of cells with  $n = 0$  and  $m = 1$  in the Hückel model is reduced to only one resonance integral  $t$  between the atoms in the center of the cell and atom A cell  $m = 1$ . Similarly, for the interaction of the central cell to the cell  $m = 2$ . They differ only phase factors: shift the first cell relative to the central vector is determined  $\vec{a}_1$ , and the second cell - vector  $\vec{a}_2$  (Fig. 1.24). Similarly receives input from cells 3 and 4.

Summation five matrices (1.148) gives the Hamiltonian (1.145)

$$\left[ h(\vec{k}) \right] = \begin{bmatrix} \varepsilon & h_0^* \\ h_0 & \varepsilon \end{bmatrix}, \tag{1.149}$$

Where

$$h_0 \equiv t + te^{+i\vec{k}\cdot\vec{a}_1} + te^{+i\vec{k}\cdot\vec{a}_2} \tag{1.150}$$

or taking into account the (1.146)

$$h_0 \equiv t \left( 1 + 2 \cos(k_y b) \exp(+ik_x a) \right). \tag{1.151}$$

Diagonalization (1.144) with (1.149) gives the dispersion relation

$$E(\vec{k}) = \varepsilon \pm |h_0(\vec{k})|, \quad (1.152)$$

which lead to the usual sight for grapheme

$$E = \pm v_0 p, \quad (1.153)$$

where  $v_0$  – Fermi velocity is about 1/300 the speed of light, it is possible by linearization  $h_0$  near the Dirac points at which

$$h_0(\vec{k}) = 0, \quad (1.154)$$

so that

$$E(\vec{k}) = \varepsilon. \quad (1.155)$$

At these points, the equilibrium the electrochemical potential is located at  $\varepsilon$  for neutral systems in which exactly half the energy levels filled (valence band) and the other half - empty (conduction band). Dirac points - three pairs (Fig. 1.25). Choose a pair of corresponding  $k_x = 0$ . Then the Hamiltonian (1.151)

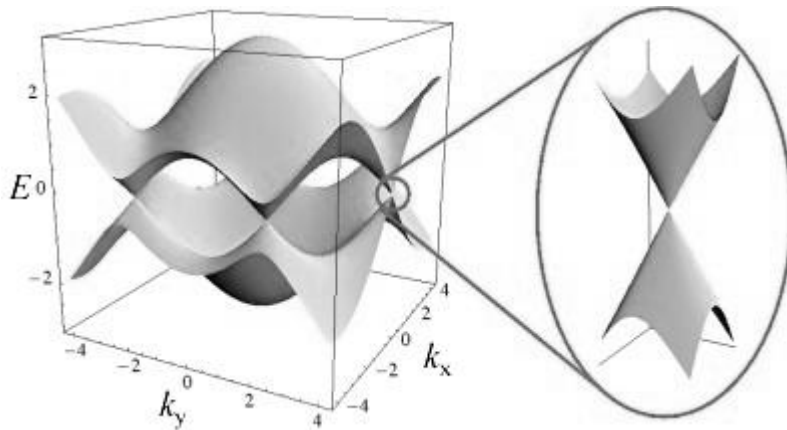


Figure 1.25 – The band structure of graphene

Enlarged view of the line spectrum of the current carriers in the vicinity of the Dirac  $k_x a = 0$  and  $k_y b = +2\pi/3$  (Fig. 1.26)

turns to zero when  $k_y b = \pm 2\pi/3$ . Decomposition of the Hamiltonian (1.151) in a Taylor series

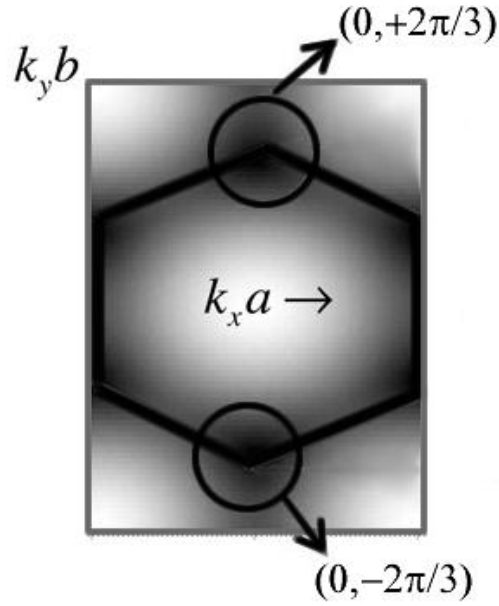


Figure 1.26 – Cross-section of the band structure of graphene at the Dirac point, the region near where blackened

close to the pair of points give

$$h_0(\vec{k}) \approx \pm ita(k_x \mp i\beta_y), \quad (1.156)$$

Where

$$\beta_y \equiv k_y \mp 2\pi / 3b. \quad (1.157)$$

After not complicated transformations we finally obtain the dispersion relation in the vicinity of the Dirac points

$$E = \varepsilon \pm at\sqrt{k_x^2 + k_y^2}, \quad (1.158)$$

that when  $\varepsilon = 0$  is equivalent to the standard record (1.153). Next, consider the construction of the contact matrices for graphene.

## 1.8 A general method for the construction of the contact matrices

Any 2D conductor with the same along the entire length of the guide section across its width may be broken into fragments that mimic each other over the entire length of the conductor. For example, in the case of such graphene fragment can be cut, repeated throughout the length of the conductor and the graphene shown in a single copy in Fig. 1.27. A fragment described by the matrix of the Hamiltonian  $[H] \equiv \alpha$  of order  $n$  by the number of employed

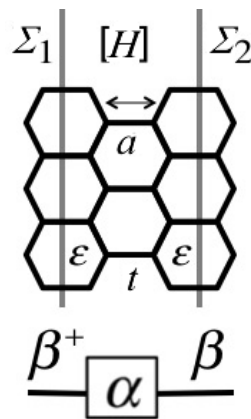


Figure 1.27 – Construction of the contact matrices for graphene

basic functions. For example, for a fragment in Fig. 1.27  $n = 12$  Hückel. Matrix fragments  $\alpha$  are interconnected matrices  $\beta$ .

Consider the right border of the conductor to the contact (Fig. 1.28).

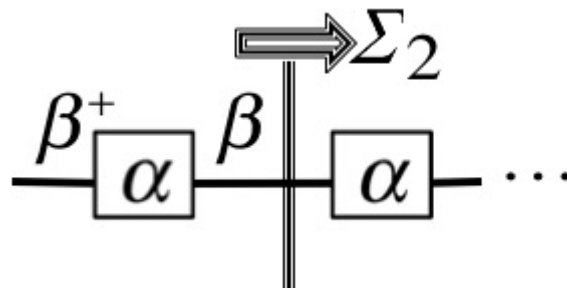


Figure 1.28 – The right border of the conductor to the contact

Contact the block matrix is zero everywhere except the last diagonal element number  $n$

$$\Sigma_2(E) = \begin{matrix} & \begin{matrix} n-2 & n-1 & n \end{matrix} \\ \begin{matrix} \dots \\ \dots \\ \dots \end{matrix} & \begin{bmatrix} \dots & & \\ 0 & 0 & \\ 0 & \beta g_2 \beta^+ & \end{bmatrix} \end{matrix} \quad (1.159)$$

This non-zero block  $g_2$  called the Green's surface function for the contact 2 and it iteratively calculated from equation

$$[g_2]^{-1} = (E + iO^+)I - \alpha - \beta^+ g_2 \beta, \quad (1.160)$$

where  $O^+$  – infinitesimal positive number, which controls the selection of the convergence of the iteration process, while the term  $iO^+I$  provides a negative imaginary part and non-Hermitian matrices  $g$  and  $\Sigma$ .

Consider the output of equation (1.160) in a more general case (see Fig. 1.29) when

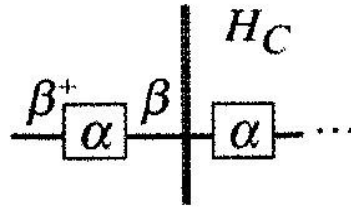


Figure 1.29 – The right border of the conductor with a contact in the general case

the last piece of the conductor associated with unlimited contact, described by the Hamiltonian  $H_c$

$$\begin{bmatrix} \alpha & B \\ B^+ & H_c \end{bmatrix}, \quad (1.161)$$

where

$$[B] \equiv [\beta \ 0 \ 0 \ \dots \ \dots]. \quad (1.162)$$

The resulting retarded Green's function is calculated from equation

$$\begin{bmatrix} A & -B \\ -B^+ & A_c \end{bmatrix}^{-1} = \begin{bmatrix} G^R & \dots \\ \dots & \dots \end{bmatrix}, \quad (1.163)$$

Where

$$A \equiv (E + i0^+)I - \alpha, \quad (1.164)$$

$$A_c \equiv (E + i0^+)I_c - H_c. \quad (1.165)$$

For calculation  $G^R$  from (1.163) Referring to the obvious equality for block matrices

$$\begin{bmatrix} A & B \\ C & D \end{bmatrix}^{-1} \times \begin{bmatrix} p & q \\ r & s \end{bmatrix} = \begin{bmatrix} I & 0 \\ 0 & I \end{bmatrix}, \quad (1.166)$$

multiplying that after simple transformations we obtain

$$p = (A - BD^{-1}C)^{-1}. \quad (1.167)$$

Using the matrix equation (1.167), for  $G^R$  from (1.163) we have

$$G^R = [A - BA_c^{-1}B^+]^{-1}, \quad (1.168)$$

so that the contact matrix

$$\Sigma = BA_c^{-1}B^+. \quad (1.169)$$

Because the matrix  $B$  (162) is the only non-zero element  $\beta$ , have

$$\Sigma = \beta g \beta^+, \quad (1.170)$$

where  $g$  is represents the upper unit matrix  $[A_c]^{-1}$

$$\begin{bmatrix} A & -\beta & 0 & 0 & \dots \\ -\beta^+ & A & -\beta & 0 & \dots \\ 0 & -\beta^+ & A & -\beta & \dots \\ \dots & \dots & \dots & \dots & \dots \end{bmatrix}^{-1} = \begin{bmatrix} g & \dots & \dots \\ \dots & \dots & \dots \\ \dots & \dots & \dots \\ \dots & \dots & \dots \end{bmatrix}. \quad (1.171)$$

Required the equation (1.160) is obtained by the equation (1.168) applied to the matrix  $N \times N$  (1.171), regarding the first block  $A$  as a conductor, and the rest  $(N - 1) \times (N - 1)$  as a contact. Then

$$g_N = [A - \beta g_{N-1} \beta^+]^{-1}, \quad (1.172)$$

where  $g_N$  complies  $g$  to the right side of the equation (1.171), if the matrix of the left side has dimensions  $N \times N$ . The equation (1.172) is solved iteratively, starting with the known  $g_1$ , further  $g_2$  and more so on until  $g_N$  does not coincide with  $g_{N-1}$  with preassigned precision, giving a solution of (1.160)

$$g = [A - \beta g \beta^+]^{-1}. \quad (1.173)$$

It is useful to get the already known value  $\Sigma$  for a homogeneous 1D conductor, using a common method of building contact matrix  $\Sigma$  by the equation (1.170). First, we find  $g$  according to equation (1.173), wherein  $A = EI - \alpha$ . For homogeneous conductor  $\alpha = \varepsilon$ ,  $\beta = t$ ,  $I = 1$ , so that

$$g^{-1} = E - \varepsilon - t^2 g$$

or

$$t^2 g^2 - (E - \varepsilon) g + 1 = 0,$$

whose solution is

$$g = \frac{(E - \varepsilon) \pm \sqrt{(E - \varepsilon)^2 - 4t^2}}{2t^2} = \frac{1}{t} \left( \cos ka \pm \sqrt{\cos^2 ka - 1} \right) = \frac{e^{\pm ika}}{t}, \quad (1.174)$$

where we have used the dispersion relation for a homogeneous 1D conductor (1.92). Substituting (1.174) into (1.170) we obtain the already known expression for the homogeneous conductor  $t \cdot \exp(ika)$ , where the exponent "+" sign is selected for physical reasons.

### 1.9 Ballistic conductance of graphene

As an illustrative example, we present the results of calculating the transmission coefficient and the density of states of graphene ribbons Hückel model for its two configurations boundaries (Fig. 1.30) - zigzag (Zigzag Graphene Nano Ribon / ZGNR) and armchair (Armchair Graphene Nano Ribon / AGNR) [36]. The calculations were performed for the tape width  $W = 53 \text{ nm}$  resonance integral  $t_0 = 2.7 \text{ eV}$ .

Because these ideal graphene ribbons are ballistic conductors, the transmission coefficients are equal to the number of modes

$$M = \text{Int} \left( \frac{2W}{h/p} \right) = \text{Int} \left( \frac{2W}{h} \frac{E}{v_0} \right), \quad (1.175)$$

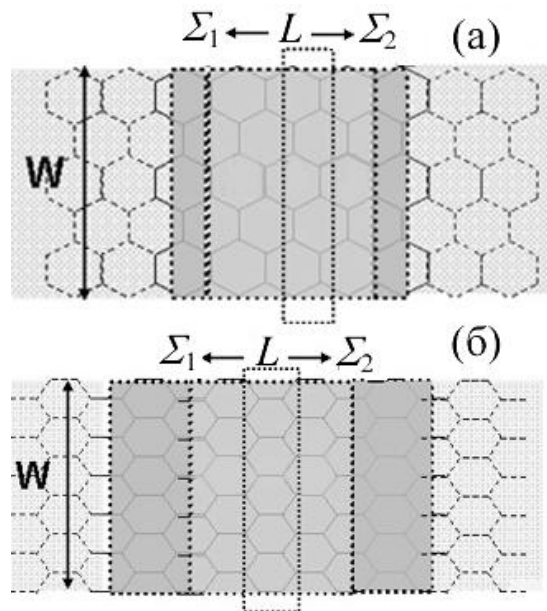


Figure 1.30 – Choice of repeating units (shown by rectangles that extend beyond the width of the tape  $W$ ) two configurations boundaries - zigzag (a) and armchair (b)

where we use the dispersion relation for the graph (1.153). Fermi velocity  $v_0$  assumed to be  $10^6$  m/s, commonly used in the literature [37].

The calculation results of the transmission coefficient and the density of states by NEGF shown in Fig. 1.31. Attention is drawn to the high density of states at  $E = 0$  for the zigzag configuration of the graphene ribbons. It's so

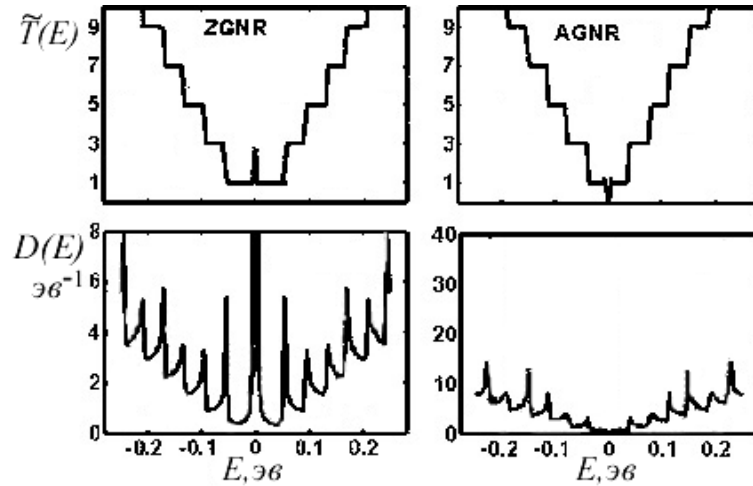


Figure 1.31 – The transmission coefficient and the density of states for the two configurations borders - zigzag ZGNR (left) and armchair AGNR (right)

called edge localized states near the Fermi level, absent in armchair configuration [38, 39]. Our task is not to analyze the results of the calculation, the more that the role of the configuration and width boundaries of graphene ribbons studied in detail [38 - 42]. We only high plausibility of the results obtained, even within such a simple graph model as an approximation of strong coupling in orthogonal basis, taking into account the interaction with parametric only neighboring atoms.

## Chapter 2 HALL EFFECT MEASURING ELECTROCHEMICAL POTENTIALS

### 2.1 Introduction

Edwin Hall in 1879 discovered the occurrence of transverse potential difference by placing a thin gold plate with a constant current in a magnetic field [1]. In the simplest embodiment, the Hall effect is manifested as follows. We place 2D conductor with an electric current in a weak magnetic field  $\vec{B}$ , perpendicular to the surface of the conductor - along the axis  $y$  in Fig. 2.1. The magnetic field is the Lorentz force

$$\vec{F} = \frac{d\vec{p}}{dt} = -q\vec{v} \times \vec{B} \quad (2.1)$$

deflects the electrons moving at speeds  $\vec{v}$  from source  $S$  to the drain  $D$ , from their path along or against the velocity vector of the lateral edges of the conductor (Fig. 2.1). The criterion of smallness of the magnetic field is usually a condition that electrons do not begin to move along a cycloid.

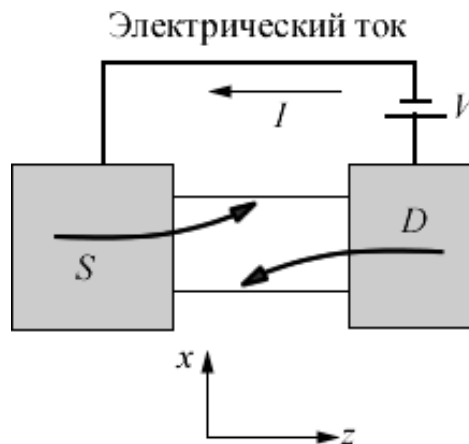


Figure 2.1 – The magnetic field perpendicular to the current-carrying conductor deflects the electrons to the edges of the conductor

Since more electrons move from source to drain, is created Hall voltage  $V_H$  in a transverse direction  $x$  (Fig. 2.2).

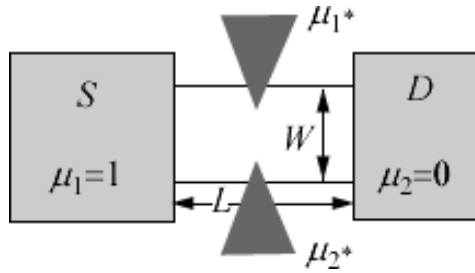


Figure 2.2 – Hall voltage generated in the transverse direction

The Hall effect has always aroused considerable interest. It is particularly increased in 1980, when Karl von Klitzing discovered that the Hall resistance

$$R_H = \frac{V_H}{I} \quad (2.2)$$

takes discrete values [2, 3], which can be calculated using the following simple formula

$$R_H = \frac{25812.80}{k}, \quad k = 1, 2, 3, \dots \quad (2.3)$$

The observed phenomenon is called integer quantum Hall effect. The accuracy of measuring the resistance is so great that the National Bureau of Standards was chosen to calibrate the Hall effect resistance [4].

K. von Klitzing demonstrated [2, 3] that the Hall resistance actually measures the ratio of two fundamental physical constants - the Planck constant and the square of the electron charge

$$R_H = \frac{h}{q^2} \cdot \frac{1}{k}, \quad k = 1, 2, 3, \dots, \quad (2.4)$$

and by the speed of light  $c$  due to the fine structure constant

$$\alpha = \frac{q^2}{\hbar c} = \frac{1}{137.0359895}, \quad (2.5)$$

it is essential for metrology of the fundamental constants of physics.

Already in 1982, has been experimentally observed fractional quantum Hall effect [5, 6]. In ferromagnets in the Hall resistance observed contribution depends directly on the magnetization of the material, and this contribution can be much larger than normal Hall resistance. This phenomenon is called anomalous Hall effect [7]. There are other, no less interesting manifestation of the Hall effect - spin Hall effect Dyakonov - Perel [8, 9], the quantum spin Hall effect in graphene [10], as well as other manifestations of the magnetic field on the electrical circuit, such as the non-reciprocity circuits, are difficult to interpret in terms of the effective resistance of ordinary [11], which is even more interesting because there is a new class of materials - topological insulators, which seemed to have nonreciprocity even in the absence of magnetic fields [12]. These and other related questions will we consider, with varying degrees of completeness in this and the following publications from the standpoint of the concept of "bottom - up" of modern nanoelectronics [13].

Let us consider the usual classical Hall effect at low magnetic fields. One of the reasons for the increased interest in the Hall effect was the fact that the Hall resistance has a different sign for  $n$ - and  $p$ -conductors, which opens up the possibility of experimentally determine the difference between them. The same purpose can be achieved by measuring the current flow through a conductor between the terminals located at different temperatures [14]. In this and in another case, usually use the term "hole" as a positive charge carriers in  $p$ -conductors. This interpretation can not be considered satisfactory, as in  $n$ - and in  $p$ -conductors carriers are only electrons.

in the case of thermoelectric measurements is determined by the direction of the current slope of the density of states  $D(E)$ , or whether this function is increasing with increasing energy ( $n$ -conductor), or falling ( $p$ -conductor) [14]. The sign of the Hall effect is determined by the sign of the effective mass is determined by (75) in [15] as the ratio of the pulse  $p$  of the speed  $dE/dp$ . As a result, although the Lorentz force (2.1) is the same for the  $n$ - and  $p$ -conductors, giving the same value of  $dp/dt$ , resulting  $dv/dt$  has different signs for the  $n$ - and  $p$ -conductors, electrons spinning in the past in the opposite direction, which leads to a change in the sign of the Hall of the potential difference.

Referring to the elementary theory of the Hall effect, as it usually is contained in textbooks on solid state physics, for example. [16] The current is given by

$$I = q(N/L) v_d , \quad (2.6)$$

where  $N/L$  is the linear density of electrons and their drift velocity is equal to the product of the mobility of electrons in the electric field along the length of the conductor

$$v_d = \bar{\mu}(V/L) . \quad (2.7)$$

In equilibrium, the transverse field compensates the Lorentz force

$$V_H / W = v_d B , \quad (2.8)$$

so that using (2.6) and (2.7) for the Hall resistance have

$$R_H = \frac{V_H}{I} = \frac{B}{q(N/LW)} . \quad (2.9)$$

This equation is widely used to determine the electron density  $N/LW$  the slope of the dependence of the Hall resistance on the magnetic field.

This elementary theory of the Hall effect is presented with certain minor nuances in all textbooks. Everywhere electric field appears in both the longitudinal and transverse direction as causes of electrical current. I agree with this can not be [15]. According to (2.9), the Hall resistance depends on the electron density on the entire range of energies, which, of course, wrong. Like any other transport coefficients [14], the Hall resistance - a property of the Fermi surface, and it depends only on the electron energies in the range of about several  $kT$  around the value  $E = \mu_0$  [15].

We show that the Hall resistance to single-mode elastic resistor is given by

$$R_H(E) = \frac{2BLW}{qD(E)v(E)p(E)}, \quad (2.10)$$

which still need to be averaged over the energy range around a few  $kT$  around the value  $E = \mu_0$ , using standard thermal broadening function  $F_T$  [15], namely:

$$\frac{1}{R_H} = \int_{-\infty}^{+\infty} dE \left( -\frac{\partial f_0}{\partial E} \right) \frac{1}{R_H(E)}. \quad (2.11)$$

We note that, in general, be averaged conductivity of  $1/R_H(E)$ , and not the resistance  $R_H(E)$ , since all the mode of conduction channels "work" in parallel and are at the same potential difference.

Equations (2.10) - (2.11) reduces to the standard expression (2.9) using the fundamental relationship [15]

$$D(E)v(E)p(E) = N(E) \cdot d \quad (2.12)$$

For 2D conductor ( $d = 2$ ) and averaging  $N(E)$ , as has been shown in [15]. If the dispersion relation for the studied Explorer is not known, it can only use the equations (2.10) - (2.11).

In any case, the equation (2.11) indicates that the Hall effect does not affect all electrons at energies of all possible. There is, however, a phenomenon that affects all of the electrons at all energy - is the existence of equilibrium currents in a conductor placed in a magnetic field (Fig. 2.3).

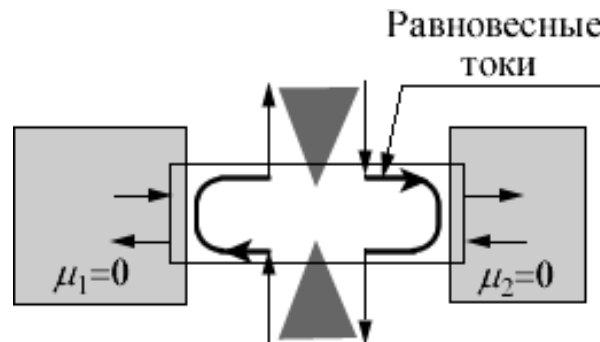


Figure 2.3 – The equilibrium currents exist in any conductor in a magnetic field

Yet, non-vanishing currents that exist even in the hydrogen atom in a magnetic field, are irrelevant to the transport coefficients. Transport models should be built in such a way that the no Fermi currents were eliminated from the outset. A similar problem with respect to the spin currents occur even without the external magnetic field [17].

Next, we consider the calculation of non-equilibrium electrochemical potentials inside the conductor, and the conductor fourterminal simulation environment using a equation [18, 19]. However, first consider the overall dynamics concisely electrons in a magnetic field.

**Why differ  $n$ - and  $p$ -conductors?** Why the Hall resistance has opposite signs for the  $n$ - and  $p$ -conductors? The main reason is that in the  $n$ -conductors and pulse rate have the samedirection, and in the  $p$ -conductors – antirected; and as  $v = dE/dp$ , and  $p$ -conductors energy decreases with increasing pulse (Fig. 2.4) [15].

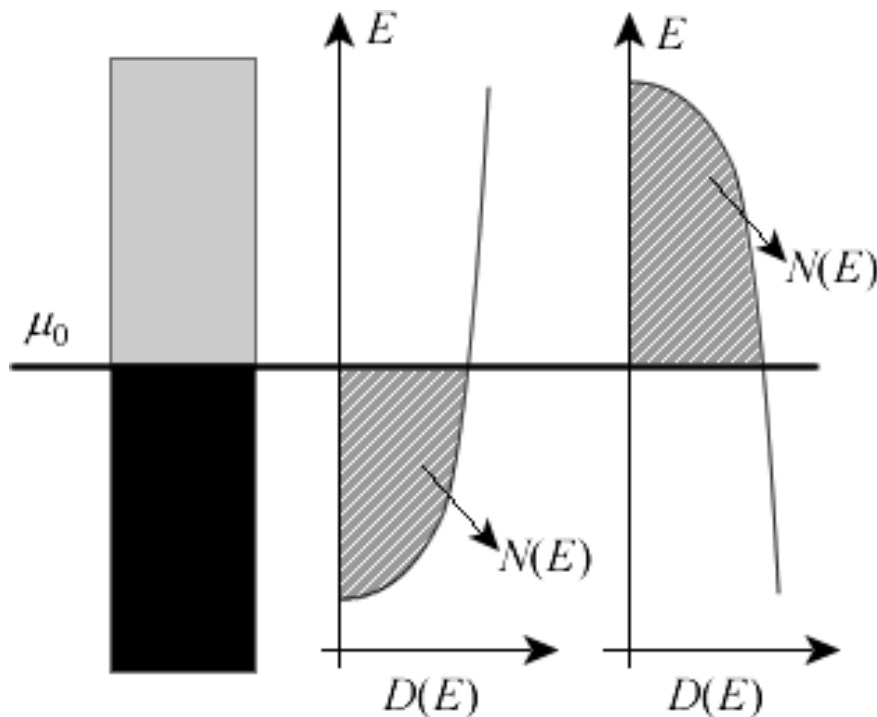


Figure 2.4 – Hall resistance has different signs for the  $n$ -conductors (left) and the  $p$ -conductors (right) and inversely proportional to  $N(E)$  at  $E = \mu_0$

To see the role played by the difference in the sign of the velocity and momentum, we turn to the Lorentz force (2.1). For any isotropic dispersion relation velocity and momentum are collinear (parallel or antiparallel) and let are, for example, at an angle  $\theta$  to the longitudinal axis  $z$  of the conductor (Fig. 2.5).

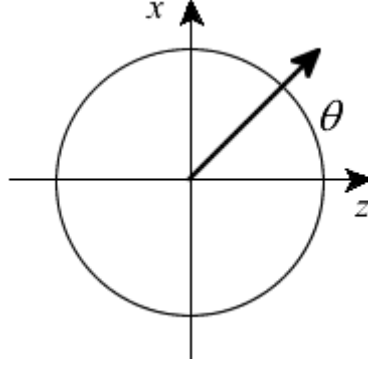


Figure 2.5 – To decompose the momentum and velocity of the electron on the projection length and breadth of 2D conductor (Fig. 2.1)

Then

$$\begin{aligned}\vec{p} &= p \cos \theta \hat{z} + p \sin \theta \hat{x} \\ \vec{v} &= v \cos \theta \hat{z} + v \sin \theta \hat{x} ,\end{aligned}\tag{2.13}$$

and after substituting in (2.1) we obtain

$$\frac{d\theta}{dt} = \frac{qvB}{p} .\tag{2.14}$$

In other words, the angle  $\theta$  varies linearly with time, and velocity vectors and pulse spin at a constant angular speed  $\omega_C$ . However, the  $n$ - and  $p$ -conductors rotation is in opposite directions, since the ratio  $p/v$  they have different signs. This ratio is defined as the mass (equation (75) in [15]) and is a constant for a parabolic dispersion (equation (78) in [15]), so that the cyclotron frequency

$$\omega_C = \left| \frac{qvB}{p} \right|_{E=\mu_0} = \left| \frac{qB}{m} \right|_{E=\mu_0} .\tag{2.15}$$

For the linear dispersion (equation (79) in [15]), the mass increases with energy, so that the cyclotron frequency (2.15) decreases with increasing density of charge carriers, which is observed in graphene [20].

The magnetic field of the rotating electrons on a circular path with a frequency  $\omega_C$ . If  $\omega_C \cdot \tau \ll 1$ , where  $\tau$  – the average time of free rotation, the rotation is never ending, which corresponds to the observation of the Hall resistance (2.9) - (2.11) in a weak magnetic field. In the strong magnetic field  $\omega_C \cdot \tau \gg 1$  observed the quantum Hall effect.

## 2.2 The spatial profile of the electrochemical potential

Here are arguments in favor of the formula (2.10) - (2.11) for the Hall resistance, based on the general theory of ballistic transport, as set out in Annex 1 [21].

The model of an elastic resistor drift velocity is determined by the potential difference

$$\delta\mu = \mu^+ - \mu^- \quad (2.16)$$

between conditions associated with the drain, and conditions associated with the source, so that instead of the equation for the current (2.6) we write equation (A1.39) in [21], namely:

$$I(E) = \frac{q}{h} M(E) \left( -\frac{\partial f_0}{\partial E} \right) \delta\mu, \quad (2.17)$$

where the number of modes to use the formula (67) in [15]

$$\frac{M(E)}{h} = \frac{D(E)\nu(E)}{\pi L}. \quad (2.18)$$

From equation (A1.15) and (A1.23) [21] instead of equation (2.7) we have the potential difference associated with the voltage applied to the ends of the conductor,

$$\delta\mu = \frac{qV\lambda}{L + \lambda} \cong q\lambda \frac{V}{L}. \quad (2.19)$$

Just as in (2.6) and (2.7) Drude formula for conductivity

$$G = \frac{I}{V} = \sigma \frac{W}{L}, \quad (2.20)$$

where the specific conductivity

$$\sigma = \frac{q\bar{\mu}N}{WL}, \quad (2.21)$$

and (2.17) and (2.18) follows a more general expression for the conductivity obtained in [15].

Now we will show that instead of the standard Hall-effect equation (2.8) we have the equation

$$\frac{V_H}{W} = \frac{2}{\pi} \frac{\delta\mu}{p} B \quad (2.22)$$

which together with (2.17) and (2.18) gives the above expression (2.10) - (2.11) for the Hall resistance singlemode elastic resistor.

Earlier, in [21] obtained an equation (A1.12)

$$v_z \frac{\partial\mu}{\partial z} = -\frac{\mu - \mu_0}{\tau}, \quad (2.23)$$

whose decisions determine the electrochemical potentials  $\mu^+$  and  $\mu^-$  (Fig. 2.6).

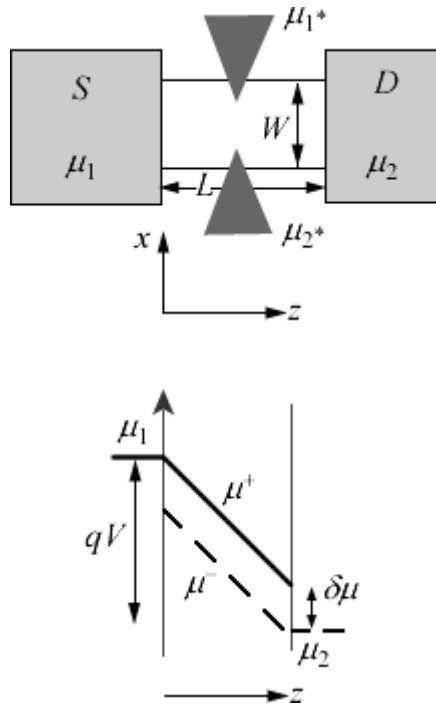


Figure 2.6 – The spatial profile of potential  $\mu^+$  and  $\mu^-$  along the length of the conductor

We show that these solutions can be written in the form

$$\mu(z, \theta) \equiv \bar{\mu}(z) + \frac{2}{\pi} \delta\mu \cos \theta . \quad (2.24)$$

Since this is an elastic resistor, in which the electrons are moving at a fixed energy and therefore have a constant pulse is convenient to use cylindrical coordinates  $p, \theta$  (Fig. 2.7) instead of Cartesian  $p_x, p_y$ .

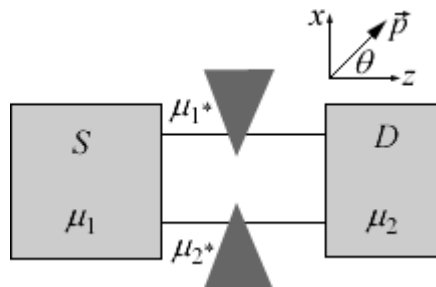


Figure 2.7 – On the orientation of cylindrical coordinates  $p, \theta$  with respect to the conduction channel

Let us consider electrons moving at a fixed angle  $\theta$ . Then in view of (2.19) we obtain

$$\mu(z) = \bar{\mu}(z) + \frac{qV}{L} v\tau \cos \theta, \quad (2.25)$$

keeping in mind that in this simple case, the mean free path

$$2v_z\tau = 2v\tau \cos \theta. \quad (2.26)$$

Comparing (2.25) and (2.24) and performing averaging over angles for the 2D conductor (formula (58) in [15]), to obtain a potential difference

$$\delta\mu \approx \frac{qV}{L} \frac{\pi}{2} v\tau, \quad (2.27)$$

and finally combining (2.25) and (2.27), we obtain the desired expression (2.24).

Now the question is how to change the decision (2.24) of (2.23) with allowance for the Lorentz force generated by the magnetic field. To do this we need to transport the Boltzmann equation in the relaxation time approximation [22]

$$v_x \frac{\partial \mu}{\partial x} + v_z \frac{\partial \mu}{\partial z} + F_x \frac{\partial \mu}{\partial p_x} + F_z \frac{\partial \mu}{\partial p_z} = -\frac{\mu - \mu_0}{\tau}, \quad (2.28)$$

where the left saved all the  $x$ - and  $z$ -component, because it is a 2D conductor in the plane  $xz$  (Fig. 2.1). This equation is compared with its special case (2.23) comprises three new terms. Two of them are connected with the Lorentz force, and can be rewritten as

$$F_x \frac{\partial \mu}{\partial x} + F_z \frac{\partial \mu}{\partial z} = \vec{F} \cdot \vec{\nabla}_\mu = \frac{F_\theta}{p} \frac{\partial \mu}{\partial \theta} + F_r \frac{\partial \mu}{\partial r}, \quad (2.29)$$

where the radial component of the Lorentz force (2.1) is missing, and the angular component

$$F_r = 0, \quad F_\theta = -qvB. \quad (2.30)$$

Now the equation (2.28) takes the form

$$v_x \frac{\partial \mu}{\partial x} + v_z \frac{\partial \mu}{\partial z} - \frac{qvB}{p} \frac{\partial \mu}{\partial \theta} = -\frac{\mu - \mu_0}{\tau}. \quad (2.31)$$

Given the fact that the solution of equation (2.23) is the equation (2.24), is not difficult to make sure that the solution of equation (2.31) will

$$\mu(z, \theta, x) = \bar{\mu}(z) + \frac{2}{\pi} \delta\mu \cos \theta - \frac{2}{\pi} \frac{\delta\mu}{p} qBx, \quad (2.32)$$

whence

$$-qV_H = \mu(x = W) - \mu(x = 0) = -\frac{2}{\pi} \frac{\delta\mu}{p} qBW \quad (2.33)$$

and accordingly the desired equation (2.22).

Before proceeding to the measurement of potential interest to us in the Hall conductor four-terminal model look more closely at the general issues of measurement of electrochemical potentials.

### **2.3 Measurement of electrochemical potential. Formula Landauer and Buttiker**

Classical Fermi distribution (equation (10) in [15]) with a high accuracy is suitable for massive contacts which are always substantially in equilibrium, but this is not necessarily true for small wires, even with small applied potential difference. Annex 1 [21] shows how important it is to introduce two separate

electrochemical potential  $\mu^+$  and  $\mu^-$  for the understanding of the physical meaning of the boundary resistance as the basis of a new formulation of Ohm's law. Non-equilibrium electrochemical potentials of this type are very useful and are widely used in practical engineering nanoelectronics, though still expressed doubts as to their conceptual values and even measurability.

The following simple example we consider the features of non-equilibrium potentials and problems of their measurability, which will link them to the concepts and formulas of Landauer and Buttiker [18, 23 - 27], which are central to the theory of transport processes of modern mesophysics.

Following Landauer [23 - 27], we consider a ballistic channel with localized defect transmissive  $T$  share falling on the defect electrons and reflects the share of  $1 - T$  back (Fig. 2.8). We could follow the logic of the arguments in Annex 1 [21] and would get the spatial profiles of potential  $\mu^+$  and  $\mu^-$  Channel defective as qualitatively shown in Fig. 2.8, and thus give to the resistance offered by the defect, as it did Landauer in 1957.

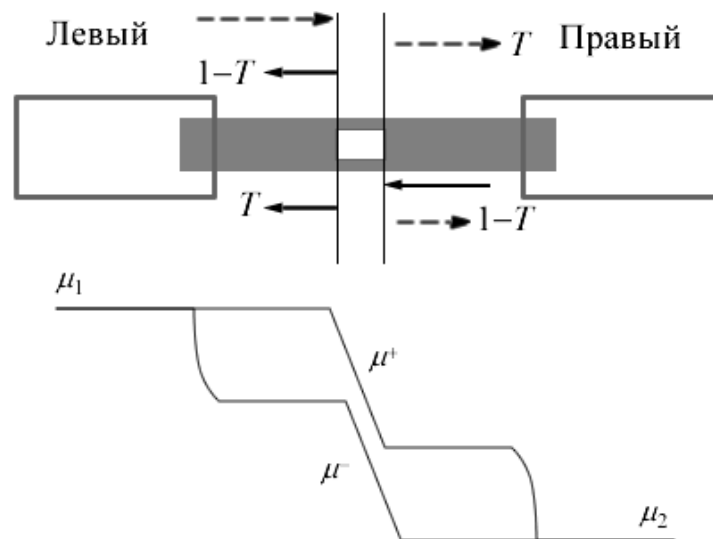


Figure 2.8 – Profile of non-equilibrium potentials in the channel with one defect

Overcome expressed doubts about the feasibility of non-equilibrium potential could four-terminal experiments (Fig. 2.9) with two additional contacts, conducting small amount of current in order to measure the voltage drop across the defect.

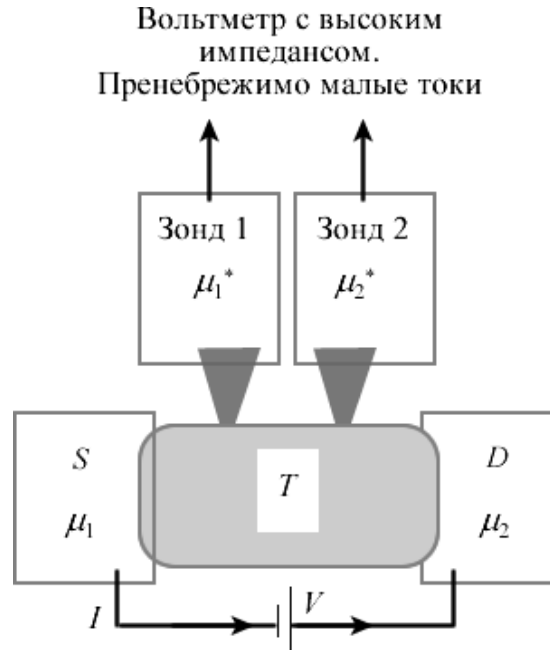


Figure 2.9 – Four-terminal experiment to measure the conductivity of 1D channel with one defect with transmittance  $T$

We show that in the case of identical and weakly bound probe contacts four-terminal conductivity

$$G_{4t} = \frac{I}{(\mu_1^* - \mu_2^*)/q} = M \frac{q^2}{h} \frac{T}{1-T}, \quad (2.34)$$

where  $M$  - the number of modes of the conductor, and two-terminal conductivity is of lesser importance

$$G_{2t} = \frac{I}{(\mu_1 - \mu_2)/q} = M \frac{q^2}{h} T, \quad (2.35)$$

so that the difference between them is the boundary resistance (Fig. 2.10)

$$\frac{1}{G_{2t}} - \frac{1}{G_{4t}} = \frac{h}{q^2 M}. \quad (2.36)$$

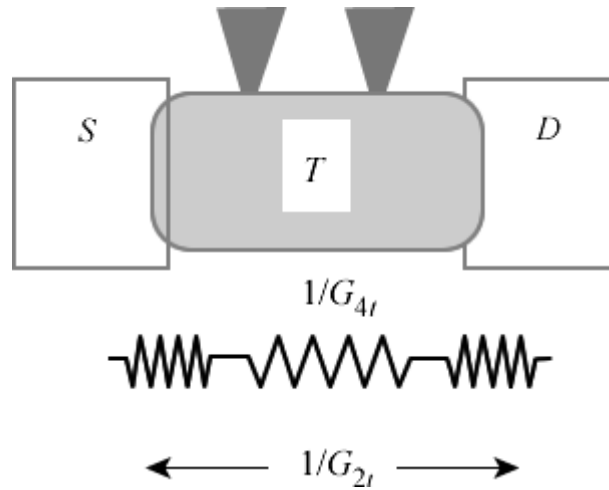


Figure 2.10 – Two-terminal resistance can be regarded as a resistance at a defect which is connected in series with a resistance boundary

Although the boundary resistance was predicted and found by Yu.V.Sharvin in metallic conductors in 1965 [28, 29], it is recognized as a ubiquitous role is still not widely today. In the first half of the 80s was a discussion about the meaning and difference between the two conduction formulas (2.34) and (2.35), when, finally, in 1986 Imrie not identify the difference between them (2.36) as a boundary resistance [30, 31]. In the evolution of mesophysics equation (2.35) was widely known and was known as the Landauer formula, whereas the original did Landauer formula (2.34) was almost forgotten. The voltage drop at a defect, contact resistance, and both formulas Landauer discussed in detail in the review Treefolk and Sadowski [32].

One of the problems in the formative years of mesophysics was that contacts were strongly associated with the main conductor and behaved as "additional defects" to eliminate that was not so easy. Buttiker [18, 27] to interpret the measurements suggested four-terminal elegant formula

$$I_m = \left( \frac{1}{q} \right) \sum_n G_{m,n} (\mu_m - \mu_n), \quad (2.37)$$

connecting current to the contact number  $m$  with electrochemical potentials in other contacts where  $G_{m,n}$  is conductivity is determined by the transmission

coefficient  $T_{m,n}$  contacts between  $m$  and  $n$ . For the two-terminal circuit measurements Buttiker formula simplifies to

$$I_1 = \left(\frac{1}{q}\right) G_{1,2} (\mu_1 - \mu_2) = -I_2 \quad (2.38)$$

and coincides with the two-terminal Landauer formula (2.35), if the conductivity  $G_{1,2}$  identified as  $(q^2/h)M$ .

If we knew all the chemical potentials  $\mu_m$ , You could benefit formula Buttiker (2.37) and calculated to all currents  $I_m$ . But the four-terminal measurements (Fig. 2.9) we do not know the electric potentials at the terminals 1\* and 2\*, so that we do not know chemical potentials  $\mu_{1^*}$  and  $\mu_{2^*}$ . However, we know the currents  $I_{1^*}$  and  $I_{2^*}$  and they should be equal to zero (Fig. 2.9). If we know each contact or  $\mu_m$ , or  $I_m$ , Buttiker formula allows to calculate the value of all the missing.

Consider Landauer voltage drop across the defect (Fig. 2.8) and show that weakly bound contact Buttiker formula gives the same results as the non-equilibrium potentials  $\mu^+$  and  $\mu^-$  inside the conductor.

The potential measured by a test contact (Fig. 2.9), there is a certain mean value of the potentials  $\mu^+$  and  $\mu^-$  (Fig. 2.11), the correct structure is determined by averaging the contacts. We model the this measurement by comparing the conductivities  $g^+$  and  $g^-$  two streams of electrons  $I^+$  and  $I^-$  (Fig. 2.11). Assuming current at zero contact trial, we have

$$g^+ (\mu^+ - \mu_{30H\partial}) + g^- (\mu^- - \mu_{30H\partial}) = 0, \quad (2.39)$$

so that

$$\mu_{30H\partial} = \frac{g^+}{g^+ + g^-} \mu^+ + \frac{g^-}{g^+ + g^-} \mu^-, \quad (2.40)$$

where the weighting coefficients

$$\frac{g^+}{g^+ + g^-} = \alpha, \quad \frac{g^-}{g^+ + g^-} = 1 - \alpha. \quad (2.41)$$

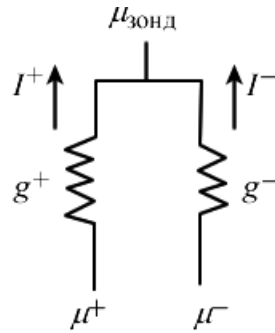


Figure 2.11 – For the calculation of the chemical potential on the test contact

Assuming that non-invasive measurements of test contacts of atomic size, it can be expected that the conductivity will be almost identical, so that the weighting coefficient  $\alpha \sim 50\%$  and the test measures the contact arithmetic mean

$$\mu_{30HД} = (\mu^+ + \mu^-) / 2. \quad (2.42)$$

If the contact is small enough and angers different flows  $I^+$  and  $I^-$ , weighting factor  $\alpha$  is different from 50%. If, moreover, the two test contact 1\* and 2\* at a measuring circuit (Fig. 2.9) different weights, the measured resistance of the defect will be different compared to Landauer value (2.34).

**Landauer Formulas.** We now return to the problem of finding equilibrium potential profile in the channel with the defect (Fig. 2.8). First, balance the outgoing and incoming currents (Fig. 2.12):

$$I_R^+ = T I_L^+ + (1 - T) I_R^-, \quad (2.43a)$$

$$I_L^- = (1 - T) I_L^+ + T I_R^-. \quad (2.43b)$$

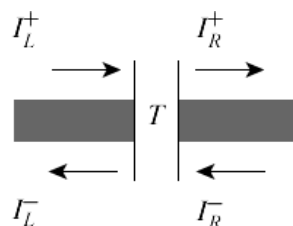


Figure 2.12 – Distribution of current on the left and right of the defect

Then, following formulas (A1.35) and (A1.36) of Annex 1 of [21], from the current move to the distribution functions

$$f_R^+ = T f_L^+ + (1 - T) f_R^-, \quad (2.44a)$$

$$f_L^- = (1 - T) f_L^+ + T f_R^-, \quad (2.44b)$$

and then to potentials

$$\mu_R^+ = T \mu_L^+ + (1 - T) \mu_R^- = T \mu_1 + (1 - T) \mu_2, \quad (2.45a)$$

$$\mu_L^- = (1 - T) \mu_L^+ + T \mu_R^- = (1 - T) \mu_1 + T \mu_2. \quad (2.45b)$$

We simplify the calculations by the potential at one contact, zero and the other equal to unity (Fig. 2.13).

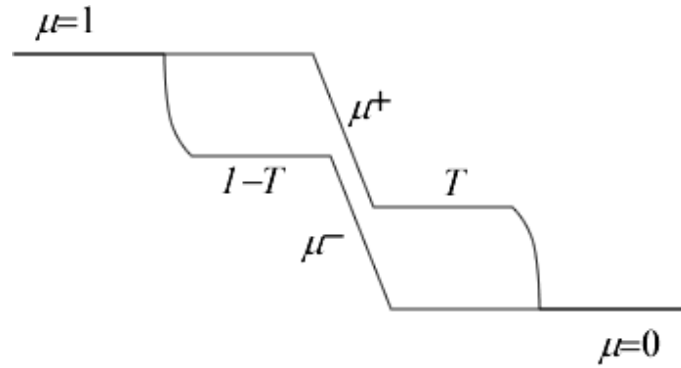


Figure 2.13 – Profiles of potential  $\mu^+$  and  $\mu^-$  on the defect, normalized to the total potential difference is equal to one

The necessary potential difference can be always taken into account by multiplication by  $\mu_1 - \mu_2 = qV$ . Then equation (2.45) simplifies to

$$\mu^+ - \mu^- = T(\mu_1 - \mu_2) \quad (2.46)$$

and together with an expression for the current

$$I = \frac{q}{h} M(\mu^+ - \mu^-) \quad (2.47)$$

provide a standard formula Landauer (2.35).

For the first Landauer formula (2.34) we jump on defect of a potential  $\mu^+$ , or  $\mu^-$ :

$$\mu_L^+ - \mu_R^+ = (1 - T)(\mu_1 - \mu_2), \quad (2.48a)$$

$$\mu_L^- - \mu_R^- = (1 - T)(\mu_1 - \mu_2), \quad (2.48b)$$

and then divide this current difference, and obtain (2.34).

Do not forget that we are interested in measuring electrochemical potentials inside the conductor. How does this relate to the measurement of the voltage non-invasive probe of a scanning tunneling microscope (STM)? Assuming that such a STM probe measures the average electrochemical potential  $\mu^+$  and  $\mu^-$ , we obtain the graph in Fig. 2.14, the comparison of which with Fig. 2.13 and suggests that non-invasive probe STM actually measures the average value of the electrochemical potential  $(\mu^+ + \mu^-)/2$ .

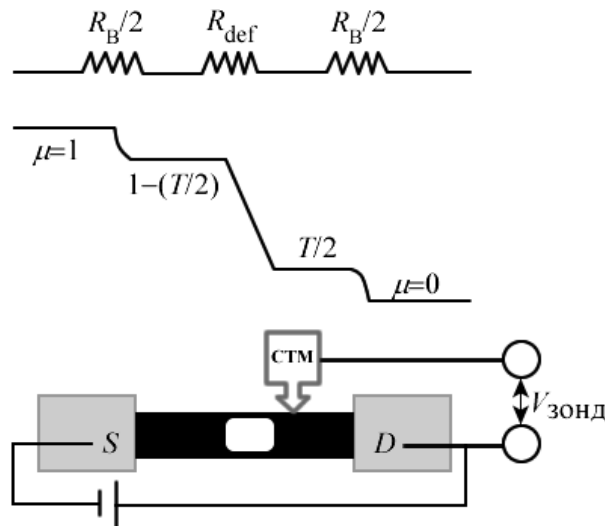


Figure 2.14 – Scanning tunneling microscope measures the average value of the electrochemical potential  $(\mu^+ + \mu^-)/2$

What if the STM probe measures the weighted average of  $\mu^+$  and  $\mu^-$  with the weight coefficient  $\alpha$  (2.40) different from 50%? Until weighting factor  $\alpha$  remains the same for both potentials  $\mu^+$  and  $\mu^-$ , jump on the defect (2.48) remains the same

$$\mu_L^{30H\partial} - \mu_R^{30H\partial} = (1 - T)(\mu_1 - \mu_2), \quad (2.49)$$

which leads to the same first Landauer formula (2.34). If the weighting coefficients are different for  $\mu^+$  and  $\mu^-$ , then (2.34) would be invalid. In the limiting case where the weighting factor  $\alpha$  is equal to zero on the left and one on the right (Fig. 2.11),

$$\mu_L^{30H\partial} - \mu_R^{30H\partial} = (1 - 2T)(\mu_1 - \mu_2), \quad (2.50)$$

which leads to a negative resistance at  $T > 0.5$ .

The concept of non-equilibrium potential  $\mu^+$  and  $\mu^-$  It leads to the intuitively correct results and is now being widely used, but its use requires caution. This defect causes the potential jump, not ballistic transport (Fig. 2.14), meaning that the resistance (2.34) is determined by the defect. We must remember that we are still considering the elastic resistors. Yes, the surge still is  $IR$  and Joule heat dissipation  $I^2R$  the conductor is absent and only occurs at the contacts.

## 2.4 Buttiker's formula

His formula (2.37) contains the measured values directly, leaving outside any issues relating to mute the internal variables. I would like to emphasize the general applicability of the Buttiker's formula, regardless of the conductor is resilient or is not. Indeed, as we shall see, for the derivation of (2.37) only need quite a bit over the usual linear theory of electrical circuits.

We define the conductivity to start multiterminal

$$G_{m,n} \equiv -\frac{\partial I_m}{\partial(\mu_n / q)}, \quad m \neq n \quad (2.51a)$$

$$G_{m,m} \equiv + \frac{\partial I_m}{\partial (\mu_m / q)}, \quad (2.51b)$$

where natural to wonder why, when  $m \neq n$  is a negative sign, unlike the case when  $m = n$ . Selecting the sign can be illustrated by the four-terminal measurement channel one defect (Fig. 2.15).

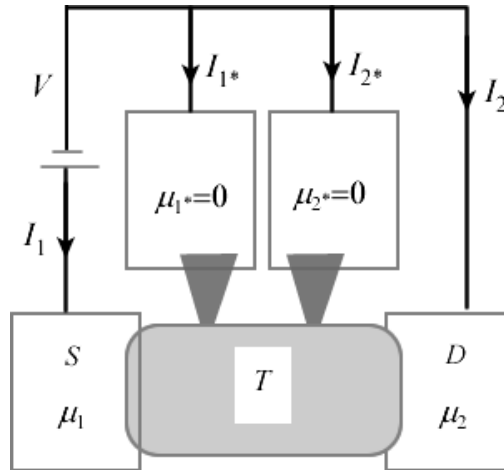


Figure 2.15 – Thought experiment with a four-terminal measurement channel with one defect as shown in Fig. 2.8

The increase in chemical potential  $\mu_1$  increases the current entering the pin 1 (positive current) and an outflow from all other contacts (negative currents). Sign in (2.51) are chosen so that the coefficients of conductivity  $G_{m,n}$  always be positive, as required intuitive meaning of conductivity.

Now the current (2.37) can be rewritten in terms of coefficients of conductivity

$$I_m = G_{m,m} \frac{\mu_m}{q} - \sum_{n \neq m} G_{m,n} , \quad (2.52)$$

The coefficients must satisfy the following two rules summability.

Firstly, if all the chemical potentials of the same (equilibrium state), all currents through (2.52) must be zero, which entails generally amounts

$$G_{m,m} = \sum_{n \neq m} G_{m,n} . \quad (2.53a)$$

Secondly, for arbitrary values of the chemical potential sum of all currents should be zero, which leads to the second rule amounts

$$G_{m,m} = \sum_{n \neq m} G_{n,m} , \quad (2.53b)$$

proof of which is not so obvious, as was the case with the first sum rule, and it can be obtained based on the equation (2.52). First sum up all the currents (2.52)

$$\sum_m I_m = 0 = \sum_m G_{m,m} \frac{\mu_m}{q} - \sum_m \sum_{n \neq m} G_{m,n} \frac{\mu_n}{q} , \quad (2.54)$$

then use the summation rules (2.53) and interchange the indices in the double sum

$$0 = \sum_m G_{m,m} \frac{\mu_m}{q} - \sum_m \sum_{n \neq m} G_{n,m} \frac{\mu_m}{q} , \quad (2.55)$$

that for arbitrary values of the chemical potential is only valid if it satisfies the second sum rule (2.53b). Finally,

$$G_{m,m} = \sum_{n \neq m} G_{m,n} = \sum_{n \neq m} G_{n,m} . \quad (2.56)$$

Using sum rules (2.56), we rewrite the first term in (2.52) as a sum and as a result we obtain the famous Buttiker's formula (2.37). We note that in the formula need not 's summation limit for  $n \neq m$ , because the summand for  $n = m$  is always zero.

Sometimes Buttiker's formula (2.37) is more convenient to record through the so-called response factors [33]

$$I_m = \sum_n g_{m,n} \frac{\mu_n}{q} , \quad (2.57)$$

are defined as follows:

$$\begin{aligned} g_{m,n} &\equiv -G_{m,n}, \quad m \neq n \\ g_{m,m} &\equiv G_{m,m} \end{aligned} \quad (2.58)$$

with the rules of summation

$$\sum_n g_{m,n} = \sum_n g_{n,m} = 0. \quad (2.59)$$

Apply Buttiker's approach to the situation in Fig. 2.14, where it is stated that the two non-invasive probes placed before and after the defect with the transmittance  $T$  respectively generate potentials  $1 - T/2$  and  $T/2$  (Fig. 2.16). Will we get the same results by Buttiker method?

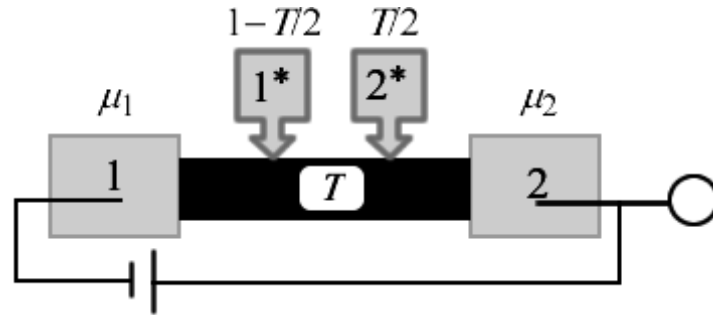


Figure 2.16 – To the probe before and after a defect with a transmittance of  $T$  potentials generated  $1 - T/2$  and  $T/2$ , accordingly

Bearing in mind that this measurement it is about four to four potentials and currents at the terminals 1, 2, 1\* and 2\*, write equation (2.57) in matrix form

$$\begin{Bmatrix} I_1 \\ I_2 \\ I_{1^*} \\ I_{2^*} \end{Bmatrix} = \frac{Mq}{h} \begin{bmatrix} A & B \\ C & D \end{bmatrix} \begin{Bmatrix} \mu_1 \\ \mu_2 \\ \mu_{1^*} \\ \mu_{2^*} \end{Bmatrix}, \quad (2.60)$$

where the matrices have the form of  $A$ ,  $B$ ,  $C$  and  $D$  have the form of  $(2 \times 2)$ .

Because

$$\begin{Bmatrix} I_{1^*} \\ I_{2^*} \end{Bmatrix} = \begin{Bmatrix} 0 \\ 0 \end{Bmatrix}, \quad (2.61)$$

then we can conductor

$$\begin{Bmatrix} \mu_{1^*} \\ \mu_{2^*} \end{Bmatrix} = -D^{-1}C \begin{Bmatrix} \mu_1 \\ \mu_2 \end{Bmatrix} \quad (2.62)$$

with the matrices  $C$  and  $D$  in the form of

$$[C \quad D] = \begin{bmatrix} -t_1 & -t_2 & r & 0 \\ -t'_2 & -t'_1 & 0 & r' \end{bmatrix}, \quad (2.63)$$

where the elements of the matrix  $C$  are interpreted as the probability intercontact transport 1 on  $1^*$ , 2 on  $1^*$ , 2 on  $2^*$  and 1 on  $2^*$  (Fig. 2.17), it being assumed that the contacts  $1^*$  and  $2^*$  loosely coupled and transport between them can be neglected.

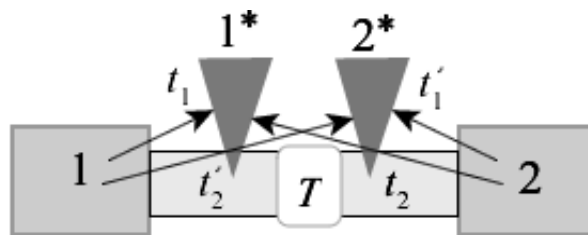


Figure 2.17 – Probabilities intercontact transport in the four-terminal measurement of the conductivity of a channel with a defective transmission factor  $T$

The sum rules (2.59) give

$$\begin{aligned} r &= t_1 + t_2 \\ r' &= t'_1 + t'_2 \end{aligned} \quad (2.64)$$

From the equations (2.62) - (2.64) we have

$$\mu_{1^*} = \frac{t_1}{t_1 + t_2} \mu_1 + \frac{t_2}{t_1 + t_2} \mu_2, \quad (2.65a)$$

$$\mu_{2^*} = \frac{t_2'}{t_1' + t_2'} \mu_1 + \frac{t_1'}{t_1' + t_2'} \mu_2. \quad (2.65b)$$

Note also that the probability  $t_1$  (Fig. 2.17) can be represented as the sum of the probability  $\tau$  of the forward transfer  $1 \rightarrow 1^*$  and probability  $(1 - T) \cdot \tau$  reflected from the defect, and then reach the contact  $1^*$ :

$$t_1 = \tau + (1 - T)\tau. \quad (2.66a)$$

Analogous considerations for a probability  $t_2$  to give

$$t_2 = T\tau, \quad (2.66b)$$

because the path of the electron with the contact 2 will first need to overcome the defect (the probability of  $T$ ), and then get on contact  $1^*$  (probability  $\tau$ ). For the same reasons,  $t_1 = t_1'$  and  $t_2 = t_2'$  (Fig. 2.17).

Using equations (2.66) and setting  $\mu_1 = 1$  and  $\mu_2 = 0$ , from equations (2.65) yields the expected value for the potentials at probes equations (2.66) and setting  $1^*$  and  $2^*$ :

$$\begin{aligned} \mu_{1^*} &= 1 - (T/2) \\ \mu_{2^*} &= T/2 \end{aligned}, \quad (2.67)$$

in what could and no doubt, as in the Buttiker's formula featured only the characteristics of contacts and actually rolled all the details related to the non-equilibrium electrochemical potentials.

**Do not trivial Buttiker's equation?** Finally, any complex circuitry can always be represented by an equivalent circuit effective transistors, such as in

Fig. 2.18 to three terminals. Will it give us a standard theory of electrical circuits, the same result as Buttiker's equation (2.37)?

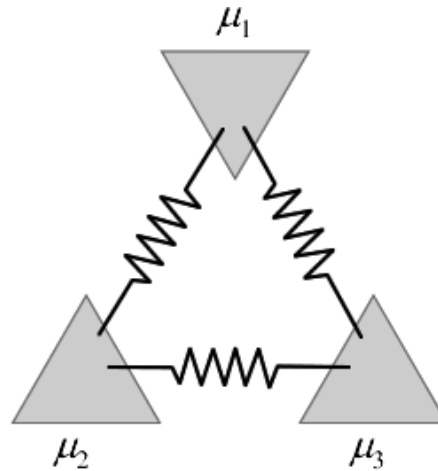


Figure 2.18 – Buttiker equation equivalent resistor network effective only if all reversible conduction ( $G_{m,n} = G_{n,m}$ )

The answer is certainly yes, but only for normal mutual electrical circuits in which conduction between all terminals are completely reversible

$$G_{m \leftarrow n} = G_{n \leftarrow m}, \quad (2.68)$$

in other words, the electrons are transported equally easily in both directions for each pair of terminals ( $m, n$ ).

The range of applicability Buttiker equation (2.37) is much broader than the normal mutual electrical circuits, for example, it is applicable for conductors in a magnetic field, when there is a one-conductivity:

$$G_{m \leftarrow n} \neq G_{n \leftarrow m} \quad (2.69)$$

For such situations to justify the applicability of the Buttiker equation (2.37) is not so easy. If Buttiker equation (2.37) conductance  $G_{m,n}$  change to  $G_{n,m}$ , then we just get an erroneous formula, applying that to the multi-terminal nonreciprocal circuits get erroneous results that do not conform to the Buttiker formula (2.37).

**Measuring Hall potential.** Referring finally to the calculation of the Hall voltage using Buttiker formula (2.37) with the four-terminal experiment, differing from that discussed above (Fig. 2.17) Accommodation test probes 1\* and 2\* across the conductor (Fig. 2.19).

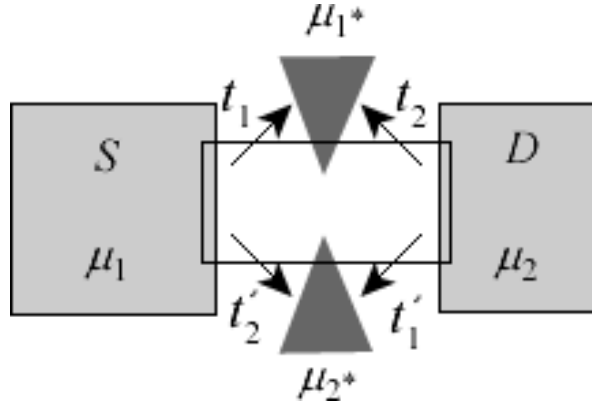


Figure 2.19 – Probabilities intercontact transport in the four-terminal measurement of the Hall voltage

In the absence of a magnetic field probe potential difference of zero. When the magnetic field is perpendicular to the surface of the conductor (plane of the drawing) electrons moving from left to right, are deflected along or against the direction of movement of the side edges of the guide (Fig. 2.1), creating a distinction between the probe potentials  $\mu_{1^*}$  and  $\mu_{2^*}$ , which we want to calculate, depending on the voltage, a current in the conductor.

The equations for the probe potentials remain the same (2.65), if the probability of a contact to make sense of transport, as shown in Fig. 2.19. The calculation of these probabilities either numerically or in the semiclassical approximation leads to Hall voltage  $V_H$

$$-qV_H = \mu_{1^*} - \mu_{2^*} \quad (2.70)$$

in accordance with the already previously obtained by equation (2.22).

Equation (2.22) was obtained based on the Boltzmann equation for transport, but it can also be obtained from (2.65) if we rewrite them in relation to the width of a thin wire somewhere in the middle of a long conductor less than the mean free path, with electrons moving to the left where the potential  $\mu^+$ , and

on the right, where the potential  $\mu^-$ , for potentials at the middle of the conductor on its side at the points simulating probes 1\* and 2\* (Fig. 2.20),

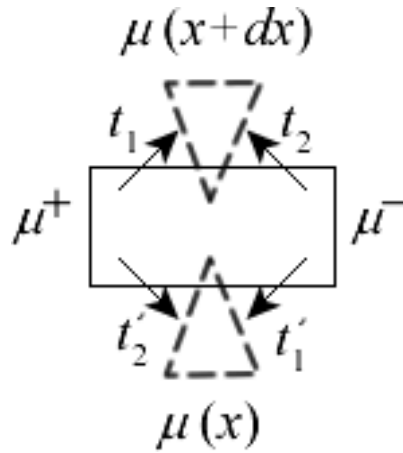


Figure 2.20 – Derivation of equation (2.22) of the probabilities intercontact transport in the four-terminal measurement of the Hall voltage

namely:

$$\mu(x+dx) = \frac{t_1}{t_1+t_2} \mu^+ + \frac{t_2}{t_1+t_2} \mu^-, \quad (2.71a)$$

$$\mu(x) = \frac{t'_2}{t'_1+t'_2} \mu^+ + \frac{t'_1}{t'_1+t'_2} \mu^-. \quad (2.71b)$$

To calculate the probabilities in (2.71), we note that in the absence of a magnetic field, the electrons with velocities lying within an angle  $\theta$  (Fig. 2.5)

$$0 < \theta < +\pi/2,$$

move upwards and lie within the

$$-\pi/2 < \theta < 0,$$

move down (Fig. 2.21).

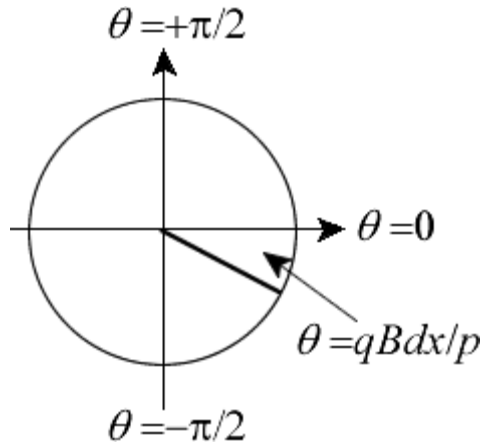


Figure 2.21 – For the calculation of the angle of the turn-up of the electron Lorentz force

The magnetic field of the electron spins upward trajectory at an angle equal to the product of the angular velocity (14) at a time  $dx/v$ , takes to cover the distance  $dx$

$$\frac{qvB}{p} \frac{dx}{v} = \frac{qBdx}{p} \quad (2.72)$$

Then the probability intercontact transport will be proportional to the corners

$$t_1 = t_1' \square \frac{\pi}{2} + \frac{qB}{p} dx, \quad (2.73a)$$

$$t_2 = t_2' \square \frac{\pi}{2} - \frac{qB}{p} dx \quad (2.73b)$$

and substituting them into equation (2.71) gives

$$\mu(x + dx) - \mu(x) = \frac{2qBdx}{\pi p} (\mu^+ - \mu^-), \quad (2.74)$$

so that

$$\frac{d\mu}{dx} = \frac{2qB}{\pi p} \delta\mu \quad (2.75)$$

B in accordance with equation (2.32) and, consequently and with (2.22).

## 2.5 Quantum Hall effect, Landau levels and edge states in graphene

One of the most spectacular applications Buttiker approach is the interpretation of the quantum Hall effect, when the magnetic field is so large that the electrons moving from the source, do not reach the probe 2\*, and electrons moving from the runoff does not reach probe 1\* (Fig. 2.19) . As a result,

$$\frac{V_H}{(\mu_1 - \mu_2) / q} = \frac{t_1 - t_2'}{t_1 + t_2'} = 1, \quad (2.76)$$

Because  $t_2 = t_2' = 0$ , so that the Hall voltage is equal to the potential difference across the ends of the conductor and the Hall resistance equal to the normal two-terminal resistance.

Interestingly, in this mode the resistance given by the expression (2.4) with the highest degree of accuracy [4]. It is possible to imagine as if we would have the perfect ballistic conductor with only the boundary resistance. The length of conductors in experiments often reaches several hundred micrometers, such ballistic nature is amazing, and it was noted that the Nobel Prize in 1985 (Klaus von Klitzing).

Referring to graphene. In a previous publication [19] formulated the method of non-equilibrium Green's functions (NEGF) in the matrix formulation as applied to the modeling of transport problems of nanoelectronics, particularly for graphene ribbons have been the results of the calculation method NEGF transmission coefficient and the density of states for the two configurations tape borders - and zigzag armchair in the strong-coupling approximation in an orthogonal basis with a view of the parametric interaction of neighboring atoms only through the Coulomb  $\varepsilon$  and resonant  $t_0$  integrals (Hückel) in full agreement with the results of calculations with more accurate model Hamiltonians. Now we consider the external magnetic field to the graphene ribbons in the same approximation and the results of the calculation of the transmission coefficient

and the density of states in a magnetic field, as well as the quantum Hall effect and conductivity of graphene ribbons in a magnetic field [34].

We studied the system is a long 2D conductor wire with two trial probes on both sides of the guide (Fig. 2.22) to measure the cross of the Hall voltage produced in the presence of a magnetic field applied perpendicular to the surface of 2D conductor.

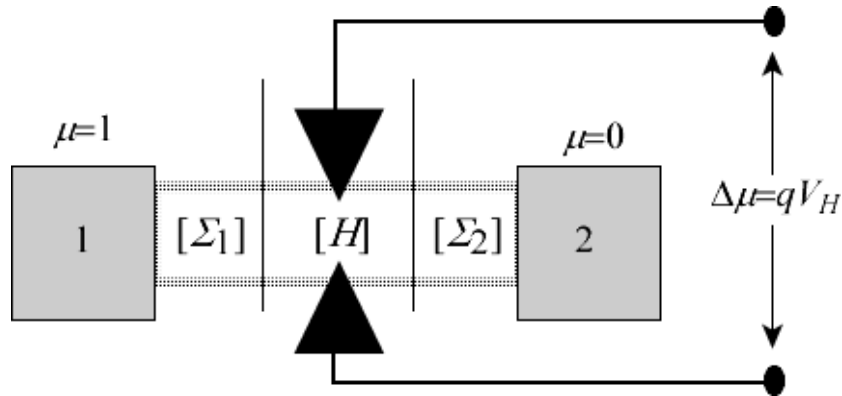


Figure 2.22 – For the measurement of the Hall voltage through the chemical potential difference generated between the transverse probes when the conductor perpendicular to the magnetic field

First, take into account the magnetic field in the Hamiltonian of the conductor  $H$  and contact matrices  $\Sigma_1$  and  $\Sigma_2$  method NEGF.

The energy of a particle of charge  $-q$  in the vector potential  $\vec{A}$  given by

$$E(\vec{r}, \vec{p}) = \frac{(\vec{p} + q\vec{A}) \cdot (\vec{p} + q\vec{A})}{2m} + U(\vec{r}). \quad (2.77)$$

To find the settings Hückel Hamiltonian with the magnetic field, consider a uniform lattice of atoms with a constant value  $E_c$  and a constant vector potential. First, consider the 1D conductor extending along an axis  $x$

$$E(p_x) = E_c + \frac{(p_x + qA_x)(p_x + qA_x)}{2m}, \quad (2.78)$$

so that the dispersion relation has the form

$$E(k_x) = E_c + \frac{(\hbar k_x + qA_x)(\hbar k_x + qA_x)}{2m} \quad (2.79)$$

and it can be approximated by a cosine function

$$E(k_x) = \varepsilon + 2t \cos\left(k_x a + \frac{qA_x a}{\hbar}\right) \quad (2.80)$$

with Hückel parameters  $\varepsilon$  and  $t$  [19]

$$\begin{aligned} \varepsilon &= E_c - 2t \\ t &= -\hbar^2 / 2ma^2 = -t_0, \end{aligned} \quad (2.81)$$

where  $a$  – is lattice constant. Unlike uniform lattice without the vector potential field [19] is only the appearance of a phase factor  $\exp(\pm iqA_x a/\hbar)$  have resonance integrals (Fig. 2.23).

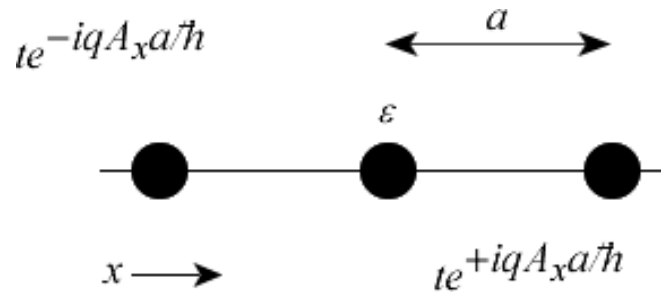


Figure 2.23 – Uniform 1D conductor in the field of the vector potential

For a homogeneous lattice 2D conductor phase factors with the phases

$$\varphi_x = \frac{qA_x a}{\hbar}, \quad \varphi_y = \frac{qA_y a}{\hbar} \quad (2.82)$$

appear in the resonance integrals in both directions of the conductor plane (Fig. 2.24).

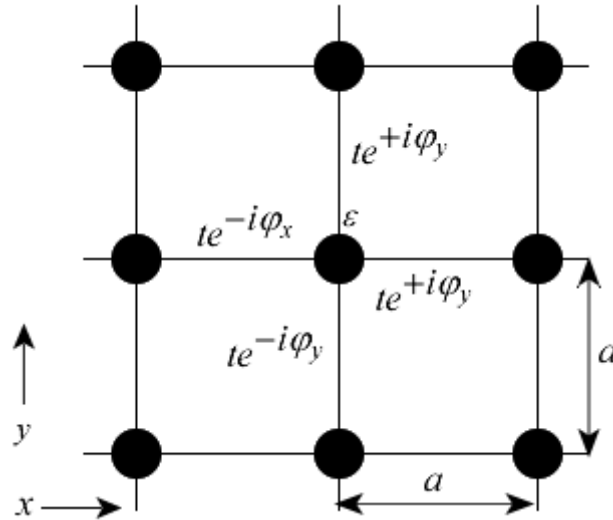


Figure 2.24 – Consideration of a magnetic field directed along the axis  $z$ , reduced to take into account the phase factors in the resonance integrals Hückel lattice

Magnetic field

$$\vec{B} = \vec{\nabla} \times \vec{A}, \quad (2.83)$$

so we are interested in a magnetic field perpendicular to the plane of the 2D conductor,

$$B_z = \frac{\partial A_y}{\partial x} - \frac{\partial A_x}{\partial y}. \quad (84)$$

Hall resistance given by the ratio of the Hall voltage to the current through the conductor (2.9). Hall voltage can be calculated in two ways. Using four-terminal measuring circuit and the Buttiker's equation, calculate the difference between the chemical potentials generated at the two transverse probe (Fig. 2.22). On the other, in the framework of NEGF [19] Next non-equilibrium Green's function  $G^n$

$$2\pi N = Tr[G^n] \quad (2.85)$$

proportional to the number of electrons, and the spectral function  $A$

$$2\pi D(E) = A \quad (2.86)$$

is proportional to the density of conditions, so that the fullness of condition  $j$  is the ratio of the corresponding diagonal elements of the Green's function and the spectral function

$$f(j) = \frac{G^n(j,j)}{A(j,j)} \cdot \quad (2.87)$$

In the linear response of the population is proportional to the chemical potential [15]. If one contact put in  $f = 0$ , and the other  $f = 1$ , so that the difference between them is  $qV$ , fullness  $f(j)$ , calculated from (2.87) by being multiplied by  $qV$ , give the value of the chemical potential

$$\mu(j) = qVf(j) \quad (2.88)$$

Fig. 2.25 shows the results of calculation of the Hall resistance, normalized to the quantum resistance  $h/q^2$ , as a function of magnetic field.

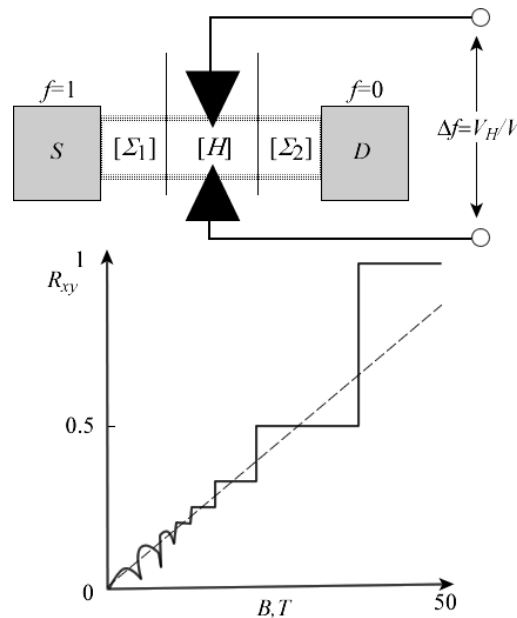


Figure 2.25 – Norm Hall resistance depends on the magnetic field to the graphene ribbon width  $W = 26 = 65 \text{ nm}$  in the Hückel approximation for energy  $E = t_0$  [19]

A remarkable result - it is the appearance of stairs in strong magnetic fields, known as the quantum Hall effect. First, however, let us turn to weak magnetic fields, where the Hall resistance, according to the standard semi-empirical theory of the Hall effect depends linearly on the magnetic field (2.9)

$$R_H = B / qn, \quad (2.89)$$

as shown in Fig. 2.25 by the dotted line, calculated for

$$n = \frac{N}{LW} = \frac{k^2}{4\pi} \quad (2.90)$$

at  $E = t_0 = 2.7 \text{ eV}$  and  $ka = \pi/3$  с  $a = 2.5 \text{ nm}$  [19].

As the magnetic field occurs gradually speed dependence of the Hall resistance of the field, obliged quantum effects in the form of the Landau levels (Fig. 2.26). In this screen shot postponed the diagonal elements of the spectral function  $A(j,j;E)$  depending on the energy  $E$  calculated by NEGF, and is a local width  $j$  of the graphene ribbons density of states for the three Landau levels.

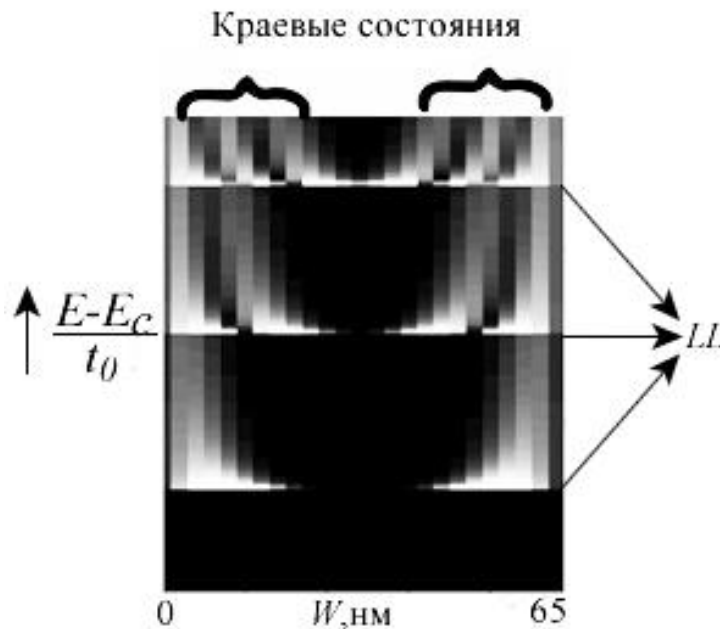


Figure 2.26 – Local by the width of the graphene ribbons density of states in the energy dependence of the Landau levels at  $B = 20 \text{ T}$

The energy of the Landau levels

$$E_n = \left( n + \frac{1}{2} \right) \hbar \omega_c, \quad (2.91)$$

where  $n$  – is integer,  $\omega_c$  – is cyclotron frequency (15). Equidistant Landau levels are arranged relative to each other with an increment

$$\hbar \omega_c = \frac{\hbar q B}{m} = \frac{2q B a^2}{\hbar} t_0, \quad (2.92)$$

expression is obtained by using (2.15) and (2.81). When used in calculating the values of  $B = 20 \text{ T}$  and  $a = 2.5 \text{ nm}$  the growth rate is found to be  $\hbar \omega_c \approx 0.37 t_0$  in good agreement with the results of the calculation method NEGF (Fig. 2.26).

The energy of the Landau levels (2.91) is the result of a purely quantum analytical solutions of the Schrödinger equation with the vector potential, which is also the basis of a numerical solution method NEGF specific geometry of the graphene ribbons. This result can be understood qualitatively, if we turn to the semi-classical model, in which the electrons move in circular orbits, making one revolution in time

$$t_c = \frac{2\pi}{\omega_c} = \frac{2\pi p}{qvB}, \quad (2.93)$$

so that the length of the orbit circle of radius  $r_c$

$$2\pi r_c = vt_c = \frac{2\pi p}{qB}. \quad (2.94)$$

If we now consider the quantum limit by which the circumference of the orbit must be such that it fit on the integer  $K$  de-Broglie wave length  $h/p$ , we obtain

$$\frac{2\pi p}{qB} = K \cdot h / p \quad (2.95)$$

Semiclassical electron can have any energy  $E = p^2/2m$ , however, the quantum limit in the form of equality of the circumference of an integer  $K$  to the wave length leads to

$$p^2 = K \cdot hqB, \quad (2.96)$$

so that the allowed values of energy

$$E = K \frac{\hbar qB}{2m} = K \frac{\hbar \omega_c}{2}, \quad (2.97)$$

which is not quite the same thing as the correct result (2.91), but the quality is quite acceptable.

If the number of edge states to identify as  $K_{es}$ , the resulting current

$$I_H = \frac{q^2}{h} V \cdot K_{es}, \quad (2.98)$$

since the Hall voltage  $V_H$  is simply equal to the voltage  $V$ , applied to the ends of the conductor, since one end of the conductor is in equilibrium with the source, and the other - to the drain.

This leads to a quantization of the Hall resistance

$$R_H = \frac{h}{q^2} \frac{1}{K_{es}}, \quad (2.99)$$

generating at normalized Hall resistance plateau at  $1/4$ ,  $1/3$ ,  $1/2$  and 1 (Fig. 2.25) as the magnetic field generates Landau levels, changing the number of boundary conditions  $K_{es}$  at energy  $E = t_0$  from 4 to 3, to 2, and to 1 (Fig. 2.26).

As for the distribution of electric current in a 2D conductor in a mode of observation of the quantum Hall effect, it is often used [35, 36] the semiclassical

model of electron motion along the so-called [37] open skipping orbits (Fig. 2.27). As a result, formed the boundary currents, providing exceptionally high ballistic conductivity.

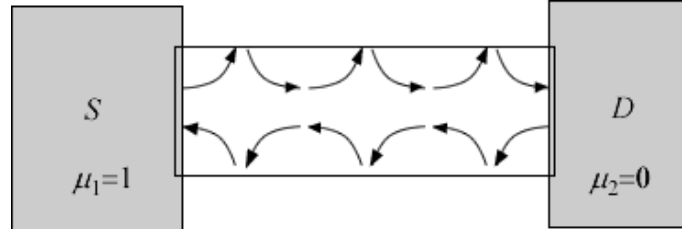


Figure 2.27 – It is believed that the electrons in the 2D conductor in a strong magnetic field move along open orbits, creating a compact track boundary currents, like localized in a quantum waveguide [37]

We have already cited the results of the calculation method NEGF transmission coefficient and the density of states of graphene ribbons for the two configurations tape borders - zigzag ZGNR / Zigzag Graphene NanoRibbon and armchair AGNR / Armchair GNR in the absence of a magnetic field [19]. The impact of a strong magnetic field is shown in Fig. 2.28.

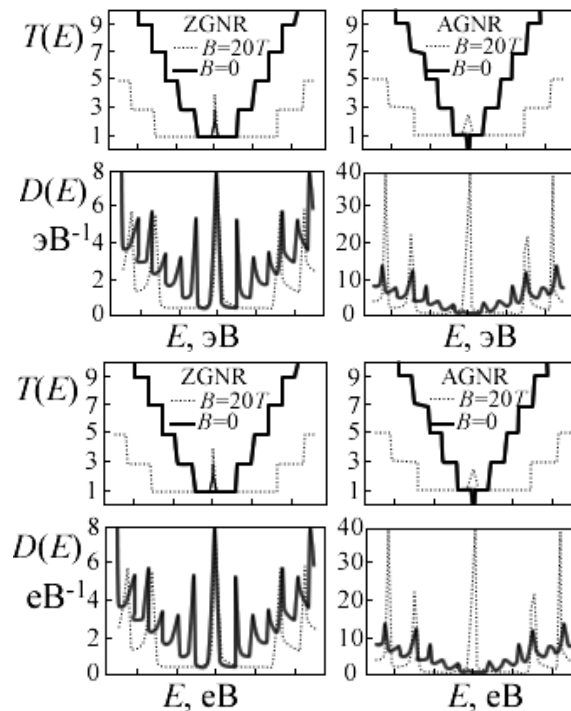


Figure 2.28 – The effect of a strong magnetic field  $B = 20 T$  on the transmission coefficient  $T(E)$  and the density of states  $D(E)$  of the graphene ribbons of width  $W = 53 nm$  for the two configurations of the borders – ZGNR and AGNR [34]

Landau levels (LL) in strong magnetic fields are formed in such 2D conductors, the width of which is sufficient for the formation of cyclotron orbits. The larger width of the conductor, the magnetic field requires minimal for generating a first LL. The energy levels of graphene Landau

$$E_n^{LL} = \pm v_0 \sqrt{2q\hbar n B}, \quad (2.100)$$

where the Fermi velocity assumed to be equal  $v_0 = 10^6 \text{ m/s}$  [38]. According to (2.100), first and second Landau levels at  $B = 20 \text{ T}$  occur when  $E_1^{LL} = 0.15 \text{ eV}$  and  $E_2^{LL} = 0.23 \text{ eV}$ . There is also a level of Landau  $E = 0$ , This zero Landau  $E_0^{LL}$  [39 – 41]. The results of the calculation method NEGF (Fig. 2.28) are fully consistent with the above estimates.

Outside of this work was the spin quantum Hall effect, which would be devoted to the following message.

## Chapter 3

### TRAFFIC SPIN MODEL NEGF AND QUANTUM SPIN HALL EFFECT

#### 3.1 Introduction

The use of magnetic contacts for generating spin current in the nonmagnetic channel conductivity even beyond the current flow using the test magnetic contact 2 with the polarization  $\vec{P}_2$  (Fig. 3.1) was considered in [1] based on the concept of chemical potential  $\mu$  of the charge and spin potential  $\vec{\mu}_s$ .

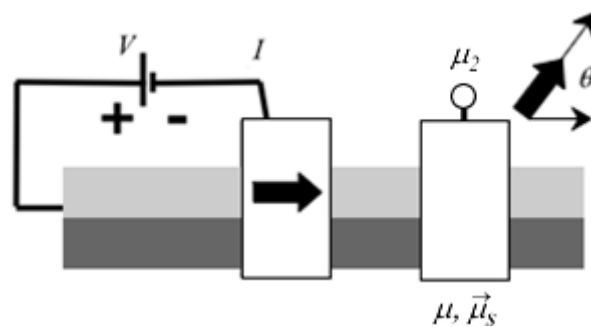


Figure 3.1 – The recording track 2 as the analyzer spin current

The relationship between the charge and spin potentials given by the simple expression

$$\mu_2 = \mu + \frac{\vec{P}_2 \cdot \vec{\mu}_s}{2}, \quad (3.1)$$

in which the polarization vector coincides with the direction of the recording pin 2 relative to the direction of the current and potential spin vector coincides with the direction of the spin polarization of the conduction channel, which has the agreement of the magnetization direction of the injection contact. Generally considered the parallel and antiparallel orientation of the magnetization of the contacts are special cases of the general expression (3.1). We have no reliable information whether to perform is actually similar experiments, i.e., injected back contact with a fixed magnetization direction, and the potential difference was measured by a rotating magnetic contact. Repeatedly, however, experiential

actually measured a similar situation, when both the magnetic contact were fixed relative to each other, and the spin of electrons in a conductor rotated by an external magnetic field.

All these effects are extremely interesting and important in themselves. We are, however, in this report We turn that show how these spin effects into account in the method of non-equilibrium Green's functions (NEGF) [2] in relation to the model of the transport problem of nanoelectronics, in particular, to consider the quantum spin Hall effect in graphene. It also shows how NEGF method leads to results corresponding to equation (3.1). Accounting for a spin in the method NEGF require the introduction of a matrix potential forms (2 x 2), which, as it turns out, can be expressed in terms of charge and spin potentials appearing in (3.1).

The spin polarization of electrons and photons are very similar, except that the notion of orthogonality for them has a different meaning. For photons orthogonal polarization is realized at  $90^\circ$ , and electrons - when  $180^\circ$ , which manifests itself in the non-local spin fluctuation building depending on the angle between the magnetic recording and injecting contacts (Fig. 3.2) [1].

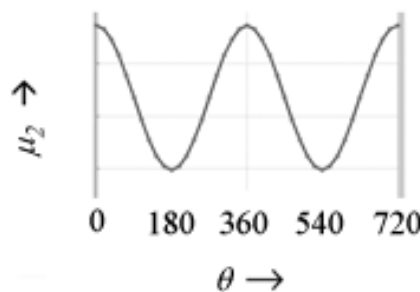


Figure 3.2 – Fluctuations nonlocal spin potential, depending on the angle between the magnetic recording and injecting contacts (Fig. 3.1)

Mathematically, an adequate description of the electron spins of orthogonality requires a spinor calculus, vector and not as in the case of the polarization of the photons. Vector is described by three real components along the axes  $x, y, z$  Cartesian coordinate system, and is described by two spinor complex components in the directions up ( $up$ ) and down ( $dn$ ):

$$\left\{ \begin{array}{c} n_x \\ n_y \\ n_z \end{array} \right\}, \quad \left\{ \begin{array}{c} \psi_{up} \\ \psi_{dn} \end{array} \right\},$$

where here and below, as before, [2] column vectors will be taking in braces, and square matrices - in rectangular.

Nevertheless, spinor should be seen as an object that has a definite direction as the vector. How consistent is the visual perception of a two-component spinor with its structure?

Spinor oriented along the direction of the unit vector  $\hat{n}$  with the projections on the axis of  $x, y, z$

$$\hat{n} \equiv \left\{ \begin{array}{c} \sin \theta \cos \phi \\ \sin \theta \sin \phi \\ \cos \theta \end{array} \right\} \quad (3.2)$$

described by two complex components  $c$  and  $s$ :

$$\left\{ \begin{array}{c} \cos \frac{\theta}{2} e^{-i\phi/2} \equiv c \\ \sin \frac{\theta}{2} e^{+i\phi/2} \equiv s \end{array} \right\}. \quad (3.3)$$

It is not obvious, but later we will show that the vector (3.2) and spin (3.3) presentation of the same abstract rotating object are identical, more isomorphic. Yet we perceive the equivalence (3.2) and (3.3) as something given.

When the spin formalism NEGF corresponding equations, of course, remain the same, but the order of the matrix - the Hamiltonian  $[H]$ , contact  $[\Sigma]$ , the non-equilibrium Green's function  $[G^n]$ , the spectral function  $[A]$  [2] is doubled by the fact that the electrons in the same quantum state coordinate, but with different spins are now described various basic functions. If earlier, when you do not take into account differences between the spins of the two electrons in the same quantum state, the number of basis functions is equal to  $N$ , but now the number of basis functions is  $2N$ . In quantum chemistry, this approach is

known as unlimited (in the back) Hartree - Fock (Unrestricted Hartee - Fock) [3, 4] or another method of different orbitals for different spins (Different Orbitals for Different Spins) [5] or split orbitals [6].

The simplest description of the conduction channel without loss of "physics", to which we always strive in Hückel approximation, better known in the physics literature as a method of strong coupling in orthogonal basis, taking into account only the interaction of neighboring atoms, the channel conductivity is considered not susceptible to back other words, the same interacts with electrons in different spin states. Hamiltonian  $[H]$  of conductor in Hückel approximation is now written in the same way as in [2], only the Coulomb  $\varepsilon$  and resonance  $t$  integrals are now written in a 2 x 2 matrix  $[\alpha]$  and  $[\beta]$  (Fig. 3.3), and namely:

$$\begin{aligned} [\alpha] &= \varepsilon[I], \\ [\beta_x] &= [\beta_y] = t[I], \end{aligned} \tag{3.4}$$

where  $[I]$  - the identity matrix of 2 x 2. In fact, there are two decoupled Hamiltonians, which does not carry any new "physics".

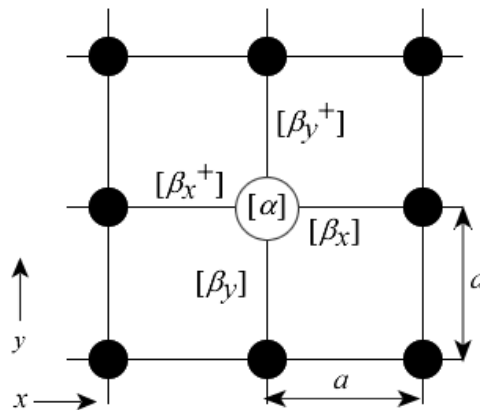


Figure 3.3 – Smooth 2D lattice with the lattice parameter  $a$ , in which each atom is described by Coulomb  $[\alpha]$  and resonance  $[\beta]$  integrals in the form of a 2 x 2 matrix

Similarly written matrix self-energy  $[\Sigma]$  contacts that this approach is equally react to different backs, multiplying their regular expressions [2] on the identity matrix  $[I_2]$ . This approach is expected to result in a trivial sense that we

seem to take into account only the back of the class, and only at the end of all the results of calculations just doubled.

All spin effects considered, for example, in [1], or arise as a result of accounting trivial contacts sensitive to the back and describe the corresponding contact matrices  $[\Sigma]$ , or the channel conductance is sensitive to the back and is described by the Hamiltonian corresponding  $[H]$  or occur both circumstances.

Now it is a look at some model transport problems by taking into account NEGF back and start with a simple one-level model of a spin valve. From the computational point of view, the only question is how to write the Hamiltonian and contact matrix, and then calculating the standard stroke [2].

### 3.2 One-level spin valve

It is known [1], reveals a different spin valve conductance  $G_P$  or  $G_{AP}$ , depending on the magnetization of the two parallel rows of contacts or antiparallel to AP. Magnetoresistance

$$MR = (G_p - G_{AP}) / G_{AP} \quad (3.5)$$

expressed in terms of the polarization  $P$  magnetic contacts

$$MR = \frac{P^2}{1 - P^2}, \quad (3.6)$$

which in turn is determined by the boundary resistance of the valve

$$P \equiv \frac{R - r}{R + r} \quad (3.7)$$

subject to the vanishing of the resistance of the channel conductivity.

In the magnetic tunnel junction (MTJ) in the expression for magnetoresistance dielectric conductor there is an additional deuce [1]:

$$MR = \frac{2P^2}{1 - P^2}, \quad (3.8)$$

the appearance of which can be seen from the tunnel conductors physics, according to which the resulting resistance of the two series-connected conductors is in proportion to their product, rather than the amount.

Now we get the same result, including multiplier device by applying the method to the one-level NEGF valve on the assumption that the equilibrium electrochemical potential  $\mu_0$  is much  $kT$  lower than the energy  $\varepsilon$  dielectric guide (Fig. 3.4).

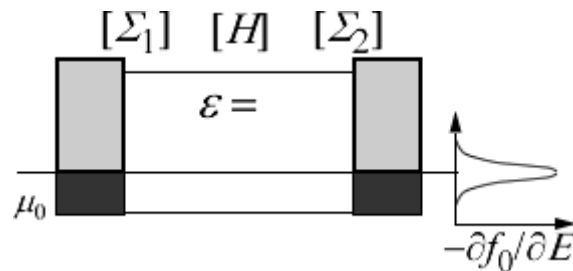


Figure 3.4 – Model equilibrium dielectric single layer conductor

According to the quantum model of single layer homogeneous 1D resistor without spin [2] and the contact Hamiltonian matrix is simply the numbers (Fig.3.5).

$$\begin{array}{ccc}
 \bullet & | & \bullet \\
 \Sigma_1 = -\frac{i}{2}[\gamma_1] & H = & -\frac{i}{2}[\gamma_2] = \Sigma_2 \\
 & [\varepsilon] & \\
 \Gamma_1 = [\gamma_1] & & [\gamma_2] = \Gamma_2 \\
 \bullet & | & \bullet
 \end{array}$$

Figure 3.5 – A homogeneous single-level 1D conductor without spin  
Own energy contacts

$$\gamma_1 = \hbar v_1, \quad (3.9a)$$

$$\gamma_2 = \hbar v_2 \quad (3.9b)$$

proportional to the speed with which the electrons leave the vehicle in the direction of contacts [2].

When taking into account the number of basis functions of spin doubles instead of numbers appear matrix of order 2: Hamiltonian, however, is simply a diagonal matrix, but the contact matrix for different spins "up"  $u$  and spin "down"  $d$  (Fig. 3.6).

$$\begin{array}{c}
 \begin{array}{ccc}
 \text{up/u} & \bullet & \\
 \text{dn/d} & \bullet & \\
 \end{array} \\
 \\
 \Sigma_1 = -\frac{i}{2} \begin{bmatrix} \gamma_{1u} & 0 \\ 0 & \gamma_{1d} \end{bmatrix} \\
 \\
 \Gamma_1 = \begin{bmatrix} \gamma_{1u} & 0 \\ 0 & \gamma_{1d} \end{bmatrix}
 \end{array}
 \quad \Bigg| \quad
 \begin{array}{c}
 \begin{array}{ccc}
 \bullet & & \\
 \bullet & & \\
 \end{array} \\
 \\
 H = \begin{bmatrix} \varepsilon & 0 \\ 0 & \varepsilon \end{bmatrix} \\
 \\
 \begin{array}{ccc}
 \bullet & & \\
 \bullet & & \\
 \end{array} \\
 \\
 \Sigma_2 = -\frac{i}{2} \begin{bmatrix} \gamma_{2u} & 0 \\ 0 & \gamma_{2d} \end{bmatrix} \\
 \\
 \Gamma_2 = \begin{bmatrix} \gamma_{2u} & 0 \\ 0 & \gamma_{2d} \end{bmatrix}
 \end{array}$$

Figure 3.6 – A homogeneous single-level 1D conductor with the spin (spin valve)

For spin valve immediately get retarded Green function [2]

$$[G^R] = \begin{bmatrix} E - \varepsilon + \frac{i}{2}(\gamma_{1u} + \gamma_{2u}) & 0 \\ 0 & E - \varepsilon + \frac{i}{2}(\gamma_{1d} + \gamma_{2d}) \end{bmatrix}^{-1} \quad (3.10)$$

and then the transmission coefficient

$$\bar{T} = Tr[\Gamma_1 G^R \Gamma_2 G^A] = \frac{\gamma_{1u} \gamma_{2u}}{(E - \varepsilon)^2 + \left(\frac{\gamma_{1u} + \gamma_{2u}}{2}\right)^2} + \frac{\gamma_{1d} \gamma_{2d}}{(E - \varepsilon)^2 + \left(\frac{\gamma_{1d} + \gamma_{2d}}{2}\right)^2}. \quad (3.11)$$

We must remember that we are now considering "not sensitive to the back" of the conduction channel.

For parallel magnetization configuration of contacts  $P$  both contacts can be considered the same, so that ( $\alpha > \beta$ )

$$\gamma_{1u} = \gamma_{2u} = \alpha, \quad (3.12a)$$

$$\gamma_{1d} = \gamma_{2d} \equiv \beta, \quad (3.12b)$$

whereas antiparallel configuration  $AP$  second contact overturns spin compared to the parallel configuration  $P$ , namely

$$\gamma_{1u} = \gamma_{2d} = \alpha, \quad (3.13a)$$

$$\gamma_{1d} = \gamma_{2u} \equiv \beta. \quad (3.13b)$$

Substituting (3.12a, 3.12b) to (3.8), we obtain  $P$ -passing coefficient

$$\bar{T}_p = \frac{\alpha^2}{(E - \varepsilon)^2 + \alpha^2} + \frac{\beta^2}{(E - \varepsilon)^2 + \beta^2}, \quad (3.14a)$$

and (3.13a, 3.13b) gives coefficient  $AP$ -passing

$$\bar{T}_{AP} = \frac{2\alpha\beta}{(E - \varepsilon)^2 + \left(\frac{\alpha + \beta}{2}\right)^2}. \quad (3.14b)$$

The measured conductivity is determined by the average value of the transmission coefficient at energies of a few  $kT$  around the value  $\mu_0$ . We are now considering a dielectric conductor (Fig. 3.4). Assuming

$$\varepsilon - \mu_0 \ll kT, \alpha, \beta, \quad (3.15)$$

we get

$$G_p \ll \bar{T}_p(E = \mu_0) = \frac{\alpha^2}{(\mu_0 - \varepsilon)^2 + \alpha^2} + \frac{\beta^2}{(\mu_0 - \varepsilon)^2 + \beta^2} \approx \frac{\alpha^2 + \beta^2}{(\mu_0 - \varepsilon)^2} \quad (3.16a)$$

and

$$G_{AP} \square \bar{T}_{AP}(E = \mu_0) \approx \frac{2\alpha\beta}{(\mu_0 - \varepsilon)^2}, \quad (3.16b)$$

and to obtain the desired magnetoresistance formula (3.8)

$$MR \equiv \frac{G_p}{G_{AP}} - 1 = \frac{\alpha^2 + \beta^2}{2\alpha\beta} - 1 = \frac{2P^2}{1 - P^2} \quad (3.17)$$

with polarization

$$P \equiv \frac{\alpha - \beta}{\alpha + \beta}. \quad (3.18)$$

Similarly, you can obtain a formula for the magnetoresistance (3.6) non-magnetic metallic conductor, if we assume that the chemical potential  $\mu_0$  is near the level of energy  $\varepsilon$ , and  $kT \gg \alpha, \beta$ .

**The rotation of the magnetic contacts.** The spin valve mode  $AP$  second contact overturns back compared with the valve in the  $P$  mode, so that

$$\Gamma_1 = \begin{bmatrix} \alpha & 0 \\ 0 & \beta \end{bmatrix}, \quad \Gamma_2 = \begin{bmatrix} \beta & 0 \\ 0 & \alpha \end{bmatrix}. \quad (3.19)$$

How to write the matrix  $\Gamma$  contact oriented in any direction of the unit vector  $\hat{n}$  by its projection (3.2) along the axes  $x, y, z$ ? Final formula is

$$\Gamma = \frac{\alpha + \beta}{2} [I] + \frac{\alpha - \beta}{2} \begin{bmatrix} n_z & n_x - in_y \\ n_x + in_y & -n_z \end{bmatrix}, \quad (3.20)$$

where  $I$  - identity matrix of order 2. The formula is not immediately obvious, but we soon got it. In the meantime, make sure that the formula contains special cases of parallel and antiparallel orientation of the magnetizations of contacts, respectively:

$$n_z = +1, \quad n_x = n_y = 0: \quad \Gamma = \begin{bmatrix} \alpha & 0 \\ 0 & \beta \end{bmatrix}, \quad (3.21a)$$

$$n_z = -1, \quad n_x = n_y = 0: \quad \Gamma = \begin{bmatrix} \beta & 0 \\ 0 & \alpha \end{bmatrix}. \quad (3.21b)$$

Verify the validity of the general formula (3.20) can be achieved by the following observation. Matrix

$$\tilde{\Gamma} = \begin{bmatrix} \alpha & 0 \\ 0 & \beta \end{bmatrix} \quad (3.22)$$

describes a magnetic contact is oriented along an arbitrary direction of the unit vector  $\hat{n}$ , if the direction of the reference axis to select the  $+\hat{n}$  and  $-\hat{n}$  instead of the standard Cartesian semiaxes  $+\hat{n}$  and  $-\hat{n}$ . Go back to the standard basis  $\pm\hat{n}$  possible by a unitary transformation matrix  $\Gamma = V \tilde{\Gamma} V^+$  (3.22):

$$\begin{array}{c} \hat{n} \quad -\hat{n} \\ \hat{z} \quad \begin{bmatrix} c & -s^* \\ s & c^* \end{bmatrix} \\ -\hat{z} \end{array} \quad \begin{array}{c} \hat{n} \quad -\hat{n} \\ \hat{n} \quad \begin{bmatrix} \alpha & 0 \\ 0 & \beta \end{bmatrix} \\ -\hat{n} \end{array} \quad \begin{array}{c} \hat{z} \quad -\hat{z} \\ \hat{n} \quad \begin{bmatrix} c^* & s^* \\ -s & c \end{bmatrix} \\ -\hat{n} \end{array}, \quad (3.23)$$

$V \qquad \qquad \qquad V^+$

where speakers unitary transformation matrix  $[V]$  are the components of the spinor  $c$  and  $s$  (3.3) in the directions  $\pm\hat{n}$ . The first column of the matrix  $V$  corresponds to the direction  $+\hat{n}$ , and the second column corresponds to the direction  $-\hat{n}$  with the components of the spinor  $-s^*$  and  $c^*$ , which are obtained from (3.3) by converting the angles

$$\theta \rightarrow \pi - \theta \quad \text{and} \quad \phi \rightarrow \pi + \phi \quad (3.24)$$

and removal of both components of the overall phase factor.

Multiply the three matrices in (3.23) gives

$$\Gamma = \begin{bmatrix} c & -s^* \\ s & c^* \end{bmatrix} \begin{bmatrix} \alpha & 0 \\ 0 & \beta \end{bmatrix} \begin{bmatrix} c^* & s^* \\ -s & c \end{bmatrix} = \begin{bmatrix} c & -s^* \\ s & c^* \end{bmatrix} \begin{bmatrix} \alpha c^* & \alpha s^* \\ -\beta s & \beta c \end{bmatrix} = \begin{bmatrix} \alpha c c^* + \beta s s^* & (\alpha - \beta) c s^* \\ (\alpha - \beta) s c^* & \alpha s s^* + \beta c c^* \end{bmatrix} \quad (3.25)$$

Using the definition of the components of the spinor  $c$  and  $s$  (3.3) and trigonometric equations

$$2 \cos^2 \frac{\theta}{2} = 1 + \cos \theta, \quad 2 \sin^2 \frac{\theta}{2} = 1 - \cos \theta \quad \text{и} \quad 2 \sin \frac{\theta}{2} \cos^2 \frac{\theta}{2} = \sin \theta, \quad (3.26)$$

rewrite (3.25) in the form

$$\Gamma = \frac{1}{2} \begin{bmatrix} (\alpha + \beta) + (\alpha - \beta) \cos \theta & (\alpha - \beta) \sin \theta e^{-i\phi} \\ (\alpha - \beta) \sin \theta e^{+i\phi} & (\alpha + \beta) - (\alpha - \beta) \cos \theta \end{bmatrix}, \quad (3.27)$$

resulting in the desired formula (3.20), to use the expression (3.2) for the components of the unit vector  $\hat{n}$  along the axes  $x, y, z$ .

If the polarization vector

$$\vec{P} \equiv P \hat{n} = \frac{\alpha - \beta}{\alpha + \beta} \hat{n} \quad (3.28)$$

to determine its value (3.18) and a unit vector  $\hat{n}$ , then the equation (3.20) can be rewritten as

$$\Gamma = \frac{\alpha + \beta}{2} \left( [I] + \begin{bmatrix} P_z & P_x - iP_y \\ P_x + iP_y & -P_z \end{bmatrix} \right) \quad (3.29)$$

or even otherwise

$$\frac{[\Gamma]}{(\alpha + \beta)/2} = \begin{bmatrix} 1 & 0 \\ 0 & 1 \end{bmatrix} + P_x \begin{bmatrix} 0 & 1 \\ 1 & 0 \end{bmatrix} + P_y \begin{bmatrix} 0 & -i \\ +i & 0 \end{bmatrix} + P_z \begin{bmatrix} 1 & 0 \\ 0 & -1 \end{bmatrix} \quad (3.30)$$

through widely used in quantum theory of Pauli spin matrices

$$\sigma_x \equiv \begin{bmatrix} 0 & 1 \\ 1 & 0 \end{bmatrix}, \quad \sigma_y \equiv \begin{bmatrix} 0 & -i \\ +i & 0 \end{bmatrix}, \quad \sigma_z \equiv \begin{bmatrix} 1 & 0 \\ 0 & -1 \end{bmatrix} . \quad (3.31)$$

Finally, equation (3.29) can be compactly rewritten as

$$\Gamma = \frac{\alpha + \beta}{2} ([I] + [\sigma_x]P_x + [\sigma_y]P_y + [\sigma_z]P_z) = \frac{\alpha + \beta}{2} ([I] + [\vec{\sigma}] \cdot \vec{P}). \quad (3.32)$$

Similarly, it is possible to rewrite the delivery matrix compactly own energy. Suppose, for example, in the basis  $\pm \hat{n}$

$$\tilde{\Sigma} = -\frac{i}{2} \begin{bmatrix} \alpha & 0 \\ 0 & \beta \end{bmatrix}, \quad (3.33)$$

then in the basis  $\pm \hat{z}$  we have:

$$\Sigma = -i \frac{\alpha + \beta}{4} [I] - i \frac{\alpha - \beta}{4} [\vec{\sigma}] \cdot \hat{n} = -i \frac{\alpha + \beta}{4} ([I] + [\vec{\sigma}] \cdot \vec{P}). \quad (3.34)$$

**The spin Hamiltonians.** Let us now discuss the spin-dependent Hamiltonians and consider keeping the classical spin-orbit and Zeeman splitting and Hamiltonian Rashba [7, 8].

**Hamiltonian with Zeeman splitting.** Let the direction of the magnetic field  $\vec{B}$  is determined by the unit vector  $\hat{n}$ . The Hamiltonian in the basis  $\pm \hat{n}$  has the form

$$\mu_{el} \begin{bmatrix} +B & 0 \\ 0 & -B \end{bmatrix}, \quad (3.35)$$

where  $\mu_{el}$  - magnetic moment of the electron. The level of positive spin moves up the value of  $\mu_{el} B$ , but with a negative spin shifted down by the same amount (Zeeman splitting).

The basis  $\pm \hat{z}$  have:

$$H_B = \mu_{el} \vec{\sigma} \cdot \vec{B}. \quad (3.36)$$

More need add to spin-independent part of the Hamiltonian. In the case of a parabolic dispersion have

$$H = \frac{\hbar^2}{2m} (k_x^2 + k_y^2) [I] + \mu_{el} \vec{\sigma} \cdot \vec{B}, \quad (3.37)$$

and for a homogeneous 2D lattice in Hückel approximation with resonant and Coulomb integrals [2]

$$t = -\hbar^2 / 2m\alpha^2, \quad (3.38)$$

$$\varepsilon = E_c - 4t \quad (3.39)$$

Hamiltonian has the form:

$$H = (\varepsilon + 2t \cos k_x a + 2t \cos k_y a) [I] + \mu_{el} \vec{\sigma} \cdot \vec{B}, \quad (3.40)$$

where  $a$  - lattice parameter. For such a lattice (Fig. 3.3) the resonant and Coulomb matrix have the form:

$$\begin{aligned} \alpha &= \varepsilon [I] + \mu_{el} \vec{\sigma} \cdot \vec{B} \\ \beta_x &= t [I], \quad \beta_y = t [I]. \end{aligned} \quad (3.41)$$

Compared with the spin-independent Hamiltonian (3.4) changes only the Coulomb matrix.

### 3.3 Rashba Hamiltonian

A more complete account of the spin-orbit interaction gives the Hamiltonian

$$H_R = \eta \hat{z} \cdot (\vec{\sigma} \times \vec{k}) = \eta (\sigma_x k_y - \sigma_y k_x), \quad (3.42)$$

where  $\eta$  - Rashba parameter [7 - 9]. This Hamiltonian relativistic origin has caused them effects commonly observed experimentally and reliably interpreted. [9] We also are now only interested in one thing - how to take into account the interaction Rashba for our homogeneous 2D lattice Hückel approximation. To that end, approximate (3.42), sinuses

$$H_R = \frac{\eta}{\alpha} (\sigma_x \sin k_y a - \sigma_y \sin k_x a) \quad (3.43)$$

and write for the sake of convenience in terms of exponentials

$$H_R = \frac{\eta}{2ia} \sigma_x (e^{+ik_y a} - e^{-ik_y a}) - \frac{\eta}{2ia} \sigma_y (e^{+ik_x a} - e^{-ik_x a}), \quad (3.44)$$

the factors to which the

$$\begin{aligned} \beta_x &= \frac{i\eta}{2a} \sigma_y, & \beta_x^+ &= -\frac{i\eta}{2a} \sigma_y \\ \beta_y &= -\frac{i\eta}{2a} \sigma_x, & \beta_y^+ &= \frac{i\eta}{2a} \sigma_x \end{aligned} \quad (3.45)$$

ensure proper dispersion relation (3.37).

We take into account the spin-independent part of the Hamiltonian 2D lattice (3.4), and a constant magnetic field (3.41) through the Zeeman splitting. Finally Coulomb and resonance homogeneous matrix 2D lattice with the Zeeman spin-orbit interaction and Rashba interaction have the form:

$$\begin{aligned} \alpha &= \varepsilon I + \mu_{el} \vec{\sigma} \cdot \vec{B}, \\ \beta_x &= tI + \frac{i\eta}{2a} \sigma_y, & \beta_x^+ &= tI - \frac{i\eta}{2a} \sigma_y, \\ \beta_y &= tI - \frac{i\eta}{2a} \sigma_x, & \beta_y^+ &= tI + \frac{i\eta}{2a} \sigma_x. \end{aligned} \quad (3.46)$$

We note that the Rashba interaction is taken into account using the parameter Rashba and the Pauli matrices in resonance matrices 2D lattice, and the Zeeman interaction - in the Coulomb matrices.

**Spinors and vectors.** We usually visually imagine the spin as a rotating object-oriented in a particular direction. He described two complex components spinor (3.3), and the vector in the same direction defined by the three actual projections (3.2) on the axis of a Cartesian coordinate system. To feel the connection between the two views of the same direction of the object - vector and spinor is useful to consider the spin precession in a magnetic field in both views.

Consider the single-level resistor with  $\varepsilon = 0$  in a magnetic field directed along the axis  $z$ . Two-component Schrödinger equation

$$\frac{d}{dt} \begin{Bmatrix} \psi_u \\ \psi_d \end{Bmatrix} = \frac{\mu_{el} B_z}{i\hbar} \begin{bmatrix} 1 & 0 \\ 0 & -1 \end{bmatrix} \begin{Bmatrix} \psi_u \\ \psi_d \end{Bmatrix}, \quad (3.47)$$

where the right is the spin matrix  $\sigma_z$ , actually has two differential equations with obvious solutions

$$\begin{aligned} \psi_u(t) &= \psi_u(0) e^{-i\omega t/2} \\ \psi_d(t) &= \psi_d(0) e^{+i\omega t/2}, \end{aligned} \quad (3.48)$$

where the frequency of precession

$$\omega \equiv \frac{2\mu_{el} B_z}{\hbar}. \quad (3.49)$$

Let the spin of the electron in the initial time  $t = 0$  is directed along the unit vector  $\hat{n}$  angles  $\theta$  and  $\varphi$  with respect to the selected reference frame (Fig. 3.7).

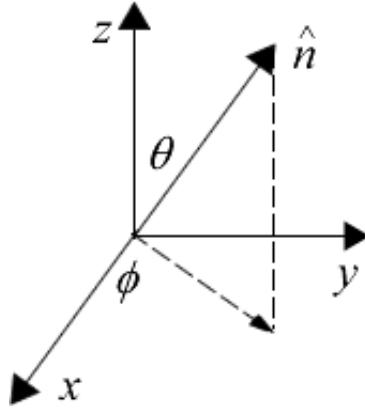


Figure 3.7 – To spin precession directed along a single vector, the angle  $\phi$

During this initial time it wavefunctions

$$\left\{ \begin{array}{l} \psi_u(0) = \cos \frac{\theta}{2} e^{-i\phi/2} \\ \psi_d(0) = \sin \frac{\theta}{2} e^{+i\phi/2} \end{array} \right\}, \quad (3.50)$$

and at subsequent times

$$\left\{ \begin{array}{l} \psi_u(t) = \cos \frac{\theta}{2} e^{-i\phi/2} e^{-i\omega t/2} \\ \psi_d(t) = \sin \frac{\theta}{2} e^{+i\phi/2} e^{+i\omega t/2} \end{array} \right\}, \quad (3.51)$$

which corresponds to the spin rotation around the axis  $z$  at a fixed angle to it  $\theta$ , while the angle  $\phi$  increases linearly over time:

$$\phi(t) = \phi(0) + \omega t. \quad (3.52)$$

According to (3.2), for the projection of the unit vector, we have:

$$\begin{aligned} n_x &= \sin \theta \cos \phi(t), \\ n_y &= \sin \theta \sin \phi(t), \\ n_z &= \cos \theta, \end{aligned} \quad (3.53)$$

where with (3.52) we obtain

$$\frac{dn_x}{dt} = -\omega n_y, \quad \frac{dn_y}{dt} = +\omega n_x \quad (3.54)$$

or in matrix form for all three components of the unit vector

$$\frac{d}{dt} \begin{Bmatrix} n_x \\ n_y \\ n_z \end{Bmatrix} = \omega \begin{bmatrix} 0 & -1 & 0 \\ +1 & 0 & 0 \\ 0 & 0 & 0 \end{bmatrix} \begin{Bmatrix} n_x \\ n_y \\ n_z \end{Bmatrix}, \quad (3.55)$$

where a square matrix, usually denoted by  $R_z$ , is the matrix of rotation around the axis of the unit vector  $z$ .

Compare the equation (3.55) with the Schrodinger equation (3.47) in the spinor representation, rewritten through the precession frequency (3.49)

$$\frac{d}{dt} \begin{Bmatrix} \psi_u \\ \psi_d \end{Bmatrix} = \frac{\omega}{2i} \begin{bmatrix} 1 & 0 \\ 0 & -1 \end{bmatrix} \begin{Bmatrix} \psi_u \\ \psi_d \end{Bmatrix}, \quad (3.56)$$

which featured Pauli matrix  $\sigma_z$ .

Suppose we wish to describe the precession of the electron spin in a magnetic field directed along  $x$ . To do this in the equation (3.55) need only perform a cyclic permutation of variables:  $x \rightarrow y$ ,  $y \rightarrow z$ ,  $z \rightarrow x$  and we obtain the equation with a rotation matrix  $R_x$ :

$$\frac{d}{dt} \begin{Bmatrix} n_x \\ n_y \\ n_z \end{Bmatrix} = \omega \begin{bmatrix} 0 & 0 & 0 \\ 0 & 0 & -1 \\ 0 & +1 & 0 \end{bmatrix} \begin{Bmatrix} n_x \\ n_y \\ n_z \end{Bmatrix}; \quad (3.57)$$

in the equation (3.55) -1 was at the intersection of row  $x$  and column  $y$ , in (3.57), it will be at the intersection of row  $y$  and column  $z$ .

Not immediately apparent how the same purpose to modify the equation (3.56). The correct answer is:

$$\frac{d}{dt} \begin{Bmatrix} \psi_u \\ \psi_d \end{Bmatrix} = \frac{\omega}{2i} \begin{bmatrix} 0 & 1 \\ 1 & 0 \end{bmatrix} \begin{Bmatrix} \psi_u \\ \psi_d \end{Bmatrix}, \quad (3.58)$$

which featured Pauli matrix  $\sigma_x$ .

Equations (3.55) and (3.56) as equations (3.57) and (3.58) describe the same physical process, namely, the rotation of the spin of an electron in a magnetic field directed along the axis  $z$ , respectively along the axis  $x$ , in the first case - three real components, and in the second - two complex. Circular permutation in the opposite direction will give us a rotation matrix  $R_y$ , and the corresponding spin matrix  $\sigma_y$  shown in the summary (3.31).

What makes the rotation matrix and spin matrices isomorphic, allowing them to describe the same physical process? The answer is that these matrices same commutation relations.

It is easy to make sure that the rotation matrix

$$R_x = \begin{bmatrix} 0 & 0 & 0 \\ 0 & 0 & -1 \\ 0 & +1 & 0 \end{bmatrix}, \quad R_y = \begin{bmatrix} 0 & 0 & +1 \\ 0 & 0 & 0 \\ -1 & 0 & 0 \end{bmatrix}, \quad R_z = \begin{bmatrix} 0 & -1 & 0 \\ +1 & 0 & 0 \\ 0 & 0 & 0 \end{bmatrix} \quad (3.59)$$

subject to the following commutation relations:

$$\begin{aligned} [R_x, R_y] &\equiv R_x R_y - R_y R_x = R_z \\ [R_y, R_z] &\equiv R_y R_z - R_z R_y = R_x \\ [R_z, R_x] &\equiv R_z R_x - R_x R_z = R_y \end{aligned} \quad (3.60)$$

where on the left there are the standard notation corresponding switches.

Pauli spin matrices obey the same commutation relations if  $R$  is formally replaced by  $\sigma/2i$ :

$$\begin{aligned} [\sigma_x, \sigma_y] &\equiv \sigma_x \sigma_y - \sigma_y \sigma_x = 2i\sigma_z \\ [\sigma_y, \sigma_z] &\equiv \sigma_y \sigma_z - \sigma_z \sigma_y = 2i\sigma_x \\ [\sigma_z, \sigma_x] &\equiv \sigma_z \sigma_x - \sigma_x \sigma_z = 2i\sigma_y \end{aligned} \quad (3.61)$$

Note that in the standard textbooks of quantum mechanics, the Pauli spin matrices are usually introduced hypothetically.

What should be the spinor components have directed along the axis  $z$ ? Since the spinor does not change during the rotation around the axis  $z$ , then its components must be eigenvectors spin matrix  $\sigma_z$  in summary (3.31):

$$\begin{Bmatrix} 1 \\ 0 \end{Bmatrix} \quad \text{or} \quad \begin{Bmatrix} 0 \\ 1 \end{Bmatrix}, \quad (3.62)$$

representing really spin "up" or spin "down" along the axis  $z$ .

If we want to learn the components of the spinor, directed along the axis of  $x$ , then you need to find your own spin vectors of a matrix  $\sigma_x$ , which are the vectors

$$\begin{Bmatrix} +1 \\ +1 \end{Bmatrix} / \sqrt{2} \quad \text{or} \quad \begin{Bmatrix} +1 \\ -1 \end{Bmatrix} / \sqrt{2}, \quad (3.63)$$

representing the direction of the spin "up" along the positive half or spin "down" along the negative semiaxis of axis  $x$ .

In general, if we want to find the components of the spinor directed along arbitrarily oriented unit vector  $\hat{n}$  (3.2) must be sought eigenvectors

$$\vec{\sigma} \cdot \hat{n} = \sigma_x \sin \theta \cos \phi + \sigma_y \sin \theta \sin \phi + \sigma_z \cos \theta = \begin{bmatrix} \cos \theta & \sin \theta e^{-i\phi} \\ \sin \theta e^{+i\phi} & -\cos \theta \end{bmatrix}, \quad (3.64)$$

designated earlier as

$$\begin{Bmatrix} c \\ s \end{Bmatrix} \quad \text{and} \quad \begin{Bmatrix} -s^* \\ c^* \end{Bmatrix},$$

the first of which corresponds to the orientation of the spin vector  $\hat{n}$  along the positive direction and are given explicitly in (3.3).

### 3.4 The spin precession

We already know how to make the Hamiltonian  $H$  and the contact matrix  $\Sigma$ , including taking into account the nontrivial spin effects, and are ready to calculate the numerical models by calculating the electron density through non-equilibrium Green's function  $G^n$ , the density of states of the spectral function of  $A$  and the current [2].

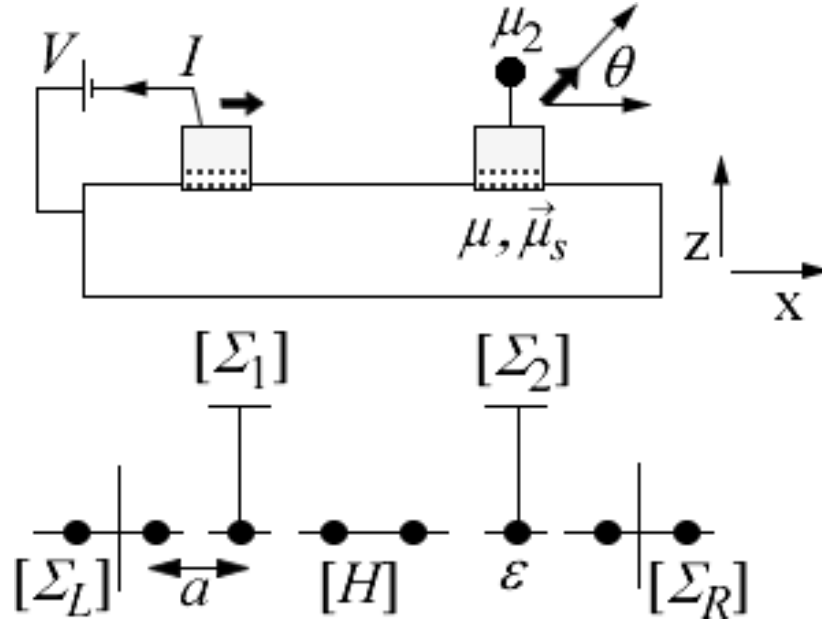


Figure 3.8 – For the measurement and calculation method NEGF spin-building within four-terminal model homogeneous 1D conductor with two magnetic probes, described the contact matrices  $\Sigma_1$  and  $\Sigma_2$

First, calculate the potential at the second probe, described the contact matrix  $\Sigma_2$ , homogeneous 1D conductor (Fig. 3.8) with a simple method NEGF Hamiltonian without spin effects depending on the angle  $\theta$  of the magnetic probe 2 with respect to the linear conductor (floating contact). The calculated results for different values of the polarization (3.7)  $P_2$  2nd probe relative 1st shown in Fig. 3.9.

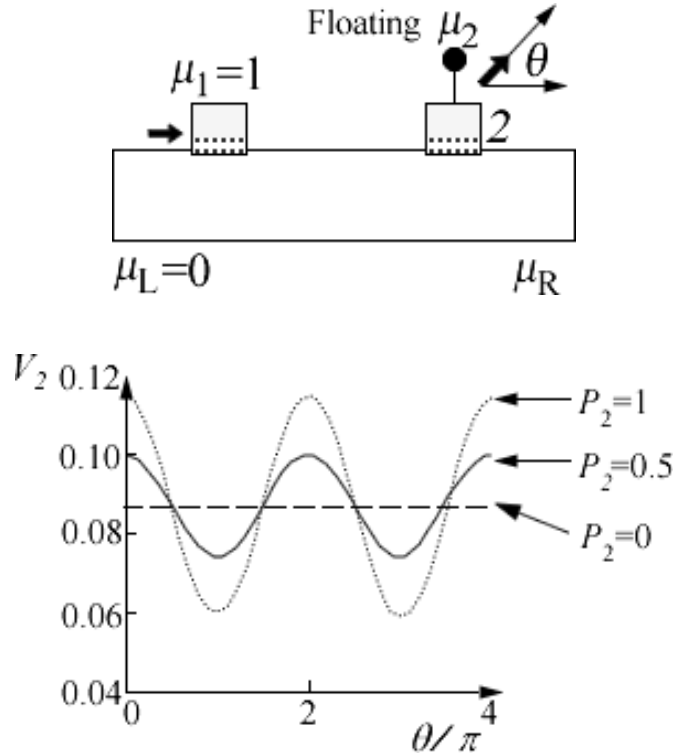


Figure 3.9 – Change in building 2nd probe relative to the 1st according to the angle of inclination, normalized to  $180^\circ$ , for different values of mutual polarization probes [10]

Fully supported by NEGF calculation formula (3.1): measured potential oscillates depending on the angle of inclination of the magnetic contact relative to another. At zero polarization measured contact potential remains constant. As mentioned at the outset, there is no evidence that similar experiments with a floating magnetic contact is really carried out. Were, however, experiments with the rotation of the spin of electrons in the conduction channel with a fixed geometry relative arrangement of the magnetic contacts.

One of the most common methods is the application of an external magnetic field that causes the precession of spin to the direction of the magnetic field with the angular frequency  $\omega$  (3.49). This means that the potential spin  $\mu_2$  at a point where the test probe 2, turn on the corner  $\omega\tau$ , where  $\tau$  is the time of passage of the electron-injecting contact way to test probe 2. Writing  $\tau = L/v$ , the equations (3.1) and (3.49) we have:

$$\mu_2 = \mu + P_2 \mu_s \cos \frac{2\mu_{el}L}{\hbar v} B_z. \quad (3.65)$$

You can expect to see an oscillating potential of the probe 2, depending on the magnitude of the applied magnetic field. However, it is usually not observed ballistic transport, and there is a large scatter in the values of the time  $\tau$ , resulting in a potential averaged over all the times  $\tau$  vanishes. Typical experiments instead of the oscillating signal, depending on the magnetic field, show a decrease in the value of building  $P_2\mu_s$  down to zero (the effect Hanley [11, 12]). Nevertheless, the effect of oscillations in Hanley observe managed by reducing the time variation  $\tau$  so that the spread was much less than the average time  $\tau$  [13].

Another approach to the rotation of the electron spin can serve Rashba effect in conductors with a strong spin-orbit interaction. It is now well established as an example of many semiconductors, the electric field along the axis  $z$  (Fig. 3.8) leads to an effective magnetic field, which depends on the momentum of the electron. This can be seen by comparing the Hamiltonian with the magnetic field (3.36) with Rashba Hamiltonian (3.42), which, for convenience, be rewritten as

$$H_R = \eta \hat{z} \cdot (\vec{\sigma} \times \vec{k}) = \eta \vec{\sigma} \cdot (\vec{k} \times \hat{z}), \quad (3.66)$$

where for the effective magnetic field, obliged Rashba interaction, we get

$$\mu_{el} \vec{B}_{eff} = \eta \hat{z} \times \vec{k}, \quad (3.67)$$

so that according to (3.65) can be expected oscillatory potential species

$$\mu_2 = \mu + P_2 \mu_s \cos \frac{2\eta k L}{\hbar v} \quad (3.68)$$

with period

$$\frac{2kL}{\hbar v} \Delta\eta = 2\pi \quad \text{or else} \quad \Delta\eta = \frac{2\pi a t_0}{kL} \sin ka. \quad (3.69)$$

This conclusion is in good agreement with the numerical results obtained by NEGF for energy corresponding to  $ka = \pi/3$  when the distance between the injector and the detector  $L = 40a$  (Fig. 3.10).

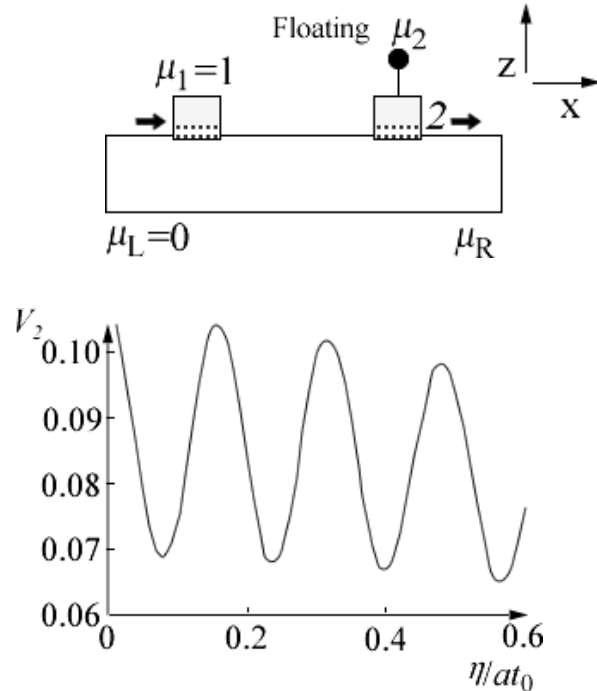


Figure 3.10 – In conductors with a large value of the coefficient  $\eta$  Rashba potential probe 2 oscillates if the magnetization of both probes are directed along the conductor (axis  $x$ ); oscillations disappear when the magnetization perpendicular to the conductor (axis  $z$ ) [10]

In this model, electrons moving along the axis  $x$  in its positive direction, are influenced by the effective magnetic field along the axis  $y$ . As the injected electrons have spin potential directed along the magnetization probes 1 and 2 (axis  $x$ ), the spin potential  $\vec{\mu}_s$  should rotate. Oscillations of the building disappear if the magnetization of both probes are directed along the axis  $y$ . This effect was confirmed experimentally [14, 15].

### 3.5 The quantum spin Hall effect

Transport polarized spins in non-magnetic materials such as copper, studied adequately and physical foundations generally clear. This is not the diffusion of spins in materials with strong spin-orbit interaction.

In the last decade, attention has been paid to the quantum spin Hall effect (COAG). In the conventional classic Hall effect electrons moving from the source to the drain along the axis  $x$ , by the magnetic field directed perpendicular to the surface of the 2D conductor, along the axis  $z$ , are twisted, so that a potential difference is created along a transverse axis  $y$  (Fig. 3.11) [24].

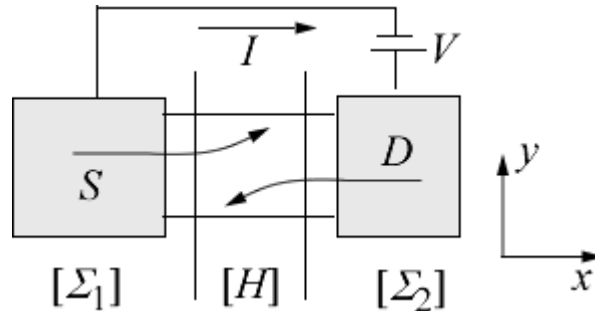


Figure 3.11 – By the choice of coordinate system when discussing the effect of the QSH

QSH effect can be understood in terms of the model, according to which the effective magnetic field spins spins polarized along semiaxes  $+z$  and  $-z$ , in opposite directions, whereas in the classical Hall effect, both varieties of spin to spin in the same direction.

Since the electrons in a conductor with a strong spin-orbit interaction are acted effective magnetic field is natural to ask whether it is possible to observe the Hall effect in the absence of an external magnetic field, but only under the influence of the internal effective magnetic field.

The answer is positive, but a similar phenomenon with a twist spin polarized along the  $+z$  and  $-z$ , in opposite directions is very delicate phenomenon as the charges are not accumulated in the transverse direction and the Hall voltage vanishes. However, the spin potential can be measured by magnetic contacts.

In the first experiments the accumulation of spins opposite polarization in the transverse direction (QSH) found in the bulk semiconductor optical probe [25], and recently QSH this type probes to measure the magnetic nanoconductors [15].

The transport model based on the method NEGF [2] adequately describes QSH, as evidenced by the results of the calculation of a homogeneous 2D conductor (Fig. 3.10) by Rashba factor  $\eta = 1 \cdot 10^{-11} \text{ eV} \cdot \text{m}$  with the energy  $E =$

$0.05t_0$  and variable width  $W$  (Fig. 3.12). For isolating the  $z$ -component of the spin density of the Green's function  $G^n$  used equation (3.65).

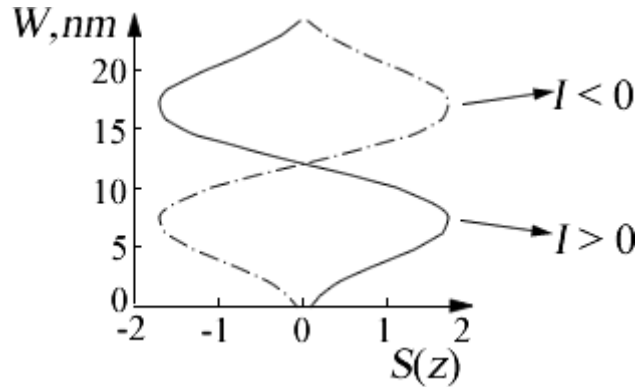


Figure 3.12 – The quantum spin Hall effect. Numerical results obtained by NEGF, show accumulation of  $+z$ -spins and  $-z$ -spins  $S(z)$  (in arbitrary units) on opposite sides of the 2D conductor with the change in direction of the current along the conductor to the opposite treatment leads to accumulated spins [10]

In the past few years significantly increased interest in transport spins in materials with strong spin-orbit interaction, especially in topological insulators [1] which exhibit very amazing manifestation of QSH [25].

### 3.6 Method NEGF and diffusive transport

Finally, we discuss the method of communication with the diffusion NEGF approach to ballistic transport, developed in [1]. We already know that the numerical results obtained by the above method NEGF, qualitatively correctly described by equation (3.1) set forth in [1] from heuristic considerations. However, the reason for this agreement is not obvious, the more so in a method for modeling transport NEGF spins initially used two-component spinors are complex, and the potential spin  $\vec{\mu}_s$  describes a three valid vector.

We have already emphasized the connection between the unit vector  $\hat{n}$  along which the spin and the spin wave functions  $\psi_{up}$  and  $\psi_{dn}$ . To establish a connection between the equation (3.1) and method of transport for NEGF spins, you need to consider such as the value of the Green's function  $G^n \sim \psi\psi^+$ , and not just the wave function  $\psi$ , because the method NEGF originally formulated

through  $G^n$ . Not to mention that it is the Green's function  $G^n$ , instead of the wave function is the observed value, suitable for communication with the experimental results.

**The electron density in the matrix representation.** We have already used the electron density in the matrix notation  $[G^n]$ , the diagonal elements that give us the number of electrons at a given point of the conductor. [2] Taking into account the spin matrix  $[G^n]$  at this point is a matrix (2 x 2), and it gives us the number of electrons or the total spin  $\vec{S}$ . You can verify this by considering an electron with spin along an arbitrary direction  $\hat{n}$  (Fig. 3.7) and is described by a wave function in the spinor representation (3.50), so that the corresponding electron density matrix  $[G^n]$  form (2 x 2) is given by

$$\psi\psi^+ = \begin{Bmatrix} c \\ s \end{Bmatrix} \begin{Bmatrix} c^* & s^* \end{Bmatrix} = \begin{bmatrix} cc^* & cs^* \\ sc^* & ss^* \end{bmatrix} \quad (3.70)$$

anyway, using (3.2) and (3.26)

$$\psi\psi^+ = \frac{1}{2} \begin{bmatrix} 1 + n_z & n_x - in_y \\ n_x + in_y & 1 - n_z \end{bmatrix} = \frac{1}{2} [I + \vec{\sigma} \cdot \hat{n}]. \quad (3.71)$$

Summing up the contributions in  $\psi\psi^+$  from all  $N$  electrons, for the matrix Green function we finally get

$$\frac{G^n}{2\pi} = \frac{1}{2} \begin{bmatrix} N + S_z & S_x - iS_y \\ S_x + iS_y & N - S_z \end{bmatrix} = \frac{1}{2} (N[I] + \vec{\sigma} \cdot \vec{S}). \quad (3.72)$$

Calculating the matrix  $[G^n]$ , the total number of electrons and the total spin can be found from

$$N = \frac{1}{2\pi} \text{Tr}[G^n], \quad \vec{S} = \frac{1}{2\pi} \text{Tr}[\vec{\sigma}G^n], \quad (3.73)$$

which follows from the vanishing trace Pauli spin matrices (3.31) and the following properties of spin matrices derived from (3.31) and (3.61), namely:

$$\begin{aligned}
\sigma_x^2 &= \sigma_y^2 = \sigma_z^2 = I \\
\sigma_x \sigma_y &= -\sigma_y \sigma_x = i\sigma_z \\
\sigma_y \sigma_z &= -\sigma_z \sigma_y = i\sigma_x \\
\sigma_z \sigma_x &= -\sigma_x \sigma_z = i\sigma_y
\end{aligned} \tag{3.74}$$

As a result, the information contained in the Hermitian matrix  $[G^n]$ , can be represented by four actual values at the point of the conductor - the total number of electrons  $N$  and three real components of the vector of the total spin  $\vec{S}$ , which can be derived from (3.73).

**Measurement of spin potential.** We came to communication between the equation (3.1) and method of transport for NEGF spins. Scalar version of equation (3.1) (equation (53) in [1]) we have received within the semiclassical model of calculating currents on the detection probe through its boundary conductivity spins the opposite direction (Fig. 12 in [1]), assuming current probe zero. Now we get the complete equation (3.1) in a vector form, based on the method NEGF (Fig. 3.13).

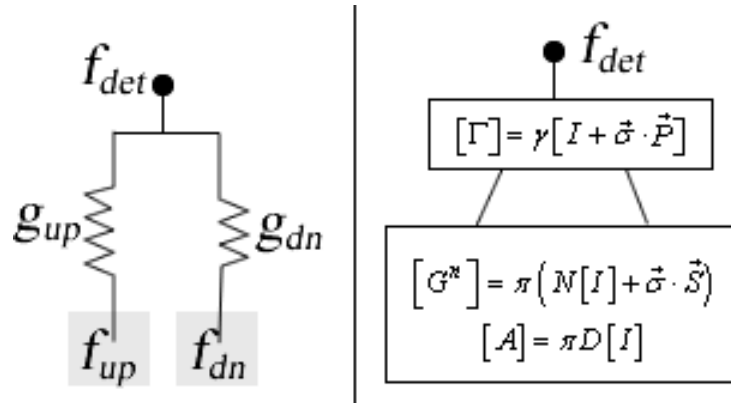


Figure 3.13 – Simulation of the detection probe in the semiclassical model and method NEGF

To have the current fourth equation formalism NEGF (equation (16) in [2])

$$I \square Tr[\Gamma][f_{det}[A] - [G^n]], \tag{3.75}$$

so that zero current on the detection probe (Fig. 3.13)

$$f_{\text{det}} = \frac{\text{Tr}[\Gamma][G^n]}{\text{Tr}[\Gamma][A]}. \quad (3.76)$$

Substituting Green function  $G^n$  (3.72), the spectral function of  $A$  expressed in terms of the spin-independent density of states  $D$

$$\frac{A}{2\pi} = \frac{D}{2}[I] \quad (3.77)$$

describing the connection of the detection probe to the channel conductivity according to (3.32)

$$\Gamma = \gamma[I + \vec{\sigma} \cdot \vec{P}], \quad (3.78)$$

and considering zero trace all Pauli matrices, we finally obtain:

$$f_{\text{det}} = \text{Tr}\left[I + \vec{\sigma} \cdot \vec{P}\right] \left[\frac{N}{D}I + \vec{\sigma} \cdot \frac{\vec{S}}{D}\right]. \quad (3.79)$$

Given the identity of two arbitrary vectors  $\vec{P}$  and  $\vec{B} \equiv \vec{S}/D$

$$[\vec{\sigma} \cdot \vec{P}][\vec{\sigma} \cdot \vec{B}] = (\vec{P} \cdot \vec{B})[I] + i\vec{\sigma} \cdot [\vec{P} \times \vec{B}], \quad (3.80)$$

we have

$$[I + \vec{\sigma} \cdot \vec{P}][bI + \vec{\sigma} \cdot \vec{B}] = (b + \vec{P} \cdot \vec{B})[I] + \vec{\sigma} \cdot [\vec{P} + \vec{B} + i\vec{P} \times \vec{B}], \quad (3.81)$$

and finally, using a zero trace the Pauli matrices, instead of (3.79) we have:

$$f_{\text{det}} = \frac{N}{D} + \vec{P} \cdot \frac{\vec{S}}{D} \equiv f + \vec{P} \cdot \frac{\vec{f}_s}{2}, \quad (3.82)$$

where the population of the charge  $f$  and spin  $f_s$  determined in such a way that their maximum values are not exceeded unity. To go from populations to the chemical potential and get the desired equation (3.1), we use the linear dependence between the linear response mode (equation (21) in [26]).

**Four component transport.** We emphasize once again that the quantum approach naturally leads to a complex matrix  $[G^n]$  form  $(2 \times 2)$  at every point of the conductor, and at the same time Green's matrix can always be rewritten in four physically real and understandable numbers such as  $(N, \bar{S})$ , or  $(\mu, \bar{\mu}_s)$ .

We have seen in [1] how many different spin transport phenomena can be described by the equation Valais - Firth (equation (23) in [1]) with the model of spin-dependent boundary resistance. However, this approach [1] has been limited to problems of transport using spin in only one direction (axis  $z$ ). Now, with the full version of the method NEGF, transport can be considered spin oriented in any arbitrary direction, although such calculations and require large computational resources.

Broadcasting matrix  $[G^n]$  in a four-format  $(N, \bar{S})$  the spin-dependent conductivity boundary [1] may be replaced by a matrix of conductivity  $G$  shaped  $(4 \times 4)$ , which will connect the four components of the potential four components of the current:

$$\begin{Bmatrix} I \\ I_{sx} \\ I_{sy} \\ I_{sz} \end{Bmatrix} = \begin{bmatrix} G \\ 4 \times 4 \end{bmatrix} \begin{Bmatrix} \Delta\mu \\ \Delta\mu_{sx} \\ \Delta\mu_{sy} \\ \Delta\mu_{sz} \end{Bmatrix}. \quad (3.83)$$

Similarly, a two-component equation Vale – Firth for  $(\mu, \mu_s)$  can be converted into four-component diffusion equation for  $(\mu, \bar{\mu}_s)$ .

As mentioned above, the accounting differences between the two spin states doubles order of all templates in the method NEGF. For example, if 1D conductor, are three of the atom, the block matrix  $[G^n]$  is the 6th order:

$$\begin{array}{cccccc}
& 1_{up} & 1_{dn} & 2_{up} & 2_{dn} & 3_{up} & 3_{dn} \\
1_{up} & & & & & & \\
1_{dn} & [N_1, \vec{S}_1] & & & & & \\
2_{up} & & & & & & \\
2_{dn} & & [N_2, \vec{S}_2] & & & & \\
3_{up} & & & & & & \\
3_{dn} & & & & & [N_3, \vec{S}_3] & 
\end{array}, \quad (3.84)$$

wherein the diagonal blocks (2 x 2) correspond to the quaternary transport format description.

What is missing in the Green's matrix (3.84), so it's off-diagonal elements linking the neighboring and more distant from each other atoms of the conductor. As will be shown below, these elements of the Green matrix generate quantum interference effects. For some transportation problems is not essential, since these effects are often leveled dephasing processes, it will be devoted to the following message.

## Chapter 4

# QUANTUM INTERFERENCE AND DEPHASING IN METHOD NON-EQUILIBRIUMGREEN'S FUNCTIONS

### 4.1 Introduction

So far we have considered only physical contact  $[\Sigma_{1,2}]$  in the quantum model of coherent transport [1], in which the electrons move coherently from the source to the drain through the channel described by static Hamiltonian  $[H]$  in the absence of electron interaction with the environment as it moves through the channel described by the self-energy  $[\Sigma_0]$  (Fig. 4.1).

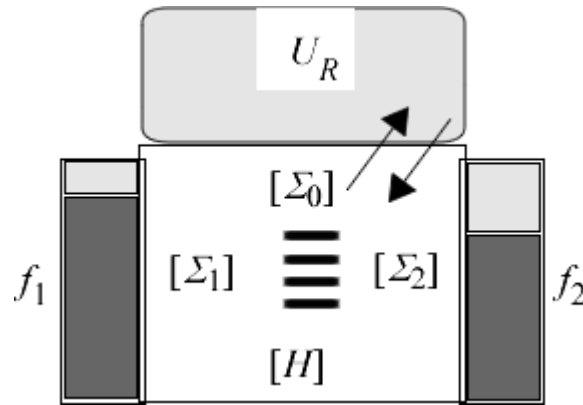


Figure 4.1 – Model of quantum transport with a simple elastic dephasing

What is the physical interaction is  $\Sigma_0$ ? From the point of view of an electron moving through a conductor, Wednesday is not a static electron described static Hamiltonian  $[H]$ , but a very turbulent environment with a randomly varying potential  $U_R$ , which fluctuates in the picosecond time scale. Even at low temperatures frozen phonon modes electron moves in the fluctuating potential produced by all other electrons (the self-consistent field approximation). Even in this case, there are phase fluctuations (dephasing), leading to fluctuations in current. The effect of averaging should be adequately model if we are to correctly interpret the experimental data.

The method of non-equilibriumGreen's functions (NEGF) was originally designed specifically for the account of inelastic processes of quantum transport in massive conductors. We are yet outlined its relation to elastic resistors [1]. Now we consider a relatively simple model of elastic dephasing.

What is the process of dephasing? Or in other words, the coherent process differs from incoherent? Coherent transport is a process of electron motion along the conductor in which the state of the other particles in the channel conductivity is not changed. Simple electron from the elastic rebound of the defect back to the conduction channel have a coherent process. If the electron transfers part of its energy, for example, lattice atom and atom began to vibrate with greater amplitude, such a process is incoherent. It seems to mean that the incoherent process must also be inelastic, originating with the exchange of energy. However, this is not necessarily so, and the classic example is the spin dephasing.

Let us have a magnetic impurity with two spin states of the same energy (degenerate). And let the electron interacting with an impurity, change the spin direction is reversed, without changing its energy. This process - elastic. Nevertheless, this process is incoherent, since the state of the electron changed.

What makes this process is incoherent? Can we consider the electron spin and the admixture as a single component system whose state has changed and therefore the process can be considered a coherent? What really makes these processes are incoherent, because these are external forces that inspire the return of an impurity spin in the unpolarized state (50% of the "up" and 50% "down"). This process of "erasing" is the essence of spin dephasing. In the general case, the dephasing is meant a process in which a quantum mechanical interference is destroyed.

**The elastic dephasing.** The processes of elastic dephasing in the method described by the matrix NEGF own energy

$$[\Sigma_0] = D \times [G^R], \quad (4.1a)$$

$$[\Sigma_0^{in}] = D \times [G^n], \quad (4.1b)$$

$$[\Gamma_0] = D \times [A], \quad (4.1c)$$

where the "cross"  $\times$  is an exploded matrix multiplication, and describe the elements of the matrix  $D$  correlation between the random values of the potential at the nodes  $i$  and  $j$  of the conductor:

$$D_{ij} = \langle U_{Ri} U_{Rj} \rangle. \quad (4.2)$$

Two limit model correlations are of interest. In the first, fully correlated random potential at all nodes along the entire length of the conduction channel has the same value for each node  $i$ , so that all the elements of the matrix  $[D]$  are both equal to  $D_0$ :

$$\text{(Model A)} \quad D_{ij} = D_0. \quad (4.3)$$

In the second model, there is no correlation between the nodes of the conductor, scalar matrix  $D$ :

$$\text{(Model B)} \quad D_{ij} = D_0 \cdot \delta_{ij}, \quad (4.4)$$

where  $\delta_{ij}$  - Kronecker delta-function. Real processes are usually described intermediate cases.

The origin of the formula (4.1) can be understood with reference to the source in the construction method NEGF in matrix form of the Schrodinger equation (equation (4) in [1])

$$E \{ \psi \} = [H + \Sigma_1 + \Sigma_2] \{ \psi \} + \{ S_1 \}, \quad (4.5)$$

where  $[\Sigma_1]$  and  $[\Sigma_2]$  - contact your own energy matrix and column matrix  $\{s_l\}$  describes the influx of electrons in a conductor with a left contact 1 (Fig. 4.1) [1].

The random potential introduced into the Schrodinger equation by analogy with the matrix self-energy

$$E \{ \psi \} = [H + \Sigma_1 + \Sigma_2] \{ \psi \} + U_R \{ \psi \} + \{ S_1 \} \quad (4.6)$$

with a corresponding current member

$$\Sigma_0^{in} A = 2\pi U_R U_R^* \{ \psi \} \{ \psi \}^+ = D_0 G^n, \quad (4.7)$$

written above for Model A. Several longer calculations lead to the same expression for the model B. As a result, we have the formula (4.1b).

To justify the formula (4.1c), we note that this formula with (4.1b) must provide zero current on the "Terminal 0", which follows from the fourth equation formalism NEGF (equation (16) in [1]), namely:

$$I_0 = \frac{q}{h} \text{Tr} \left[ \Sigma_0^{in} A - \Gamma_0 G^n \right] = D_0 \frac{q}{h} \text{Tr} \left[ G^n \Gamma_0 - \Gamma_0 G^n \right] = 0 \quad (4.8)$$

and is a must, because the "terminal 0" is not a physical contact, where the electrons can move into a conductor or leave it.

Indeed, at one time Buttiker proposed to account for the incoherent process of entering a dummy contact (Buttiker probe), the electrochemical potential is selected in such a way as to guarantee this zero current contact [2, 3]. The formalism NEGF this leads to the assertion that

$$\Sigma_0^{in} = \Gamma_0 f_P \quad (4.9)$$

where the number of  $f_P$  is selected such as to provide a zero current to the dummy terminal. This is equivalent to the arguments above, if the connection  $\Gamma_0$  "terminal" with a guide to select proportional spectral function  $[A]$  as required under (4.1c).

We draw attention to the fact that the equation (4.1) presuppose a self-consistent calculation procedure as  $\Sigma$ ,  $\Sigma^{in}$  depend on  $G^R$  and  $G^n$ , which in turn, according to the equation (4.6) and equation (13) in [1], dependent on  $\Sigma$  and  $\Sigma^{in}$ ; and that the model A (4.3) involves calculating the full Green's function that, for sufficiently large devices leads to a very large matrix calculation order, while model B (4.4) does not require substantial computing resources such as computation subject only to the diagonal elements of the Green's matrix.

Significant conceptual differences between the models A and B is that destroys phasing model A, but does not affect the pulses, while model B also destroys pulses [4]. Dephasing process can be thought of as "extraction" of the electron conductor in a state  $[G^n]$  and then "injected" it back to a conductor in a state  $D \times G^n$ . A model involves matrix multiplication Green  $[G^n]$  by a constant so that the electron "reinjects" at exactly the same state in which it was

"extracted", without the loss of momentum, while model B are dropped off-diagonal elements of the matrix  $D$  and "reinjected" change the trajectory of an electron to a certain arbitrary compared to the path with which it has been "removed." The whole situation will become clearer below with respect to specific examples.

Instead of considering the elastic dephasing through the matrix self-energy  $[\Sigma_0]$  could be included in the random potential  $U_R$  in Hamiltonian with further averaging it possible random realizations  $U_R$ . Both approaches though not exactly equivalent, but in some cases lead to the same results, as we shall see below as specific examples.

The sake of completeness, we note that in the general case  $D$  is a tensor of the 4th rank, connecting with each other a pair of matrices, namely:

$$[\Sigma_0]_{ij} = \sum_{k,l} D_{ijkl} [G^R]_{kl}, \quad (4.10a)$$

$$[\Sigma_0^{in}]_{ij} = \sum_{k,l} D_{ijkl} [G^n]_{kl}, \quad (4.10b)$$

and the elastic dephasing (4.1) is realized through  $D_{ijkl}$  nonzero for  $i=k$  and  $j=l$ .

## 4.2 1D conductor with two or more scattering centers

Previously [1] considered in detail 1D conductor with a scattering center, characterized by the probability of passing the  $T$ . In [5] it was shown that the resistance of the conductor  $R_l$  can be split into two parts - the resistance of the scattering center and the boundary resistance (respectively, the equation (34) and (35) in [5]):

$$R_l = \frac{h}{q^2 M} \left( \frac{1-T}{T} + 1 \right). \quad (11)$$

The question arises, what is the conductor resistance  $R_2$  with two identical scattering centers, each with a probability of transmission  $T$ . This conductor can be considered as a series connection of two conductors, each with the same scattering center (Fig. 4.2).

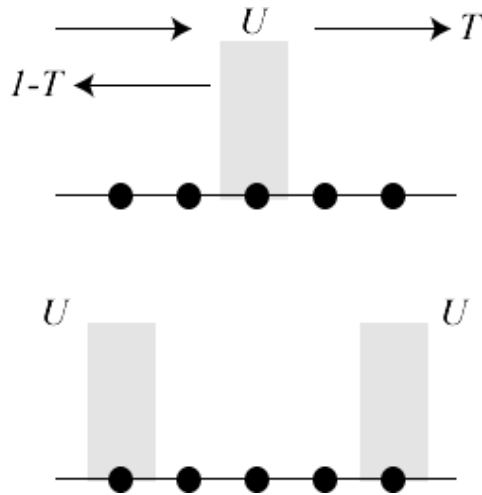


Figure 4.2 – Conductor with one or two identical scattering centers

We can expect that in a conductor with two centers of the contribution from double scattering centers:

$$R_2 = \frac{h}{q^2 M} \left( 2 \frac{1-T}{T} + 1 \right) = \frac{h}{q^2 M} \frac{2-T}{T}, \quad (4.12)$$

so that

$$R_2 = R_1 (2 - T). \quad (4.13)$$

If the probability of scattering centers passage  $T$  is close to unity, then the ballistic limit conduction  $R_2 \approx R_1$ : two identical conductor, each with the same scattering center and connected in series, carried out in the same manner as one of them, since all the resistance is a boundary.

If  $T=1$ , there is a ohmic limit  $R_2 \approx 2R_1$ : two such conductor connected in series, a dual resistance wire, because all resistance connected to the channel conductivity.

But can  $R_2$  be less than  $R_1$ ? If electrons obey the laws of classical mechanics, then, of course not. Increasing the number of obstacles on the road highway can not increase the limit of the traffic on this highway. But at the quantum "highway" it is quite possibly due to the quantum (wave) interference.

To solve the problems of this type use the model of a homogeneous 1D conductor in the Hückel approximation [1]. Recall the behavior of the

transmission coefficient in a conductor with a scattering center  $U = 2t_0$  (Fig. 4.3) and compare it with the same conductor, but with two identical such as scattering centers (Fig. 4.4).

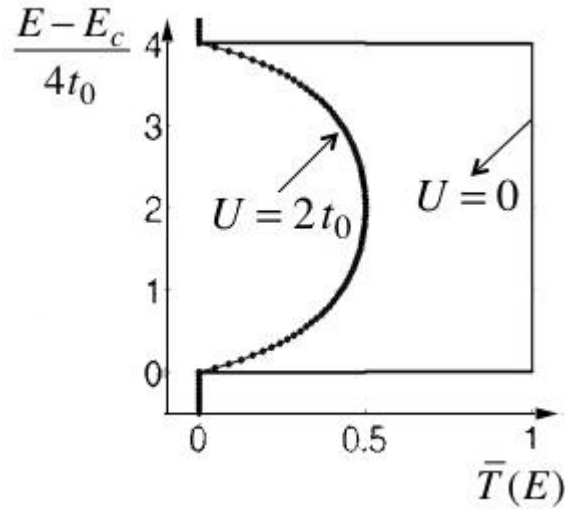


Figure 4.3 – The transmission coefficient in a uniform 1D conductor with one point scattering center ( $U = 2t_0$ ) and without ( $U = 0$ ) [1]

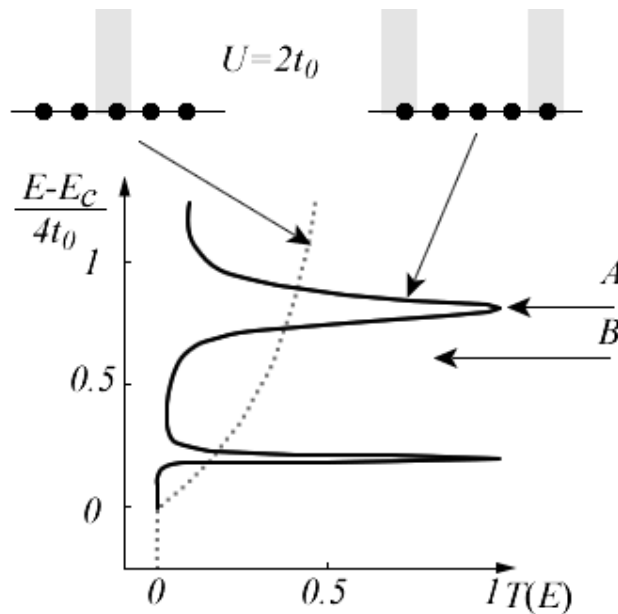


Figure 4.4 – The transmission coefficient in the single-1D conductor with one or two identical scattering centers with  $U = 2t_0$

If the electrochemical potential of the device to a conductor with two scattering centers will be at B (Fig. 4.4), the transmittance will be less than one center conductor; In other words, resistance  $R_2$  will be greater than  $R_1$ . If it happens that the chemical potential would be at level A (see Fig. 4.4), then  $R_2$  will be even smaller than  $R_1$ .

Consider a conductor with randomly distributed scattering centers. A quantum calculation method NEGF six such centers shows that the conductivity is very, very low (nearly ohmic behavior), excluding the numerous bursts of conductivity, rarely up to values close to unity (Fig. 4.5).

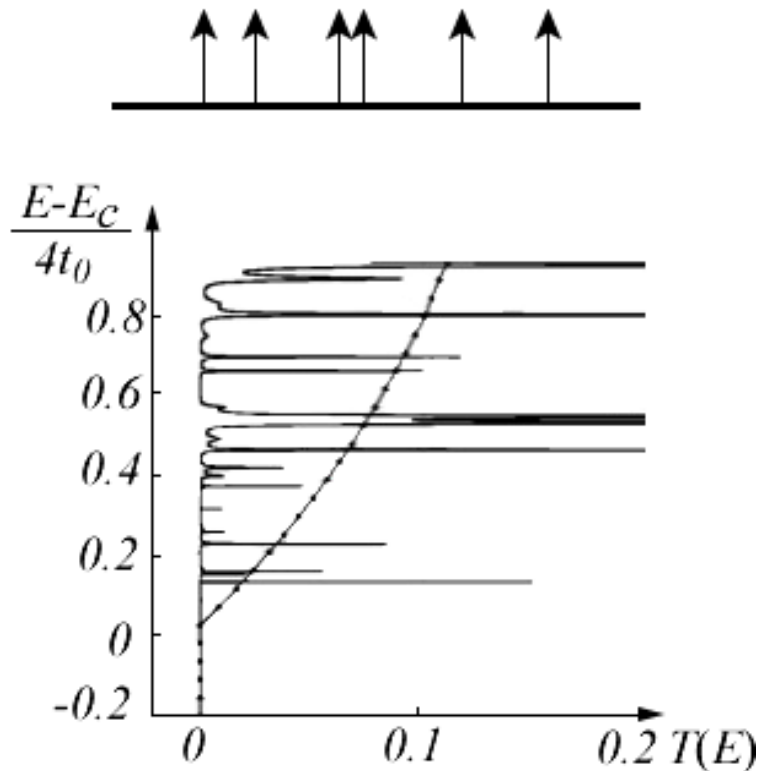


Figure 4.5 – The transmission coefficient in the single 1D conductor with the same six randomly distributed scattering centers with  $U = 2t_0$  [6].

The dots shows the result of the semiclassical calculation (Fig. 4.3) based on the six points

The figure also shows a semi-classical points result obtained initially for a single scattering center (Fig. 4.3), then a contribution from increased six times. For the resistance of the conductor have

$$R_6 = \frac{h}{q^2 M} \left( 6 \frac{1-T}{T} + 1 \right) = \frac{h}{q^2 M} \frac{6-5T}{T}, \quad (4.14)$$

where the first term in brackets is due six scattering centers, and the second term - the boundary resistance.

Quantum calculations show similar behavior and multimode conductors as classic transmittance  $M\lambda/L$  is less than one, where  $\lambda$  - the mean free path and  $L$  - length of the conductor. Such conductors say they are in the regime of strong localization. Curiously, even if  $M\lambda/L$  is greater than one, the quantum of conductance is only slightly less than the classical value; of such conductors say they are in the regime of weak localization.

Such localization effects usually observed experimentally only at low temperatures. At room temperature, it is extremely rare to meet with a deviation from Ohm's law. Consider, for example, copper wire with a cross section of  $10 \text{ nm} \times 10 \text{ nm}$ , which contains about 1000 atoms, and hence the number of modes  $M \approx 1000$ . Let the mean free path  $\lambda \approx 40 \text{ nm}$ . Then, this wire length of no more than  $M\lambda \approx 40 \text{ }\mu\text{m}$  should detect non-ohmic behavior that is not supported by experimental observations. The reason is that the effects caused by the localization of quantum interference and are observed only when there is a phase coherence over the entire length of the conductor. Copper wire length  $L \approx 40$  microns phase incoherent, especially at room temperature. Conceptually real conductor can be considered as a sequence of individual coherent conductors, each of length equal to the length of phase coherence  $L_p$ . We see or do not see the effects of localization does not depend  $M\lambda/L$ , but from  $M\lambda/L_p$ .

The main conclusion is that the interpretation of the experiments at room temperature formalism NEGF, as a rule, it is necessary to some extent to consider dephasing processes, as described above. Until we somehow do not take into account the dephasing in quantum models of electron transport manifest interference effects, leading to strong localization or resonant tunneling. In support of this, we consider the potential change along the channel conductor with defects using NEGF [6].

### 4.3 The potential jump on defects

Profile-building single-mode conductor with one defect of transparency  $T$  considered in [1, 5]. The conductivity of the conductor is given by (34) in [5]. Then, the resistance of the conductor, normalized to the quantum of resistance,

$$R_{Norm} = (1 - T)/T. \quad (4.15)$$

Semiclassical expression for the transmission coefficient  $T$  is given by the formula (113) in [1]. Then, the normalized resistance defect equal

$$R_{Norm} = (Ua/\hbar v)^2. \quad (4.16)$$

Semiclassical potential profile with a jump in the boundary resistance  $h/q^2$ , according to (36) in [5], and the resistance to the defect (4.16) is shown in Fig. 4.6 together with the results obtained by NEGF without dephasing.

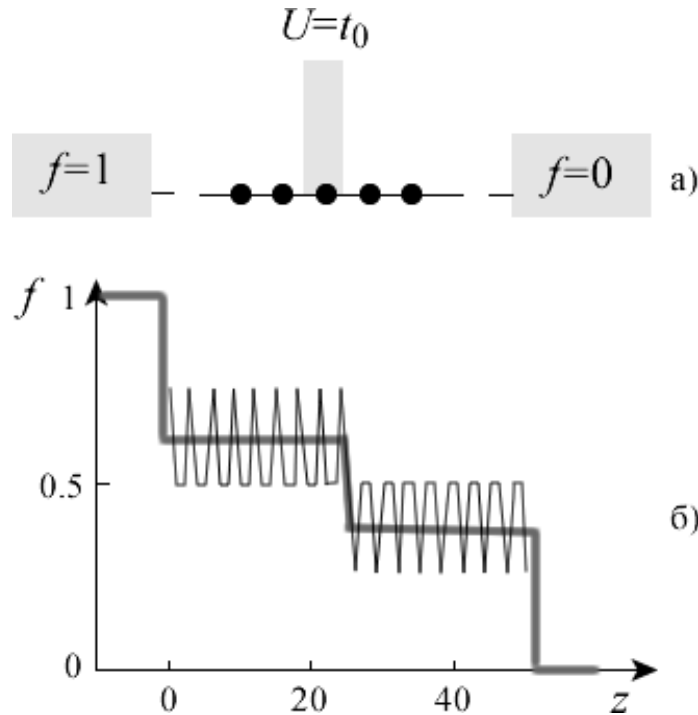


Figure 4.6 – (a) Schematic of single-mode conductor defective  $U = t_0$ ; (b) Quantum oscillations in the method NEGF without dephasing ( $D_0 = 0$ ) mode coherence at  $E = t_0$  jumps on a background of semi-classical building

Engineering of calculation population  $f$  in the method NEGF the Green's function and the spectral function and then the electrochemical potential is described in [5, formulas (87) and (88)].

The population in the calculation method NEGF a result of quantum interference oscillates so much that it becomes difficult to see the potential jump at the defect (Fig. 4.6).

Experimentally, the potential profile is usually measured with a scanning tunneling microscope (Fig. 14 in [5]) and at room temperature quantum oscillations are usually not visible because of the dephasing processes inevitably occurring in such conditions. The above example shows again that the simulation and interpretation of actual traffic measurements at room temperature must be a greater or lesser extent into account dephasing quantum interference effects.

Indeed, if the same model of the conductor (Fig. 4.6a) in the calculation method NEGF include dephasing considering only the phase relaxation (model A, equation (4.3)), we obtain the potential profile with a clearly pronounced jump at the defect in accordance with the semiclassical model (Fig. 4.7).

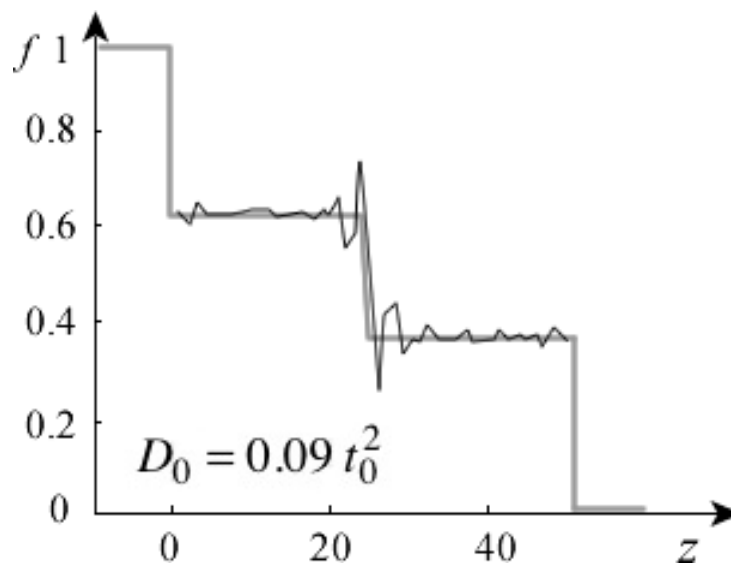


Figure 4.7 – Quantum oscillations in the method NEGF dephasing when taking into account only the relaxation phase (model A) for  $E = t_0$  does not veil the potential jump on the defect

Interestingly, if we consider also the relaxation pulse (model B, equation (4.4)), the potential throughout the conductor takes practically linearly (Fig. 4.8), as should be expected for uniformly distributed elastic resistors over the entire length of the conductor (application 1 in [7]).

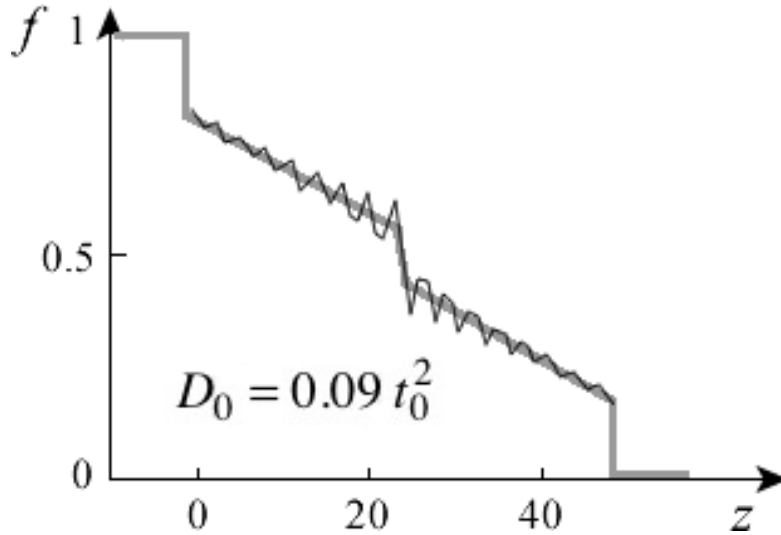


Figure 4.8 – Accounting method in NEGF both phase and relaxation impulse (model B) virtually eliminates the potential jump on the defect, making a conductor with a defect in a sequence of elastic resistors

The resistance per one unit of such a uniform conductor 1D can be obtained from (4.16) by replacing  $U^2$  on  $D_0$ :

$$R_{Norm} = D_0 (a/\hbar v)^2 (L/a), \quad (4.17)$$

where  $L/a$  gives the number of sites in the conductor.

Another useful example is already discussed above with two similar conductor scattering centers (Fig. 4.4). Values of electrochemical potential at levels A and B correspond to the constructive ( $R_2 < R_1$ ) and destructive ( $R_2 > R_1$ ) quantum interference. The difference between them is evident in the calculation of the conductor by NEGF coherent mode of transport, without dephasing with  $D_0 = 0$  (Fig. 4.9).

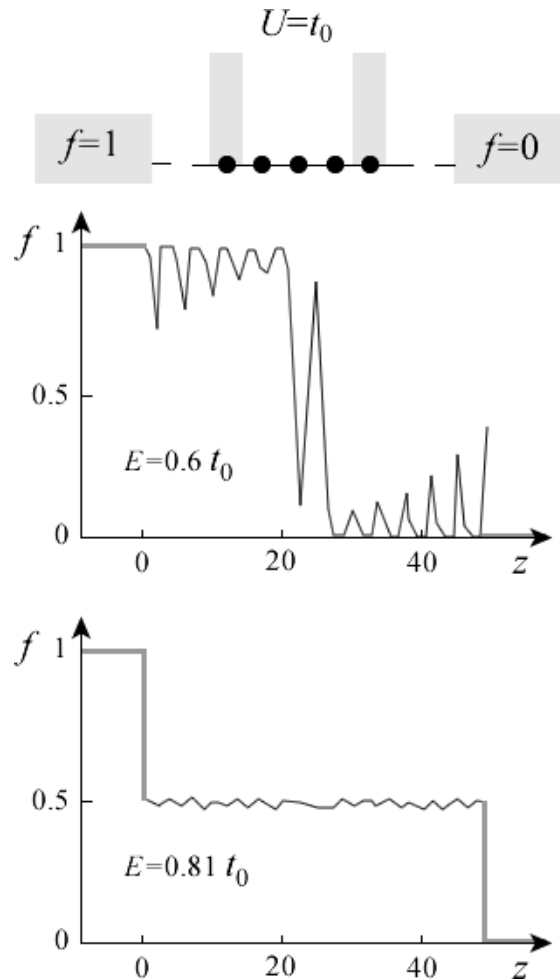


Figure 4.9 – Quantum oscillations per conductor with two identical scattering centers with  $U = t_0$  by NEGF without dephasing ( $D_0 = 0$ ) mode coherence at  $E = 0.6t_0$  evidence of destructive interference (mode B with  $R_2 > R_1$ ), and for  $E = 0.81t_0$  - of constructive interference (mode A with  $R_2 < R_1$ )

At the level of potential profile it looks as if we are dealing with a large jump in the potential defect, and even imposed on him by two bursts (destructive interference). The slight increase in the electrochemical potential to  $E = 0.81t_0$  (Level A) dramatically changes the potential profile. Now it looks like this (Fig. 4.9), as one would expect for a ballistic conductor with jumps only at the boundaries of the potential contacts (constructive interference).

In the above question "whether  $R_2$  be less than  $R_1$ ?" The answer is simple - "Yes, maybe": two defects can create less resistance than one such defect. And this "strange" result is bound to quantum interference.

One only, in both cases A and B (Fig. 4.9) to consider dephasing in a phase relaxation with sufficient non-zero value  $D_0$ , as the potential profile once it becomes like a semi-classical profile of the resistor (Fig. 4.10).

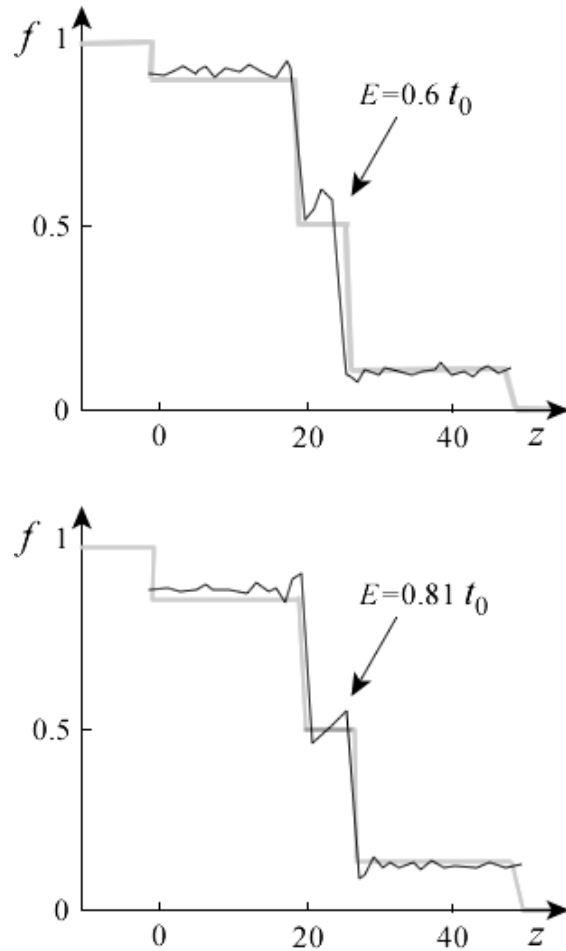


Figure 4.10 – Quantum oscillations in the method NEGF dephasing when taking into account only the relaxation phase ( $D_0 = 0.09 t_0^2$ ) when both values of electrochemical potential  $0.6t_0$  and  $0.81t_0$  jumps on a background of semiclassical building

Computationally pay attention to the fact that in the method of accounting dephasing NEGF algorithmically not difficult, but if in a coherent approach ( $D_0=0$ ) or, subject only to the pulse relaxation (model B, equation (4.4)), it suffices to calculate only diagonal elements of the Green's function, in the case of recording a phase relaxation is necessary to calculate the total Green's

function, which significantly increases the computing time and requires much more computing resources.

It is reasonable to also raise the question: what if, instead of taking into account the dephasing through the matrix  $\Sigma_0$  own energy potential  $U_R$  included in the Hamiltonian  $H$ , and the then average it over all possible implementations, it lead to the same results?

For short resistors, such as in Fig. 4.4, the answer is likely to be positive, but for long resistors, as shown in Fig. 4.5, the answer is no. In the case of a conductor in the strong localization (Fig. 4.5), it is difficult to imagine how the averaging of coherent quantum state of many possible configurations will lead to semi-classical results.

Method NEGF to dephasing, without going into details, it can not be reduced simply to averaging over many configurations, and also includes an average of individual fragments of configurations, with the result that is achieved semiclassical description of conduction, so well established in the interpretation of the actual measurements at room temperature.

Services in the four-spin format. Returning to the description of the quaternary spin transport [8], but now with the dephasing. He cited the example of the Green's matrix of a linear conductor of three atoms:

$$\begin{array}{cccccc}
 & 1up & 1dn & 2up & 2dn & 3up & 3dn \\
 1up & & & & & & \\
 1dn & \left[ N_1, \vec{S}_1 \right] & & & & & \\
 2up & & & & & & \\
 2dn & & \left[ N_2, \vec{S}_2 \right] & & & & \\
 3up & & & & & & \\
 3dn & & & & & \left[ N_3, \vec{S}_3 \right] & 
 \end{array} , \quad (4.18)$$

wherein the diagonal blocks (2 x 2) comprise four real number ( $N, \vec{S}$ ), and the non-diagonal blocks, and a connecting adjacent spaced apart atoms have been omitted; it is the off-diagonal blocks generate quantum interference effects. In this regard, we note that the spin relaxation times are of the order of nanoseconds, and the phase relaxation time on the order of three or even more smaller. If so, it is important to maintain the information stored in the diagonal

blocks, even if you do not take into account information from the non-diagonal blocks.

The formalism NEGF need to pick a suitable matrix  $D$  in equation (4.1b):

$$[\Sigma^{in}] = D \times [G^n],$$

because the process of dephasing can be visually represented as the "extraction" of the electron conductor in a state  $[G^n]$  and then "injected" it back to a conductor in a state  $D \times G^n$ .

Have already been introduced in two models for the matrix  $[D]$  - A and B models described by equations, respectively, (4.3) and (4.4). Model A is equivalent to multiplying the matrix  $[D]$  by a constant: in other words, the electron is "injected" in the same state from which it has been "removed" so that the electron momentum is maintained. The model in the off-diagonal elements vanish, leading to loss of information about the momentum of the electron, which is well illustrated in Fig. 4.8.

We define a model with one in which the matrix  $[D]$  stores all the information about the backs and vanish momentum relaxation, namely:

$$\frac{[D]}{D_0} = \begin{matrix} & \begin{matrix} 1up & 1dn & 2up & 2dn & 3up & 3dn \end{matrix} \\ \begin{matrix} 1up \\ 1dn \\ 2up \\ 2dn \\ 3up \\ 3dn \end{matrix} & \begin{bmatrix} 1 & 1 \\ 1 & 1 \\ 0 & 0 \\ 0 & 0 \\ 0 & 0 \\ 0 & 0 \end{bmatrix} & \begin{bmatrix} 0 & 0 \\ 0 & 0 \\ 1 & 1 \\ 1 & 1 \\ 0 & 0 \\ 0 & 0 \end{bmatrix} & \begin{bmatrix} 0 & 0 \\ 0 & 0 \\ 1 & 1 \\ 1 & 1 \end{bmatrix} & , & \end{matrix} \quad (4.19)$$

in other words, the model C remind the model B in against conductor lattice, and the model A regarding spin information.

Rewrite the Green's matrix

$$G^n = G^R \Sigma^{in} G^A \quad (4.20)$$

how

$$[G^n]_{ii} = \sum [G^R]_{ij} [\Sigma^{in}]_{jj} [G^A]_{ji} = D_0 \sum [G^R]_{ij} [G^n]_{jj} [G^A]_{ji}, \quad (4.21)$$

where the indices  $i, j$  enumerate the lattice atoms of the conductor and takes into account the fact that in the model with the matrix in the lattice basis  $\Sigma^{in}$  diagonal.

We already know that for any lattice site guide its diagonal matrix (2 x 2) Green's matrix (4.18) can be written in terms of the number  $(N, \vec{S})$ , so that the equation (4.21) by simple transformations can be written as

$$\begin{Bmatrix} N \\ S_x \\ S_y \\ S_z \end{Bmatrix}_i = \sum_j \begin{bmatrix} \text{Resonance} \\ \text{matrix} \\ (4 \times 4) \end{bmatrix}_{ij} \begin{Bmatrix} N \\ S_x \\ S_y \\ S_z \end{Bmatrix}_j, \quad (4.22)$$

where "resonance" matrix (4 x 4) may be interpreted as an interaction  $(N, \vec{S})$  at a node  $i$  with  $(N, \vec{S})$  at the nodes  $j$ , located away from the  $i$  in one step on a lattice. A similar one-dimensional equation resembles the standard description of Brownian motion on the grid and led to the diffusion equation drift.

#### 4.4 The quantum nature of the classics

There is nothing surprising or unexpected in the title of this section. From the above example we have seen that to understand the physics and for the interpretation of real experimental measurements are usually quite semiclassical consideration. Almost everything that we have discussed in this series, is a consequence of the transport of the Boltzmann equation. Moreover, all the billions of transistors in current notebook consisting of only a few hundred atoms are essentially classical electronics devices controlled mainly electrostatic rather than the laws of quantum mechanics. Recently made a thorough and

comprehensive measurements and calculations 2D metallic conductivity of the conductor cross-section (1 x 4) atoms [9] demonstrated its normal ohmic behavior. It is reasonable to ask Will, based on the apparent success of our fantastic Nanophysics and nanoelectronics, create a fundamentally different quantum devices that will take us beyond the current "charge" the paradigm of information processing. Mention only some considerations in this regard. [10]

**The spin coherence.** The difference between quantum and classical physics is best observed on such a fundamental property of the electron spin. Consider, for example, an experiment with spin injection in the further conduction channel second potential measurement probe [8]

$$\mu_2 = \mu + \frac{\vec{P}_2 \cdot \vec{\mu}_s}{2}, \quad (4.23)$$

dependent on the cosine of the angle between the magnetic recording and injecting contacts (Fig. 2 in [8]). Green's matrix has the form (4.18) with diagonal blocks (2 x 2)

$$\begin{bmatrix} N + S_z & S_x - iS_y \\ S_x + iS_y & N - S_z \end{bmatrix}, \quad (4.24)$$

elements of which contain physically understandable quantities of electronic and spin density ( $N, \vec{S}$ ). Formalism NEGF results [8] further to the equation (4.23) ( $\mu, \vec{\mu}_s$ ), broadcast in the ( $N, \vec{S}$ ) according to the equation (83) in [8].

This simple example allows to illustrate the link between the quantum and classical description. If you cross the components of the matrix (4.24) is negligible, only two numbers  $N$  and  $S_z$  is sufficient to describe the entire physics of transport. The remaining non-zero diagonal components can be interpreted

$N + S_z$  as the number of electrons with spin "up"

$N - S_z$  as the number of electrons with spin "down"

and then discharged semiclassical equations for the two kinds of electrons. In fact, this approach is implemented in [7].

When running such a model? One of the possibilities available when the contacts are collinear magnetization, as in [7], and the spin-orbit interaction in the channel conductivity is absent, so that the angle  $\theta$  is an integer multiple of  $180^\circ$  (Fig. 2 in [8]). Another possibility is realized when the spin dephasing so significant that cross the spin component in the diagonal block matrix (2 x 2) Green's matrix (4.24) can be neglected. Finally, if you can be neglected and the z-component of spin, then on account of the spin is not the issue.

What if collinear magnetic contacts are not directed along the axis  $z$ , but axis  $x$ ? In this case, the blocks (2 x 2) Green's matrix is diagonal (the icon  $\rightarrow$  read "rewritten in the form"):

$$\frac{[G^n]}{2\pi} \rightarrow \begin{bmatrix} N & S_x \\ S_x & N \end{bmatrix}$$

and semiclassical description is likely to be impossible. In this case, you need to choose a different coordinate system, or in general, otherwise choose the expansion of the basis functions. Select needed basis so that objects, such as a spin with the direction "up" and "down", have focused, respectively, along the  $+x$  and  $-x$ ; then the blocks will be the Green matrix diagonal:

$$\frac{[G^n]}{2\pi} \rightarrow \begin{bmatrix} N + S_{up} & 0 \\ 0 & N + S_{dn} \end{bmatrix}.$$

Recommendation choose another basis may seem trivial, but it is not so, as we shall now see.

**Pseudospins.** The formalism of Pauli spin matrices [7] is remarkable in that it is not confined only to the electron spin, but extends to any object with a two-component structure in the complex plane. Recall the graph. The carbon atoms in graphene topologically equivalent and can be either class A or class B (Fig. 23 in [1]). The wave function of the unit cell of graphene is described by a two-component vector in the complex plane [11]

$$\{\psi\} = \begin{Bmatrix} \psi_A \\ \psi_B \end{Bmatrix},$$

so that the corresponding Green's function (equation (10) in [1]) can be formally rewritten as follows:

$$\frac{[G^n]}{2\pi} = \begin{bmatrix} \psi_A \psi_A^* & \psi_A \psi_B^* \\ \psi_B \psi_A^* & \psi_B \psi_B^* \end{bmatrix} \rightarrow \begin{bmatrix} N + S_z & S_x - iS_y \\ S_x + iS_y & N - S_z \end{bmatrix},$$

that is irrelevant to the real back and only formally mathematically corresponds to (4.24). Directions pseudospins in graphene is shown in Fig. 29b in [7].

Consider another example of using the less familiar concept pseudospin pursuing primarily pedagogic purpose. Returning to the model in Fig. 4.6a.

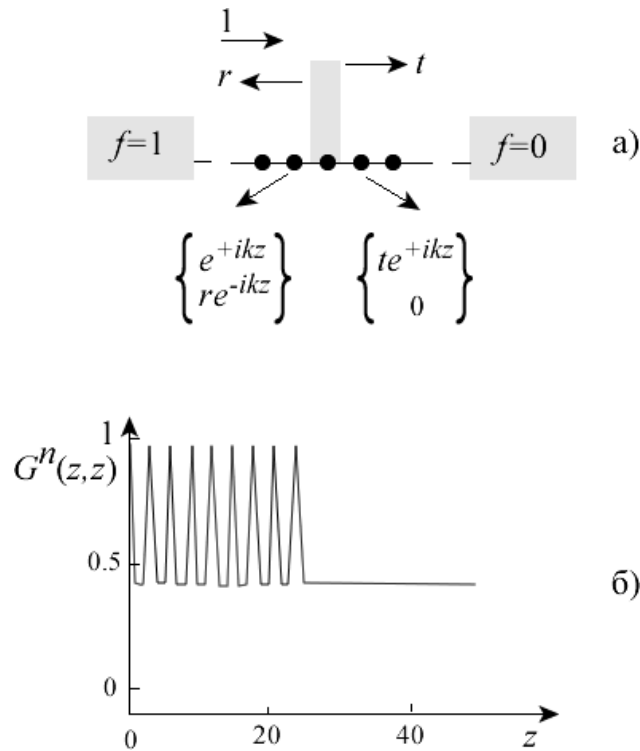


Figure 4.11 – (a) Schematic of single-mode conductor with one defect characterized by the transmission coefficient  $t$  and the reflection coefficient  $r$ ; arrows indicate a pseudo spinor wave functions of the electron before and after the passage of the defect. (b) The behavior of the diagonal matrix elements of the Green's left and right of the defect

Let's look at the behavior of the diagonal elements of the Green's matrix  $[G^n]$  on the left and right of the defect (Fig. 4.11b). To the left of the defect to

"observe" the oscillations of the electron density, whereas after passing the defect density is constant. Note that, in the same model in Fig. 4.6 – 4.10 oscillations take place and the right of the defect. But there it was on the oscillations of the populations, which is calculated from  $G^n/A$ , and the spectral function of  $A$ , which is proportional to the density of states  $D$ , oscillates, both before and after the passage of the defect, so that to our situation, these oscillations to the right in Fig. 4.6 – 4.10 have no relationship.

See how you can use the concept of pseudospin understand the behavior of the Green's matrix of diagonal elements in Fig. 4.11b. The following shows a pseudo spinor wave function of an electron and electron density on the left/ $L$  and right/ $R$  of the defect and the presentation of the latter with the use of the concept pseudospin:

$$\{\psi\} \rightarrow \left\{ \begin{array}{c} e^{+ikz} \\ re^{-ikz} \end{array} \right\}_L, \left\{ \begin{array}{c} re^{+ikz} \\ 0 \end{array} \right\}_R ;$$

$$\{\psi\}\{\psi\}^+ \rightarrow \left[ \begin{array}{cc} 1 & r^* e^{+i2kz} \\ re^{-i2kz} & rr^* \end{array} \right]_L, \left[ \begin{array}{cc} tt^* & 0 \\ 0 & 0 \end{array} \right]_R \rightarrow \left[ \begin{array}{cc} N + S_z & S_x - iS_y \\ S_x + iS_y & N - S_z \end{array} \right].$$

Assuming the coefficients  $t$  and  $r$  valid values for E pseudodensity and pseudospin density on the left and right of the barrier, respectively, we obtain:

$$\begin{aligned} N &= (1 + r^2) / 2 & N &= r^2 / 2 \\ S_x &= +r \cos 2kz & S_x &= 0 \\ S_y &= -r \sin 2kz & S_y &= 0 \\ S_z &= (1 - r^2) / 2 & S_z &= r^2 / 2 \end{aligned} \quad (4.25)$$

In other words, on the left of barrier pseudospin rotates in a plane  $xy$ . When plotting  $G^n(z, z)$  in Fig. 11b was the sum of two components pseudospin, and then took her square, which is equivalent to

$$Tr \left\{ \begin{array}{cc} 1 & 1 \\ 1 & 1 \end{array} \right\} \{\psi\}\{\psi\}^+ \left\{ \begin{array}{c} 1 \\ 1 \end{array} \right\} = Tr \left[ \begin{array}{cc} 1 & 1 \\ 1 & 1 \end{array} \right] \{\psi\}\{\psi\}^+. \quad (4.26)$$

In fact, we are dealing with a pseudo magnet with

$$\Gamma = \begin{bmatrix} 1 & 1 \\ 1 & 1 \end{bmatrix}, \quad (4.27)$$

which is 100% polarized along x. Thus, according to (4.23) measures the capacity to be proportional to what is left of the barrier to the oscillations of the cosine, and the right - to the absence of oscillations

$$N + \hat{x} \cdot \vec{S} \rightarrow \frac{1+r^2}{2} + r \cos 2kz \Big|_L ; \frac{r^2}{2} \Big|_R ,$$

which agrees well with the results of the calculation method NEGF (Fig. 4.11b).

Beyond our study are numerous questions and unsolved problems, among them nanophysics informational aspects of spintronics, which would have to devote a separate publication.

## References to Chapter 1 and 2

1. Kruglyak Yu. A., Kruglyak N. Yu., Strikha M.V. Lessons nanoelectronics: spintronics in the concept of "bottom - up"// Sensor Electronics and Microsystem Technologies. – 2013. – V. 4(10), N 2.–P. 5.
2. Glushkov A.V., Approximate quasiparticle functional in a density functional theory// Ukrainian Physical Journal. -1989.-Vol., N9.-P.1422-1425; Glushkov A.V., Relativistic quantum theory. Quantum mechanics of atomic systems. Odessa: Astroprint, 2008.
3. Datta Supriyo. Lessons from Nanoelectronics: A New Perspective on Transport. – Hackensack, New Jersey: World Scientific Publishing Company. – 2012. – pp. 474.
4. Datta Supriyo. Nanoelectronic devices: A unified view // The Oxford Handbook on Nanoscience and Nanotechnology: Frontiers and Advances, Eds. A.V. Narlikar and Y.Y.Fu. – Oxford University Press. – 2012. – V. 1, Chapter 1. – pp. 26.
5. Datta Supriyo. Quantum Transport: Atom to Transistor. – Cambridge: Cambridge University Press. – 2005. – pp. 404.
6. Datta Supriyo. Nanodevices and Maxwell's demon // Lecture Notes in Nanoscale Science and Technology, Vol. 2, Nanoscale Phenomena: Basic Science to Device Applications, Eds. Z.K. Tang and P. Sheng, Berlin: Springer. – 2008. – pp. 18
7. Caroli C., Combescot R., Nozieres P., Saint-James D. A direct calculation of the tunneling current: IV. Electron phonon interaction effects // J. Phys. C: Solid State Phys. – 1972. – V. 5. – P. 21.
8. Kubo R. Statistical-Mechanical Theory of Irreversible Processes.I. General Theory and Simple Applications to Magnetic and Conduction Problems // J.Phys.Soc. Japan. – 1957. – V. 12. – P. 570 – 586.
9. Sears F.W., Salinger G.L. Thermodynamics, Kinetic Theory, and Statistical Thermodynamics. – Boston: Addison-Wesley. – 1975. – pp. 331 – 336, 355 – 361.
10. Martin P.C., Schwinger J. Theory of many-particle systems. I // Phys. Rev. – 1959. – V. 115, N 6. – P. 1342 – 1373.
11. Kadanoff L.P., Baym G. Quantum Statistical Mechanics. – New York: W.A.Benjamin. – 1962.

12. Keldysh L.V. The diagram technique for nonequilibrium processes // JETP. – 1964. – T. – 47. – C. 1515 – 1527; Keldysh L.V. Diagram Technique for Non-Equilibrium Processes // Sov. Phys. JETP. – 1965. – V. 20. – P. 1018.
13. Landauer Rolf. Spatial variation of currents and fields due to localized scatterers in metallic conduction // IBM J. Res. Dev. – 1957. – V. 1, N 3. – P. 223 – 231.
14. Landauer Rolf. Electrical resistance of disordered onedimensional lattices // Philos. Mag. – 1970. – V. 21. – P. 863 – 867.
15. Landauer Rolf. Spatial variation of currents and fields due to localized scatterers in metallic conduction // J. Math. Phys. – 1996. – V. 37, N 10. – P. 5259.
16. Datta S. Steady-state quantum kinetic equation // Phys. Rev., 1989. – V. B40. – P. 5830.
17. Datta S. A simple kinetic equation for steady-state quantum transport // J. Phys., Cond. Matt. – 1990. – V. 2. – P. 8023 – 8052.
18. Meir Y., Wingreen N.S. Landauer formula for the current through an interacting electron region // Phys. Rev. Lett. – 1992. – V. 68. – P. 2512 – 2515.
19. Datta Supriyo. Electronic Transport in Mesoscopic Systems.- Cambridge: Cambridge University Press. – 2001. – pp. 377.
20. Smit R.H.M., Noat Y., Untiedt C., Lang N.D., van Hemert M.C., van Ruitenbeek J.M. Measurement of the conductance of a hydrogen molecule // Nature. – 2002. – V. 419, N 3. – P. 906 – 909.
21. Buttiker M. Symmetry of Electrical Conduction // IBM J. Res. Dev. – 1988. – V. 32, N 3. – P. 317 – 334.
22. Anderson P.W. Absence of Diffusion in Certain Random Lattices // Phys. Rev. – 1958. – V. 109, N 5. – P. 1492 – 1505.
23. Anderson P.W. New method for scaling theory of localization. II. Multichannel theory of a "wire" and possible extension to higher dimensionality // Phys. Rev. B. – 1981. – V. 23, N 10. – P. 4828 – 4836.
24. Kruglyak Yu. A., Kvakush V. S., Dyadyusha G. G., Khilchenko V. I. Methods of calculations in quantum chemistry. Calculation of  $\pi$ -electronic structure of molecules by simple methods of molecular orbitals // Kiev: Naukova Dumka. – 1967. – 150 p.

25. Kruglyak Yu. A., Ukrainsky I.I. Study of the electronic structure of alternant radicals by the DODS method // *Intern. J. Quantum Chem.* – 1970. – V. 4, N 1. – P. 57 – 72.
26. van Wees B.J., van Houten H., Beenakker C.W.J., Williamson J.G., Kouwenhoven L.P., van der Marel D., Foxon C.T. Quantized Conductance of Point Contacts in a Two-Dimensional Electron Gas // *Phys. Rev. Lett.* – 1988. – V. 60, N 9. – P. 848–850.
27. Wharam D.A., Thornton T.J., Newbury R., Pepper M., Ahmed H., Frost J.E.F., Hasko D.G., Peacock D.C., Ritchie D.A., Jones G.A.C. One-Dimensional Transport and the Quantisation of the Ballistic Resistance // *J. Phys. C: Solid State Phys.* – 1988. – V. 21, N 8. – P. L209 – L214.
28. Mojarad R.G., Zainuddin A.N.M., Klimeck G., Datta S. Atomistic non-equilibrium Green's function simulations of graphene nano-ribbons in the quantum hall regime // *J. Comput. Electron.* – 2008. – V. 7. – P. 407 – 410.
29. Berger C., Zhimin Song, Xuebin Li, Xiaosong Wu, Brown N., Naud C., Mayou D., Tianbo Li, Hass J., Marchenkov A.N., Conrad E.H. First P.N., de Heer W.A. Electronic Confinement and Coherence in Patterned Epitaxial Graphene // *Science.* – 2006. – V. 312. – P. 1191 – 1196.
30. Fujita M., Wakabayashi K., Nakada K., Kusakabe K. Peculiar Localized State at Zigzag Graphite Edge // *J. Phys. Soc. Japan.* – 1996. – V. 65, N 7. – P. 1920.
31. Nakada K., Fujita M., Dresselhaus G., Dresselhaus M.S. Edge state in graphene ribbons: Nanometer size effect and edge shape dependence // *Phys. Rev. B.* – 1996. – V. 54, N 24. – P. 17954.
32. Brey Luis, Fertig H.A. Electronic states of graphene nanoribbons studied with the Dirac equation // *Phys. Rev. B.* – 2006. – V. 73, N 23. – P. 235411.
33. Wakabayashi K., Takane Y., Yamamoto M., Sigrist M. Electronic transport properties of graphene nanoribbons // *New J. Phys.* – 2009. – V. 11. – P. 095016.
34. Koch, M., Ample F., Joachim C., Grill L. Voltage-dependent conductance of a single graphene nanoribbon // *Nature Nanotechnology.* – 2012. – V. 7. – P. 713 – 717.
35. Peres N.M., Castro Neto A.H., Guinea F. // *Phys. Rev. B.* – 2006. – V. 73. – P. 195411.

36. Abanin D.A., Lee P.A., Levitov L.S. Spin-filtered edge states and quantum Hall effect in Graphene // *Phys. Rev. Lett.* – 2006. – V. 96. – P. 176803.
37. Ashcroft N., Mermin N. *Solid State Physics*, vol. 1, 2. – M: Mir. – 1979.
38. Rashba E.I. Spin Currents in Thermodynamic Equilibrium: The Challenge of Discerning Transport Currents // *Phys. Rev. B.* – 2003. – V. 68, N 24. – P. 241315R.
39. Buttiker M. Symmetry of Electrical Conduction // *IBM J. Res. Dev.* – 1988. – V. 32, N 3. – P. 317 – 334.
40. Landauer Rolf. Electrical resistance of disordered onedimensional lattices // *Philos. Mag.* – 1970. – V. 21. – P. 863 – 867.
41. Hall E.H. On a New Action of the Magnet on Electric Currents // *Amer. J. Mathematics.* – 1879. – V. 2, N 3. – P. 287 – 292.
42. von Klitzing K., Dorda G., Pepper M. New Method for High-Accuracy Determination of the Fine-Structure Constant Based on Quantized Hall Resistance // *Phys. Rev. Lett.* – 1980. – V. 45. – P. 494 – 497.
43. von Klitzing K. Quantum Hall effect: Nobel Lecture // *APS.* – 1985. – T. 150, B. 1. – P. 107 – 126.
44. Reedtz G.M., Cage M.E. An Automated Potentiometric System For Precision Measurement Of the Quantized Hall Resistance // *J. Res. Nation. Bureau Standards.* – 1987. – V. 92, N 5. – P. 303 – 310.
45. Tsui D.S., Stormer H.L., Gossard A.C. Two-dimensional magnetotransport in the extreme quantum limit // *Phys. Rev. Lett.* – 1982. – V. 48, N 22. – P. 1559 – 1962.
46. Stepanovski Yu. P. Fractional quantum Hall effect // *Electromagnetic phenomena.* – 1998. – T. 1, № 3. – P. 427 – 442.
47. Nagaosa Naoto, Sinova Jairo, Onoda Shigeki, MacDonald A.H., Ong N.P. Anomalous Hall effect // *Rev. Mod. Phys.* – 2010. – V. 82, N 2. – 1539 – 1592.
48. Dyakonov M.I., Perel V.I. Possibility of orientating electron spins with current // *Sov. Phys. JETP Lett.* – 1971. – V. 13. – P. 467.
49. Dyakonov M.I., Perel V.I. Current-induced spin orientation of electrons in semiconductors // *Phys. Lett. A.* – 1971. – V. 35, N 6. – P. 459 - 460.
50. Kane C.L., Mele E.J. Quantum Spin Hall Effect in Graphene // *Phys. Rev. Lett.* – 2005. – V. 95. – P. 226801/1 – 4.

51. Srinivasan S., Sarkar A., Behin-Aein B., Datta S. All-Spin Logic Device with inbuilt Non-Reciprocity // IEEE Trans. Magnetics.– 2011. – V. 47, N 10. – P. 4026 – 4032.
52. Kane C. L., Moore J. E. Topological Insulators // Physics World. – 2011. – V. 24. – P. 32 – 36: [www.physics.upenn.edu/~kane/pubs/p69.pdf](http://www.physics.upenn.edu/~kane/pubs/p69.pdf).
53. Datta Supriyo. Lessons from Nanoelectronics: A New Perspective on Transport. – Hackensack, New Jersey: World Scientific Publishing Company. – 2012. – pp. 473.
54. Kruglyak Yu.A., Kondratenko P.A., Lopatkin Yu.M., J. Nanoelectron. Physics 5, N 2, (2013); Kruglyak Yu.A., Kondratenko P.A., Lopatkin Yu.M., J. Nanoelectron. Physics 5, N 1, (2013).
55. Glushkov A.V., Approximate quasiparticle functional in a density functional theory// Ukrainian Physical Journal. -1989.-Vol., N9.-P.1422-1425;
56. Glushkov A.V., Relativistic quantum theory. Quantum mechanics of atomic systems.-Odessa: Astroprint, 2008.
57. Kruglyak Yu.A., Kondratenko P.A., Lopatkin Yu.M., J. Nanoelectron. Physics 5, N 4, (2013).
58. Sears F.W., Salinger G.L. Thermodynamics, Kinetic Theory, and Statistical Thermodynamics. – Boston: Addison-Wesley. – 1975.
59. Landauer Rolf. Spatial variation of currents and fields due to localized scatterers in metallic conduction // IBM J. Res. Dev. – 1957. – V. 1, N 3. – P. 223 – 231.
60. Landauer Rolf. Spatial variation of currents and fields due to localized scatterers in metallic conduction // IBM J. Res. Dev. –1988. – V. 32. – P. 306.
61. Landauer Rolf. Spatial variation of currents and fields due to localized scatterers in metallic conduction // J. Math. Phys. – 1996. – V. 37, N 10. – P. 5259.
62. Buttiker M. Four-terminal phase-coherent conductance // Phys.Rev. Lett. – 1986. – V. 57. – P. 1761.
63. Sharvin Yu.V. A possible method of studying the Fermi surface // JETP. – 1965. – T. 48, № 3. – P. 984 – 985 // Sov. Phys. JETP. – 1965. – V. 21. – P. 655 – 656.

64. Sharvin Yu.V., Bogatina N.I. Investigation of Focusing of Electron Beams in a Metal by a Longitudinal Magnetic Field // *Sov. Phys. JETP*. – 1969. – V. 29, N 3. – P. 419 – 423 // *JETP*. – 1969. – T. 56, № 3. – P. 772 – 779.
65. Imry Y. in *Directions in Condensed Matter Physics*, ed. G. Grinstein, G. Mazenko. – Singapore: World Scientific. – 1986. – P. 101.
66. Imry Y., Laughlin Rolf. Conductance viewed as transmission // *Rev.Mod.Phys.* – 1999. – V. 71, N 2. – P. S306 – S312.
67. Lesovik G.B., Sadowski I.A. Description of quantum electron transport using the scattering matrix // *APS*.- 2011.- T. 181, № 10.- P. 1041 - 1096.
68. Stone A.D., Szafer A. What is measured when you measure a resistance? – The Landauer formula revisited // *IBM J. Res. Dev.* –1988. – V. 32, N 3. – P. 384 – 413.
69. Mojarad R.G., Zainuddin A.N.M., Klimeck G., Datta S. Atomistic non-equilibrium Green's function simulations of graphene nano-ribbons in the quantum hall regime // *J. Comput. Electron.* – 2008. – V. 7. – P. 407 – 410.
70. Haug R.J. Edge-state transport and its experimental consequences in high magnetic fields // *Semicond. Sci. Technol.* – 1993. – V. 8. – P. 131 – 153.
71. Cage M.E. Current Distributions in Quantum Hall Effect Devices // *J. Res. Natl. Inst. Stand. Technol.* – 1997. – V. 102. – P. 677.
72. Martinez -Duarte J.M., Martin-Palma R.J., Agulla-Rueda F. *Nanotechnology for micro- and optoelectronics*. – Moscow: Technosphere. – 2007. – 368 p.
73. Berger C., Zhimin Song, Xuebin Li, Xiaosong Wu, Brown N., Naud C., Mayou D., Tianbo Li, Hass J., Marchenkov A.N., Conrad E.H. First P.N., de Heer W.A. Electronic Confinement and Coherence in Patterned Epitaxial Graphene // *Science*. – 2006. – V. 312. – P. 1191 – 1196.
74. Brey L., Fertig H.A. Edge states and quantized Hall effect in Graphene // *Phys. Rev. B*. – 2006. – V. 73. – P. 195408.

### References to Chapter 3 and 4

1. Kruglyak Yu.A., Preuss H., Janoshek R. Nonempirical calculations of the electronic structure benzyl radical // Ukrainian Journal of Physics. – 1970. – T. 15, N 6.- P. 977 – 985.
2. Glushkov A.V., Approximate quasiparticle functional in a density functional theory// Ukrainian Physical Journal. -1989.-Vol., N9.-P.1422-1425;
3. Kruglyak Yu. A., Ukrainsky I.I. Study of the electronic structure of alternant radical method of splitting orbitals // Ukrainian Journal of Physics. – 1970. – T. 15, N 7.- P. 1068 – 1081.
4. Bychkov Yu.A., Rashba E.I. Oscillatory effects and the magnetic susceptibility of carriers in inversion layers // J. Phys. C. – 1984. – V. 17, N 33. – P. 6039 – 6045.
5. Datta Supriyo. Lessons from Nanoelectronics: A New Perspective on Transport. – Hackensack, New Jersey: World Scientific Publishing Company. – 2012. – pp. 473.
6. Hanle Wilhelm. Uber magnetische Beeinflussung der Polarisation der Resonanzfluorescenz // Z. Physik. – 1924. – V. 30, N 1. – P. 93 – 105.
7. Van Dyck R., Stoltenberg J. Pengra D. The Hanle Effect. – Washington: The University of Washington. – 2006.
8. Huang B., Jang Hyuk-Jae, Appelbaum Ian. Geometric dephasing-limited Hanle effect in long distance lateral silicon spin transport devices // Appl. Phys. Lett. – 2008. – V. 93, N 16. – P. 162508/1 – 3.
9. Koo H.C., Kwon J.H., Eom J., Chang J., Han S.H., Johnson M. Control of Spin Precession in a Spin-Injected Field Effect Transistor // Science. – 2009. – V. 325. – P. 1515.
10. Wunderlich J., Park Byong-Guk, Irvine Andrew C., Zârbo Liviu P., Rozkotová Eva, Nemeč Petr, Novák Vít, Sinova Jairo, Jungwirth Tomáš. Spin Hall Effect Transistor // Science. – 2010. – V. 330, N 6012. – P. 1801 – 1804.
11. Drune C., Roth A., Buhmann H., Hankiewicz E.M., Molenkamp L.W., Maciejko J., Xiao-Liang Q, Shou-Cheng Zhang. Spin polarization of the

- quantum spin Hall edge states // *Nature Physics*. – 2012. – V. 8. – P. 485 – 490.
12. Jun-Won Rhim. Quantum Spin Hall Effect in Graphene Nanoribbons: Effect of Edge Geometry // *Phys. Rev. B*. – 2011. – V. 84, N 3. – P. 035402/1 – 7.
  13. Son-Hsien Chen. Inverse quantum spin Hall effect generated by spin pumping from precessing magnetization into a graphene-based two-dimensional topological insulator // *Phys. Rev B*. – 2010. – V. 81. – P. 035428.
  14. Xiao-Liang Qi, Shou-Cheng Zhang. The Quantum Spin Hall Effect and Topological Insulators // *Physics Today*. – 2010. – V. 63, N 1. – P. 33.
  15. Cangas R., Hidalgo M.A. Rashba spin-orbit coupling in a two dimensional electron system under quantum Hall regime // *Physica E: Low-dimensional Systems and Nanostructures*. – 2009. – V. 41, N 7. –P. 1306 – 1309.
  16. Konig M., Buhmann H., Molenkamp L. W., Hughes T., Liu C. X., Qi X. L., Zhang S. C. The Quantum Spin Hall Effect. Theory and Experiment // *J. Phys. Soc. Japan*. – 2008. – V. 77, N 3. – P. 031007.
  17. Kane C.L., Mele E.J. Quantum Spin Hall Effect in Graphene // *Phys. Rev. Lett*. – 2005. – V. 95. – P. 226801/1 – 4.
  18. Jun-Won Rhim. Quantum Spin Hall Effect in Graphene Nanoribbons: Effect of Edge Geometry // *Phys. Rev. B*. – 2011. – V. 84, N 3. – P. 035402/1 – 7.
  19. Kruglyak Yu.A., Kondratenko P.A., Lopatkin Yu.M., *J. Nanoelectron. Physics* 6, N 1, (2014) (Article № 5 on the Hall Effect)
  20. Sih V., Lau W.H., Myers R.C, Horowitz V.R., Gossard A.C., Awschalom D.D. Generating Spin Currents in Semiconductors with the Spin Hall Effect // *Phys. Rev. Lett*. – 2006. – V. 97, N 9. – P. 096605/1 – 4.
  21. Kruglyak Yu. A., Kruglyak N. Yu., Strikha M.V. Lessons nanoelectronics. Non-equilibrium Green's function method and model of the transportation problem in the concept of "bottom - up" // *Sensor Electronics Microsys. Tech*. – 2013. – V. 4(10), N 3. – P. 5.
  22. Golizadeh-Mojarad R., Datta S. Non-equilibrium Green's function based model for dephasing in quantum transport // *Phys. Rev. B*. – 2007. – V. 75, N 8. – P. 081301/1 – 4.
  23. Kruglyak Yu. A., Kruglyak N. Yu., Strikha M.V. Hall effect measurements and electrochemical potentials in the concept of "bottom - up"// *Sensor Electronics Microsys. Tech*. – 2013. – V. 4(10), N 4. – P. 5.

24. Datta Supriyo. Lessons from Nanoelectronics: A New Perspective on Transport. – Hackensack, New Jersey: World Scientific Publishing Company. – 2012. – pp. 473.
25. Glushkov A.V., Svinarenko A.A., Khetselius O.Yu., Buyadzhi V.V., Florko T.A., Shakhman A.N., Relativistic Quantum Chemistry: Advanced Approach to Construction of the Green's Function of the Dirac Equation with Complex Energy and Mean-Field Nuclear Potential// Frontiers in Quantum Methods and Applications in Chemistry and Physics. (Springer).- 2015-Vol.29.-P.197-218.
26. Weber B., Mahapatra S., Ryu H., Lee S., Fuhrer A., Reusch T.C.G., Thompson D.L., Lee W.C.T., Klimeck Gerhard, Hollenberg L.C.L., Simmons M.Y. Ohm's Law Survives to the Atomic Scale // Science. – 2012. – V. 335. – P. 64 – 67.
27. Zurek W.H. Decoherence, Einselection and the Quantum Origins of the Classical // Rev. Mod. Phys. – 2003. – V. 75. – P. 715 – 775.
28. Kruglyak Yu.A., Kruglyak N.E. Methodological aspects of calculation of the band structure of graphene with the  $\sigma$ -core. Theoretical Foundations // Messenger of Odessa state environmental university. – 2012, V. 13. – P. 207 – 218.
29. Glushkov A.V., Atom in electromagnetic field.-Kiev: KNT, 2005.
30. Glushkov A.V., Relativistic and correlation effects in spectra of atomic systems.-Odessa: Astroprint, 2006.
31. Glushkov A.V., Relativistic Quantum Theory. Quantum, mechanics of Atomic Systems.-Odessa: Astroprint, 2008.
32. Khetselius O.Yu., Hyperfine structure of atomic spectra.-Odessa: Astroprint, 2008.
33. Khetselius, O.Yu. Quantum structure of electroweak interaction in heavy finite Fermi-systems. Astroprint: Odessa, 2011.
34. Glushkov A.V., Khetselius O.Yu., Gurnitskaya E.P., Loboda A.V., Florko T.A., Sukharev D.E., Lovett L., Gauge-Invariant QED Perturbation Theory Approach to Calculating Nuclear Electric Quadrupole Moments, Hyperfine Structure Constants for Heavy Atoms and Ions//Frontiers in Quantum Systems in Chemistry and Physics, Series: Progress in Theoretical Chemistry and Physics; Eds. S.Wilson, P.J.Grout, J. Maruani, G. Delgado-Barrio, P. Piecuch (Springer, Dordrecht), 2008.-Vol.18.-P.507-524.

35. Glushkov A.V., Khetselius O.Y., Malinovskaya S.V., New laser-electron nuclear effects in the nuclear  $\gamma$  transition spectra in atomic and molecular systems// *Frontiers in Quantum Systems in Chemistry and Physics. Series: Progress in Theoretical Chemistry and Physics* Eds. S.Wilson, P.J.Grout, J. Maruani, G. Delgado-Barrio, P. Piecuch (Springer, Dordrecht).-2008.-Vol.18.-525-541.
36. Glushkov A.V., Khetselius O.Yu., Loboda A.V., Svinarenko A.A., QED approach to atoms in a laser field: Multi-photon resonances and above threshold ionization//*Frontiers in Quantum Systems in Chemistry and Physics, Series: Progress in Theoretical Chemistry and Physics*; Eds. S.Wilson, P.J.Grout, J. Maruani, G. Delgado-Barrio, P. Piecuch (Springer, Dordrecht), 2008.-Vol.18.-P.543-560.
37. Ivanova E.P., Ivanov L.N., Glushkov A.V., Kramida A.E., High Order Corrections in the Relativistic Perturbation Theory with the Model Zeroth Approximation, Mg-Like and Ne-Like Ions//*Phys. Scripta.*-1985.-Vol.32,N5.-P.513-522.
38. E.P.Ivanova, A.V.Glushkov, Theoretical investigation of spectra of multicharged ions of F-like and Ne-like isoelectronic sequences// *Journal of Quantitative Spectroscopy and Radiative Transfer.*-1986.-Vol.36(2).-P. 127-145.
39. Glushkov A.V., Ivanov L.N., Ivanova E.P., Radiation decay of atomic states. Generalized energy approach// *Autoionization Phenomena in Atoms.*- M.: Moscow State University.-1986. -P.58-160.
40. Glushkov A.V., Effective quasi-particle valence hamiltonian of molecules in the comprehensive semi-empirical theory// *Sov. Journ. Struct. Chem.*-1988.-Vol.29(4).-P.3-10.
41. Glushkov A V, Negative ions of inert gases// *JETP Lett.*-1992.-Vol.55, Issue 2.-P.97-100.
42. Glushkov A.V., Ivanov L.N., Radiation decay of atomic states: atomic residue polarization and gauge noninvariant contributions//*Phys.Lett.A.*-1992.-Vol. 170, N1.-P.33-36.
43. Glushkov A V, Ivanov L N, DC Strong Field Stark Effect for Non-hydrogenic Atoms: Consistent Quantum Mechanical Approach // *Journal of Physics B: Atomic, Molecular and Optical Phys.*-1993.-Vol.26,N14.-P.L379-386.

44. Glushkov A.V., Calculation of parameters of the interaction potential between excited alkali atoms and mercury atoms-the Cs-, Fr-Hg interaction//*Optika i Spekr.*-1994.-Vol.77 (1).-P.5-10.
45. AV Glushkov, SV Dan'kov, G Prepelitsa, VN Polischuk, AE Efimov, Qed theory of nonlinear interaction of the complex atomic systems with laser field multi-photon resonances//*Journal of Techn.Physics.*-1997.-Vol.38, Issue 2.-P.219-222.
46. Glushkov A.V., Malinovskaya S.V., Ambrosov S.V., Shpinareva I.M., Troitskaya O.V., Resonances in quantum systems in strong external fields consistent quantum approach//*Journal of Techn.Physics.*-1997.-Vol.38, Issue 2.-P.215-218.
47. Glushkov A.V., Malinovskaya S.V., New approach to the formation of model potential for valence-electrons//*Zhurn. Fiz. Khimii.*-1988.-Vol.62(1).-P.100-104.
48. AV Glushkov, AF Kivganov, VN Khokhlov, TV Buyadzhi, LA Vitavetskaya, VP Borovskaya, VN Polishchuk, Calculation of the spectroscopic characteristics of biatomic van der Waals molecules and ions: Inert gas atom—halogen-type inert gas ion in the ground state//*Russian physics journal.*-1998.-Vol.41(3).-p. 223-226
49. AV Glushkov, AV Malinovskii, VA Efimov, AF Kivganov, VN Khokhlov, LA Vitavetskaya, GA Borovskaya, Calculation of alkaline metal dimers in terms of model perturbation theory//*Journal of structural chemistry.*-1998.-Vol.39(2).-P. 179-185.
50. A V Glushkov, L A Vitavetskaya, Accurate QED perturbation theory calculation of the structure of heavy and superheavy element atoms and multicharged ions with the account of nuclear size effect and QED corrections// *Herald of Uzhgorod Univ. Ser. Phys.*-2000.-Vol.8(2).-P.321-324.
51. Glushkov, A.V.; Malinovskaya S.V. Co-operative laser nuclear processes: border lines effects In *New Projects and New Lines of Research in Nuclear Physics*. Fazio, G., Hanappe, F., Eds.; World Scientific: Singapore, 2003, 242-250.
52. Turin A.V., Chernyakova Yu. G., Prepelitsa G.P., Characteristic features of the emission spectra of K plasma in a law inductive vacuum spark: Relativistic calculation// *Phys. Aerodisp. Syst.*-2003.-Vol.40.-P.327-332.

53. Glushkov A V, Ambrosov S V, Loboda A V, Chernyakova Yu, Svinarenko A A , Khetselius O Yu, QED calculation of the superheavy elements ions: energy levels, radiative corrections, and hfs for different nuclear models//Journal Nucl.Phys. A.: nucl. and hadr. Phys.-2004.-Vol.734.-P.21
54. AV Glushkov, SV Malinovskaya, YG Chernyakova, AA Svinarenko, Cooperative laser-electron-nuclear processes: QED calculation of electron satellites spectra for multi-charged ion in laser field// Int. Journal Quantum Chem.-2004.-Vol.99 (6).-P.889-893.
55. Glushkov A.V., Ambrosov S.V., Ignatenko A.V., Korchevsky D.A., DC strong field Stark effect for nonhydrogenic atoms: Consistent quantum mechanical approach// Int.Journ.Quant.Chem.-2004.-Vol.99,N6.-P.936-939.
56. V.D. Rusov, A.V. Glushkov, V.N. Vaschenko, D.A. Korchevsky, A.V. Ignatenko, Stochastic dynamics of the atomic systems in the crossed electric and magnetic field: the rubidium atom recurrence spectra//Bulletin of Kiev Nat. Univ.: Ser. Phys.-Math.-2004.-Issue 4.-P.433-438.
57. Malinovskaya S V, Dubrovskaya Yu. V., Zelentzova T.N. The atomic chemical environment effect on the  $\beta$  decay probabilities: Relativistic calculation// Herald of Kiev Nat. Univ. Ser.: Phys.-Math., -2004.-Issue 4.-P.427-432
58. Glushkov A.V., Energy Approach to Resonance states of compound superheavy nucleus and EPPP in heavy nuclei collisions// Low Energy Antiproton Phys. AIP Conference Proceedings.-2005.-Vol.796 (1).-P.206-210.
59. Glushkov A.V., Ambrosov S.V., Loboda A.V., Gurnitskaya E.P., Prepelitsa G.P., Consistent QED approach to calculation of electron-collision excitation cross sections and strengths: Ne-like ions// Int. Journal Quantum Chem.-2005.-Vol.104, Issue 4.-P.562–569.
60. S. Ambrosov, V. Ignatenko, D. Korchevsky, V. Kozlovskaya, Sensing stochasticity of atomic systems in crossed electric and magnetic fields by analysis of level statistics for continuous energy spectra// Sensor Electronics and Microsyst. Techn.-2005.-Issue 2.-P.19-23
61. A.V. Glushkov, S.V. Malinovskaya, V.Dubrovskaya Yu, Sensing the atomic chemical composition effect on the  $\beta$  decay probabilities//Sensor Electr. & Microsyst. Techn.-2005.-N1.-P.16-20.

62. AV Glushkov, SV Malinovskaya, AA Svinarenko, LA Vitavetskaya, Sensing spectral hierarchy, quantum chaos, chaotic diffusion and dynamical stabilisation effects in a multi-photon atomic dynamics with intense laser field// *Sensor Electronics and Microsystems Techn.*-2005.-Vol.2(2).-P. 29-36.
63. Glushkov A.V., Malinovskaya S.V., Loboda A.V., Shpinareva I.M., Gurnitskaya E.P., Korchevsky D.A., Diagnostics of the collisionally pumped plasma and search of the optimal plasma parameters of x-ray lasing: Calculation of electron-collision strengths and rate coefficients for Ne-like plasma// *Journal of Physics: Conf.Ser.*-2005.-Vol.11.-P.188-198.
64. A V Glushkov, S V Malinovskaya, G P Prepelitsa and V Ignatenko, Manifestation of the new laser-electron nuclear spectral effects in the thermalized plasma: QED theory of co-operative laser-electron-nuclear processes// *Journal of Physics: Conf.Ser.*-2005.-Vol.11.-P.199-206.
65. Khetselius O.Yu., Hyperfine structure of radium// *Photoelectronics.*-2005.-Vol.14.-P.83-85.
66. A-V Glushkov, S-V Ambrosov, A-V Loboda, E-P Gurnitskaya, O-Y Khetselius, QED calculation of heavy multicharged ions with account for correlation, radiative and nuclear effects// *Recent Advances in the Theory of Chemical and Physical Systems (Springer, Dordrecht)*-2006.-Vol.15.-P.285-299.
67. Malinovskaya S.V., Glushkov A.V., Dubrovskaya Yu.V., Vitavetskaya L.A., Quantum calculation of cooperative muon-nuclear processes: discharge of metastable nuclei during negative muon capture// *Recent Advances in the Theory of Chemical and Physical Systems (Springer, Dordrecht)*.-2006.-Vol.15.-P.301-307.
68. Glushkov A.V., Malinovskaya S.V., Gurnitskaya E.P., Khetselius O.Yu., Dubrovskaya Yu.V., Consistent quantum theory of recoil induced excitation and ionization in atoms during capture of neutron// *Journal of Physics: Conf. Series (IOP)*.-2006.- Vol.35(1).-P.425-430.
69. Glushkov A V, Malinovskaya S V, Loboda A V, Shpinareva I M and Prepelitsa G P, Consistent quantum approach to new laser-electron-nuclear effects in diatomic molecules // *Journal of Physics: Conf. Series (IOP)*.-2006.- Vol.35(1).-P.420-424.

70. Glushkov A.V., Khetselius O.Yu., Dubrovskaya Yu.V., Loboda A.V., Sensing the capture of negative muon by atoms: Energy approach// *Sensor Electr. and Microsyst. Techn.*-2006.-N4.-P.31-35.
71. Khetselius O.Y., Gurnitskaya E.P., Sensing the electric and magnetic moments of a nucleus in the N-like ion of Bi// *Sensor Electr. and Microsyst. Techn.*-2006.-N3.-P.35-39.
72. AV Glushkov, VN Khokhlov, Yu Bunyakova, AA Svinarenko, TV Solonko, Sensing the correlation between atmospheric teleconnection patterns and sea ice extent: micro technology "Geomath"//*Sensor Electr. and Microsyst. Techn.*-2006.-N2.-P.16-19.
73. Glushkov A.V., Khetselius O.Yu., Gurnitskaya E.P., Florko T.A., Sensing of nuclei available in little quantities by means of laser spectroscopy of hyperfine structure for isotopes: new theoretical scheme (U ,Hg) // *Sensor Electr. and Microsyst. Techn.*-2007.-N3.-P.8-12.
74. Glushkov A.V., Khetselius O.Yu., Malinovskaya S.V., Optics and spectroscopy of cooperative laser-electron nuclear processes in atomic and molecular systems - new trend in quantum optics// *Europ.Phys.Journ. ST.*-2008.-Vol.160,N1.-P.195-204.
75. Glushkov A.V., Khetselius O.Yu., Malinovskaya S.V., Spectroscopy of cooperative laser-electron nuclear effects in multiatomic molecules// *Molec. Physics (UK)*.-2008.-Vol.106.-N9-10.-P.1257-1260.
76. Khetselius O.Yu., Relativistic Calculating the Spectral Lines Hyperfine Structure Parameters for Heavy Ions // *Spectral Line Shapes, AIP Conference Proceedings*.-2008.-Vol.1058.-P.363-365.
77. S.V. Ambrosov, O.Y. Khetselius, A.V. Ignatenko, Wannier-Mott exciton and H, Rb atom in a DC electric field: Stark effect// *Photoelectronics*.-2008.-Vol.17.-P.82-85.
78. Khetselius O.Yu., On possibility of sensing nuclei of the rare isotopes by means of laser spectroscopy of hyperfine structure//*Sensor Electronics and Microsystem Technologies*.-2008.-Vol.3.-P.28-33.
79. Glushkov A.V., Khetselius O.Yu., Loboda A.V., Ignatenko A., Svinarenko A., Korchevsky D., Lovett L., QED Approach to Modeling Spectra of the Multicharged Ions in a Plasma: Oscillator and Electron-ion Collision Strengths// *Spectral Line Shapes. AIP Conference Proceedings*.-2008.-Vol.1058.-P.175-177.

80. E P Gurnitskaya, O Yu Khetselius, A V Loboda, L A Vitavetskaya, Consistent quantum approach to quarkony energy spectrum and semiconductor superatom and in external electric field. Photoelectronics. 2008. Vol.17. P.127-130.
81. A V Glushkov, Ya I Lepikh, S V Ambrosov, O Yu Khetselius, Yu G Chernyakova, Computer modelling optimal schemes of the laser photoionization method for preparing the films of pure composition at atomic level// Photoelectronics. 2008. Vol.17. P.53-55.
82. Glushkov A.V., Loboda A.V., Gurnitskaya E.P., Svinarenko A.A., QED theory of radiation emission and absorption lines for atoms in a strong laser field//Physica Scripta.-2009.- Vol.T.135.-P. 014022.
83. Glushkov A.V., Khetselius O.Y., Lovett L., Electron- $\beta$ -Nuclear Spectroscopy of Atoms and Molecules and Chemical Bond Effect on the  $\beta$ -Decay Parameters. In: Piecuch P., Maruani J., Delgado-Barrio G., Wilson S. (eds) Advances in the Theory of Atomic and Molecular Systems. Progress in Theoretical Chemistry and Physics, vol 20. Springer, Dordrecht.-2009.-Vol.20.-P. pp 125-152
84. Khetselius O.Yu., Relativistic perturbation theory calculation of the hyperfine structure parameters for some heavy-element isotopes// Int. Journal Quantum Chem.-2009.-Vol.109 (14).-P.3330-3335.
85. Khetselius O Yu, Relativistic calculation of the hyperfine structure parameters for heavy elements and laser detection of the heavy isotopes// Phys. Scripta.-2009.-Vol.T135.-P.014023
86. Malinovskaya S.V., Glushkov A.V., Khetselius O.Yu., Svinarenko A.A., Mischenko E.V., Florko T.A., Optimized perturbation theory scheme for calculating the interatomic potentials and hyperfine lines shift for heavy atoms in the buffer inert gas//Int. Journ. of Quantum Chemistry.-2009.- Vol.109,N14.-P.3325-3329.
87. AV Glushkov, SV Malinovskaya, OY Khetselius, AV Loboda, DE Sukharev, L Lovett, Green's function method in quantum chemistry: New numerical algorithm for the Dirac equation with complex energy and Fermi-model nuclear potential//Int. Journal Quant.Chem.-2009.- Vol.109 (8).-P.1717-1727.
88. Glushkov A.V., Lovett L., Khetselius O.Yu., Gurnitskaya E.P., Dubrovskaya Yu.V., Loboda A.V., Generalized multiconfiguration model

- of decay of multipole giant resonances applied to analysis of reaction ( $\mu$ -n) on the nucleus  $^{40}\text{Ca}$ //International Journal of Modern Physics A.-2009.-Vol. 24, N.2-3.-P.611-615.
89. AV Glushkov, O Khetselius, E Gurnitskaya, A Loboda, D Sukharev, Relativistic quantum chemistry of heavy ions and hadronic atomic systems: spectra and energy shifts//AIP Conference Proceedings 2009.-Vol.1102 (1).-P.168-171.
  90. Sukharev D.E., Khetselius O.Yu., Dubrovskaya Yu.V., Sensing strong interaction effects in spectroscopy of hadronic atoms// Sensor Electr. and Microsyst. Techn.-2009.-N3.-P.16-21.
  91. Glushkov A.V., Svinarenko A.A., Nuclear quantum optics: Energy approach to multi-photon resonances in nuclei // Sensor Electr. and Microsyst. Techn.-2010.-N2.-P.5-10.
  92. Glushkov A.V., Khetselius O.Yu., Svinarenko A.A., Prepelitsa G.P., Energy Approach to Atoms in a Laser Field and Quantum Dynamics with Laser Pulses of Different Shape//In: Coherence and Ultrashort Pulse Laser Emission (InTech).-2010.-P.159-186.
  93. Khetselius O. Yu., Lopatkin Yu. M., Dubrovskaya Yu. V., Svinarenko AA Sensing hyperfine-structure, electroweak interaction and parity non-conservation effect in heavy atoms and nuclei: New nuclear-QED approach// Sensor Electr. and Microsyst. Techn.-2010.-Vol.7(2).-P.11-19.
  94. Bunyakova Yu., Glushkov A., Analysis and forecast of the impact of anthropogenic factors on air basein of an industrial city. Odessa, Ecology, 2010.
  95. A.A. Svinarenko, A.V. Glushkov, A.V. Loboda, D.E. Sukharev, Y.V. Dubrovskaya, N.V. Mudraya, I.N. Serga, Green's Function of the Dirac Equation with Complex Energy and Non-singular Central Nuclear Potential//AIP Conference Proceedings.-2010.-Vol.1232(1).-P.259-266.
  96. Khetselius O.Yu., TA Florko, LV Nikola, AA Svinarenko, IN Serga, TB Tkach, EV Mischenko, Hyperfine Structure, Scalar-pseudoscalar Interaction and Parity Non-Conservation Effect in Some Heavy Atoms and Ions//AIP Conference Proceedings.-2010.-Vol.1232(1).-P.243-250.
  97. A.S. Kvasikova, A.V. Ignatenko, T.A. Florko, D.E. Sukharev, Y.G. Chernyakova, Photoeffect and spectroscopy of the hydrogen atom in the

- crossed dc electric and magnetic field//Photoelectronics.-2011.-Vol.20.-P.71-75.
98. Malinovskaya S.V., Glushkov A.V., Khetselius O.Yu., Lopatkin Yu.M., Loboda A.V., Svinarenko A.A., Nikola L.V., Pereyigina T.B., Generalized energy approach to calculating electron collision cross-sections for multicharged ions in a plasma: Debye shielding model// International Journal of Quantum Chemistry.-2011.-Vol.111,N2.-P.288-296.
  99. A V Glushkov, A A Svinarenko, A V Ignatenko, Spectroscopy of autoionization resonances in spectra of the lanthanides atoms//Photoelectronics .-2011.-Vol.20.-P. 90-94.
  100. Glushkov, A.V. Methods of a Chaos Theory. OSENU: Odessa, 2012.
  101. Glushkov A.V., Khetselius O.Yu., Svinarenko A.A., Relativistic theory of cooperative muon- $\gamma$ -nuclear processes: Negative muon capture and metastable nucleus discharge// Advances in the Theory of Quantum Systems in Chemistry and Physics. Series: Frontiers in Theoretical Chemistry and Physics, Eds. P.Hoggan, E.Brandas,J.Marvani, G. Delgado-Barrio, P.Piecuch (Springer, Dordrecht).-2012.-Vol.22.-P.51-68.
  102. Khetselius O.Yu., Relativistic energy approach to cooperative electron- $\gamma$ -nuclear processes: NEET Effect// Quantum Systems in Chemistry and Physics: Progress in Methods and Applications. Ser.: Progress in Theoretical Chemistry and Physics, Eds. K.Nishikawa, J. Marvani, E. Brändas, G. Delgado-Barrio, P.Piecuch (Springer).-2012-Vol.26.-P.217-229.
  103. Glushkov, A.V. Advanced relativistic energy approach to radiative decay processes in multielectron atoms and multicharged ions. In Quantum Systems in Chemistry and Physics: Progress in Methods and Applications, Series: Progress in Theoretical Chemistry and Physics; Nishikawa, K., Marvani, J., Brandas, E., Delgado-Barrio, G., Piecuch, P., Eds.; Springer: Dordrecht, 2012; Vol. 26, pp 231–252.
  104. AV Glushkov, Spectroscopy of cooperative muon-gamma-nuclear processes: Energy and spectral parameters//J. Phys.: Conf. Series.-2012.-Vol.397(1).-P. 012011
  105. Khetselius O.Yu., Spectroscopy of cooperative electron-gamma-nuclear processes in heavy atoms: NEET effect// Journal of Physics: Conf. Series.-2012.-Vol.397(1).-P.012012

106. Khetselius O.Yu., Quantum Geometry: New approach to quantization of the quasistationary states of Dirac equation for super heavy ion and calculating hyper fine structure parameters// Proceedings of International Geometry Center.-2012.-Vol.5,№ 3-4.-P.39-45.
107. Kuznetsova A.A., A. S. Kvasikova, A. N. Shakhman, L. A. Vitavetskaya Calculating the radiative vacuum polarization contribution to the energy shift of 2p-2s transition in mu-hydrogen// Photoelectronics. - 2012. – Vol. 21. – P.116-120.
108. Glushkov, A.V. Operator Perturbation Theory for Atomic Systems in a Strong DC Electric Field. In Advances in Quantum Methods and Applications in Chemistry, Physics, and Biology, Series: Progress in Theoretical Chemistry and Physics; Hotokka, M., Brändas, E., Maruani, J., Delgado-Barrio, G., Eds.; Springer: Cham, 2013; Vol. 27, pp 161–177.
109. Glushkov A.V., Khetselius O.Yu., Svinarenko A.A., Theoretical spectroscopy of autoionization resonances in spectra of lanthanide atoms// Physica Scripta.-2013.-Vol.T153.-P.014029.
110. Khetselius O.Yu., Florko T.A., Svinarenko A.A., Tkach T.B., Radiative and collisional spectroscopy of hyperfine lines of the Li-like heavy ions and Tl atom in an atmosphere of inert gas//Physica Scripta (IOP).-2013.-Vol.T153-P.014037.
111. Khetselius, O.Yu. Forecasting evolutionary dynamics of chaotic systems using advanced non-linear prediction method In Dynamical Systems Applications; Awrejcewicz, J., Kazmierczak, M., Olejnik, P., Mrozowski, J., Eds.; Wyd. Politech. Łódz.: Łódz, 2013; Vol T2, pp 145-152.
112. Glushkov A.V., Kuzakon V., Ternovsky V.B., Buyadzhi V.V., Dynamics of laser systems with absorbing cell and backward-wave tubes with elements of a chaos// Dynamical Systems Theory, eds. J. Awrejcewicz, M. Kazmierczak, P. Olejnik, and J. Mrozowski (Lodz).-2013.-Vol.T1.-P.461-466
113. Glushkov, A.V.; Prepelitsa, G.P.; Svinarenko, A.A. ; Zaichko, P.A. Studying interaction dynamics of the non-linear vibrational systems within non-linear prediction method (application to quantum autogenerators) In Dynamical Systems Theory; Awrejcewicz, J., Kazmierczak, M., Olejnik, P., Mrozowski, J., Łódz, 2013; Vol T1, pp 467-477.

114. Glushkov, A.V.; Buyadzhi, V.V.; Ternovsky V.B. Geometry of Chaos: Consistent combined approach to treating of chaotic self-oscillations in backward-wave tube. Proc. Intern. Geometry Center. 2013, 6(2), 6-12.
115. Yu G Chernyakova, Yu V Dubrovskaya, TA Florko, A V Romanova, L A Vitavetskaya, An advanced approach quantization of the quasistationary states of Dirac-Slater equation// Proc.Intern. Geom. Center.-2013.-Vol.6(2).-P. 29-34.
116. A V Glushkov, A A Svinarenko, V V Buyadzhi, P A Zaichko, V B Ternovsky, Chaos geometric attractor and quantum neural networks approach to simulation chaotic evolutionary dynamics during perception process In Advances in Neural Networks, Fuzzy Systems and Artificial Intelligence, Series: Recent Advances in Computer Engineering; Balicki, J., Ed.; WSEAS Press: Gdansk, 2014; Vol 21, pp 143-150
117. Glushkov, A.V.; Khetselius, O.Yu.; Brusentseva, S.V.; Zaichko, P.A.; Ternovsky, V.B. Studying interaction dynamics of chaotic systems within a non-linear prediction method: Application to neurophysiology In Advances in Neural Networks, Fuzzy Systems and Artificial Intelligence, Series: Recent Advances in Computer Engineering; Balicki, J., Ed.; WSEAS Press: Gdansk, 2014; Vol 21, pp 69-75.
118. Svinarenko A.A., Khetselius O.Yu., Buyadzhi V.V., Florko T.A., Zaichko P.A., Ponomarenko E.L., Spectroscopy of Rydberg atoms in a Black-body radiation field: Relativistic theory of excitation and ionization// Journal of Physics: Conf.Ser.-2014.-Vol.548.-P.012048.
119. Svinarenko A.A., Study of spectra for lanthanides atoms with relativistic many- body perturbation theory: Rydberg resonances// Journal of Physics: Conf.Ser.-2014.-Vol.548.-P.012039.
120. Glushkov A.V., Khetselius O.Yu., Lopatkin Yu.M., Florko T.A., Kovalenko O.A., Mansarliysky V.F., Collisional shift of hyperfine line for rubidium in an atmosphere of the buffer inert gas// Journal of Physics: Conf.Ser.-2014.-Vol.548.-P.012026.
121. Glushkov A.V., Spectroscopy of atom and nucleus in a strong laser field: Stark effect and multiphoton Resonances// Journal of Physics: Conf. Ser.-2014.-Vol.548.-P.012020.
122. Glushkov A.V., Kondratenko P.A., Buyadzhi V.V., Kvasikova A.S., Shakhman A.S., SakunT.N., Spectroscopy of cooperative laser electron- $\gamma$

- nuclear processes in polyatomic molecules// Journal of Physics: Conf. Ser.-2014.-Vol.548.-P.012025.
123. V.V. Buyadzhi, A.V. Glushkov, L. Lovett, Spectroscopy of atom and nucleus in a strong laser field: stark effect and multiphoton resonances// Photoelectronics.-2014.-Vol.23.-P. 38-43
  124. Glushkov, A.V.; Buyadzhi, V.V.; Ponomarenko, E.L. Geometry of Chaos: Advanced approach to treating chaotic dynamics in some nature systems// Proc. Intern. Geom. Center. 2014 7(1),24-30.
  125. Prepelitsa, G.; Glushkov, A.V.; Lepikh, Ya.; Buyadzhi, V.; Ternovsky, V.; Zaichko, P. Chaotic dynamics of non-linear processes in atomic and molecular systems in electromagnetic field and semiconductor and fiber laser devices: new approaches, uniformity and charm of chaos. Sensor Electr. and Microsyst.Techn. 2014, 11, 43-57.
  126. Glushkov A.V., Khetselius O.Yu., Bunyakova Yu.Ya., Buyadzhi V.V., Brusentseva S.V., Zaichko P.A., Sensing interaction dynamics of chaotic systems within a chaos theory and microsystem technology geomath with application to neurophysiological systems// Sensor Electronics and Microsystems Technologies-2014.-Vol.11,N3.-P.62-69.
  127. Ternovsky V.B., Florko T.A., Ignatenko A.V., Svinarenko A.A., Tkach T.B., Advanced relativistic model potential approach to calculation of the radiation transition and ionization characteristics for rydberg atoms// Photoelectronics.-2014.-Vol.23.-P.91-95.
  128. Serga I.N., Relativistic theory of spectra of pionic atoms with account of the radiative corrections: hyperfine structure// Photoelectronics.-2014.-Vol.23.-P.171-175.
  129. Glushkov, A; Khetselius, O; Svinarenko, A.; Buyadzhi, V. Spectroscopy of autoionization states of heavy atoms and multiply charged ions. Odessa: TEC, 2015.
  130. Glushkov A.V., Svinarenko A.A., Khetselius O.Y., Buyadzhi V.V., Florko T.A., Shakhman A.N. Relativistic Quantum Chemistry: An Advanced Approach to the Construction of the Green Function of the Dirac Equation with Complex Energy and Mean-Field Nuclear Potential. In: Nascimento M., Maruani J., Brändas E., Delgado-Barrio G. (eds) Frontiers in Quantum Methods and Applications in Chemistry and

- Physics. Progress in Theoretical Chemistry and Physics, vol 29. Springer, Cham.-2015.-P.197-217
131. Khetselius O.Yu., Optimized perturbation theory for calculating the hyperfine line shift and broadening of heavy atoms in a buffer gas// Frontiers in Quantum Methods and Applications in Chemistry and Physics. Series: Frontiers in Theoretical Chemistry and Physics, Eds. M.Nascimento, J.Marvani, E.Brändas, G.Delgado-Barrio (Springer, Cham).-2015-Vol.29.-P.55-76.
  132. Buyadzhi V.V., Glushkov A.V., Mansarliysky V.F., Ignatenko A.V., Svinarenko A.A., Spectroscopy of atoms in a strong laser field: New method to sensing AC Stark effect, multiphoton resonances parameters and ionization cross-sections//Sensor Electr. and Microsyst. Techn.-2015.-Vol.12,N4.-P.27-36.
  133. Ternovsky V.B., Glushkov A.V., Zaichko P.A., Khetselius O.Yu., Florko T.A., New relativistic model potential approach to sensing radiative transitions probabilities in spectra of heavy Rydberg atomic systems/ // Sensor Electr. and Microsyst. Techn.-2015.-Vol.12,N4.-P.19-26.
  134. Buyadzhi V.V., Laser multiphoton spectroscopy of atom embedded in Debye plasmas: multiphoton resonances and transitions//Photoelectronics-2015.-Vol.24.-P.128-133.